

2023

# Antimicrobial phototherapy: mechanisms and translation

---

<https://hdl.handle.net/2144/46249>

*"Downloaded from OpenBU. Boston University's institutional repository."*

BOSTON UNIVERSITY  
COLLEGE OF ENGINEERING

Dissertation

**ANTIMICROBIAL PHOTOTHERAPY:  
MECHANISMS AND TRANSLATION**

by

**SEBASTIAN EUREKO JUSUF**

B.S., Cornell University, 2017

Submitted in partial fulfillment of the  
requirements for the degree of  
Doctor of Philosophy

2023



Approved by

First Reader

---

Ji-Xin Cheng, Ph.D.  
Moustakas Chair Professor in Photonics and Optoelectronics  
Professor of Biomedical Engineering  
Professor of Electrical and Computer Engineering  
Professor of Materials Science and Engineering  
Professor of Chemistry  
Professor of Physics

Second Reader

---

Ahmad S. Khalil, Ph.D.  
Associate Professor of Biomedical Engineering

Third Reader

---

Jerome C. Mertz, Ph.D.  
Professor of Biomedical Engineering  
Professor of Electrical Engineering  
Professor of Physics

Fourth Reader

---

Shyamsunder Erramilli, Ph.D.  
Professor of Biomedical Engineering  
Professor of Materials Science and Engineering  
Professor of Physics

Fifth Reader

---

George Y. Liu, MD, Ph.D.  
Associate Professor of Pediatrics  
Director of the Infectious & Immunological Diseases Research Center  
University of California San Diego, School of Medicine

“If I don’t have red, I’ll use blue.” – Pablo Picasso

## **DEDICATION**

I would like to dedicate this work to everyone who has supported me through my doctoral journey, especially my parents, Gani and Caroline Jusuf.

## ACKNOWLEDGMENTS

I would like to thank my advisor Dr. Ji-Xin Cheng for the endless guidance and assistance he has provided me throughout my time working within his lab and the creation of this dissertation. I would also like to thank all the current and former members of my defense committee, including my committee head Dr. Ahmad Khalil, Dr. Jerome Mertz, Dr. Shyamsunder Erramilli, Dr. George Y. Liu, and Dr. Allyson Sgro. Their input on my projects has been incredibly beneficial for my growth as a researcher.

For the contents of the dissertation, I would like to acknowledge the contributions of Dr. Pu-Ting Dong, Dr. Jie Hui, Dr. Meng Zhang, Yuewei Zhan, and the Mansour Lab at Massachusetts General Hospital, all of whom helped me tremendously with the contents of this work. I would like to highlight the guidance of Dr. Dong in laying the initial foundation and performing the early experiments for this light-based catalase deactivation project as well as Yuewei Zhan's amazing work performing the neutrophil co-culture experiments and histology analysis. Their assistance in conducting the *in vivo* experiments was also invaluable. For the Mansour Lab, I would like to thank Dr. Michael K. Mansour as well as Natalie Alexander and Adam Viens for not only collaborating with me on various projects, but also for graciously providing me with any resources or advice I may have needed to conduct my experiments. I would also like to thank the rest of the Cheng Group for assisting me through my time in the Cheng Lab.

On a personal level, I would like to thank my family, especially my parents Gani and Caroline as well as my siblings Arista and Darion for the support they provided me throughout not only my PhD career, but also my entire life. I would also like to thank all

the good friends I made in the BME PhD program like Yoseph, Robbie, Nate, Jourdan, and Sam that have helped me through my career and personal life.

**ANTIMICROBIAL PHOTOTHERAPY:  
MECHANISMS AND TRANSLATION**

**SEBASTIAN EUREKO JUSUF**

Boston University College of Engineering, 2023

Major Professor: Ji-Xin Cheng, Ph.D., Moustakas Chair Professor in Photonics and Optoelectronics; Professor of Biomedical Engineering; Professor of Electrical and Computer Engineering; Professor of Materials Science and Engineering; Professor of Chemistry; Professor of Physics

**ABSTRACT**

Over the past few decades, the global healthcare community has witnessed the rise and spread of drug resistance across a broad spectrum of both bacterial and fungal pathogens, due to a combination of medical overuse and slowing pharmaceutical drug development. As a result, technology like blue light phototherapy has emerged as novel non-drug reliant alternatives based on their broad-spectrum antimicrobial capabilities, although the mechanism of action of this phenomenon is still disputed. While blue light has been found to target of multitude of molecular targets including porphyrins, flavins, and pigments, recent findings have discovered that the antioxidant catalase can act as a broad spectrum target off blue light, reducing its activity through structural deactivation.

In this thesis, we have extensively investigated the role of antioxidant catalase within antimicrobial blue light, observing the impact of antioxidant presence on blue light's antimicrobial activity and demonstrating the significant role that catalase photodeactivation plays in inducing broad spectrum ROS sensitization across bacteria. Based on these results, we reveal the translatability of this catalase photodeactivation

therapy to fight against bacterial infections by utilizing blue light to potentiate bacterial pathogens against conventional antibiotics, the host immune system, and within an *in vivo* murine model. Next, we extend our observations on the effects of antimicrobial blue light to more complex eukaryotic fungal pathogens, discovering that the catalase deactivating effects of blue light can suppress the hyphae forming capabilities of pathogenic *Candida* fungi through lipogenesis inhibition and demonstrating the translatability of this technology to target *Candida* skin infections within an *in vivo* murine model and an *ex vivo* human skin model. Finally, we explore the translatability of this technology by synergizing the effects of catalase deactivating blue light with a clinically relevant topical antibiotic silver sulfadiazine within both *in vitro* and *in vivo* environments.

## TABLE OF CONTENTS

DEDICATION .....	v
ACKNOWLEDGMENTS .....	vi
ABSTRACT .....	viii
TABLE OF CONTENTS.....	x
LIST OF FIGURES .....	xv
LIST OF ABBREVIATIONS .....	xxi
GLOSSARY .....	xxiii
CHAPTER ONE: Introduction .....	1
Rise and Spread of Antibiotic Resistance .....	1
Phototherapy: Antimicrobial Blue Light .....	3
CHAPTER TWO: Antimicrobial Phototherapy Increases Bacterial ROS Sensitivity Via Catalase Deactivation .....	7
Introduction.....	7
Bacterial Skin Infections .....	7
Current Knowledge on the Effects of Antimicrobial Blue Light on Bacteria.....	8
Antimicrobial Blue Light Deactivates Bacterial Catalase .....	10
Methods and Materials.....	12
Blue Light Source .....	12
Bacterial Strains and Cell Lines .....	13
Bacterial Preparation and Blue Light Treatment.....	13
ROS Measurement.....	14

Bacterial Transformation and Catalase Rescue .....	14
Iron Chelator Application.....	15
Antibiotic Treatment of Light Treated Bacteria .....	15
Catalase Deactivation of Bacteria-Macrophage Co-Culture .....	16
Mammalian Cell Toxicity .....	18
<i>In Vivo</i> Bacterial Infection Murine Model .....	19
Statistical Analysis.....	20
Study Approval.....	20
Results.....	21
Antioxidant Enzyme Removal and Blue Light Antimicrobial Activity .....	21
Catalase Photodeactivation Sensitizes Bacteria to Exogenous H <sub>2</sub> O <sub>2</sub> .....	23
Catalase Deactivation and Antibiotic Potentiation .....	29
Catalase Deactivation and Immune Cells .....	31
Bacterial Catalase Deactivation Mammalian Translation.....	33
<i>In Vivo</i> Bacterial Catalase Deactivation Murine Model .....	35
Discussion and Conclusion .....	36
CHAPTER THREE: Antimicrobial Phototherapy Reduces Fungal Virulence within <i>In</i>	
<i>Vitro</i> and <i>In Vivo</i> Environments.....	43
Introduction.....	43
Fungal Skin Infections .....	43
Catalase Deactivation and <i>Candida</i> .....	45
Fungal Hyphae Development.....	46

Methods and Materials.....	49
Blue Light Source .....	49
Fungal Strains and Cell lines.....	49
Fungal Preparation and Catalase Deactivation Phototherapy .....	50
Neutrophil Isolation and Co-Culture .....	52
Confocal and Phase Contrast Imaging .....	53
D <sub>2</sub> O Metabolism Stimulated Raman Spectroscopy Imaging .....	53
Gas Chromatography – Mass Spectroscopy.....	55
Mammalian Cell Toxicity .....	56
<i>In Vivo</i> Candida Infection Murine Model .....	58
<i>Ex Vivo</i> Candida Infection Human Model .....	59
Statistical Analysis.....	60
Study Approval.....	60
Results.....	61
Blue Light Treatment and Catalase Deactivation in <i>Candida</i> Species.....	61
Fungal Metabolism of Catalase Deactivated <i>C. albicans</i> .....	65
<i>C. albicans</i> and Neutrophil Co-Culture .....	68
Fungal Catalase Deactivation Mammalian Translation .....	69
<i>In Vivo</i> Fungal Murine Models.....	71
Catalase Deactivation on Non- <i>Candida</i> Fungi.....	74
Discussion and Conclusion .....	75

CHAPTER FOUR: Blue Light Induced Catalase Deactivation Improves Antimicrobial Efficiency of Silver Sulfadiazine .....	84
Introduction.....	84
Clinical Relevance of Hydrogen Peroxide.....	84
Silver Sulfadiazine: Mechanisms and Clinical Usage .....	85
Methods and Materials.....	87
Bacterial Strains.....	87
Silver Sulfadiazine Preparation .....	87
<i>In Vitro</i> Blue Light and Silver Sulfadiazine Treatment .....	87
Catalase Rescue and Salvaging .....	88
ROS Detection and Quantification .....	89
<i>In Vivo</i> Murine Model.....	89
Statistical Analysis.....	90
Study Approval.....	90
Results.....	91
Blue Light and Silver Sulfadiazine Exhibit Synergistic Behavior .....	91
Mechanisms of Blue Light and Silver Sulfadiazine Interactions .....	94
Blue Light Improves Silver Sulfadiazine Performance <i>In Vivo</i> .....	96
Discussion and Conclusion .....	97
CHAPTER FIVE: Conclusion and Future Directions .....	101
Conclusion .....	101
Further Directions of Antimicrobial Phototherapy.....	101

Applications of Pulsed Light.....	101
Higher Wavelength Explorations .....	102
APPENDIX.....	105
Blue Light Application Devices .....	105
BIBLIOGRAPHY .....	106
CURRICULUM VITAE.....	124

## LIST OF FIGURES

- Figure 1: Blue Light Disrupts Catalase Structure and Activity. a) PyMOL simulation of *P. aeruginosa* catalase, highlighting heme subunits (red) within structure. b) Raman spectra of bovine liver catalase before and after exposure to 30 J/cm<sup>2</sup> of 410 nm light. The 754 cm<sup>-1</sup> catalase peak is highlighted. c) Remaining catalase activity of bovine liver catalase following exposure to varying wavelengths of blue light. Data published in Dong et al., *JCI Insight.*, 2022.<sup>34</sup> .....4
- Figure 2: Potential Contribution of Catalase to Antimicrobial Blue Light Activity. As blue light is known to photoexcite endogenous porphyrins to produce toxic ROS, it is possible that the inactivation of catalase by blue light prevents the neutralization of ROS. This allows for both ROS formed by endogenous porphyrin excitation and ROS generated by exogenous sources to induced oxidative damage. ....9
- Figure 3: Antimicrobial Blue Light Deactivates Active Catalase within Bacteria. Under 15 J/cm<sup>2</sup> of blue light, 410 to 420 nm light significantly reduces the catalase activity found within both stationary phase a) MRSA and b) *P. aeruginosa*. Data published in Dong et al., *JCI Insight.*, 2022.<sup>34</sup> ..... 11
- Figure 4: CFU and ROS of Light Treated *E. coli* Mutants. CFU measurements of a) wild type *E. coli* MG1655, b) catalase deficient *E. coli*  $\Delta katGE$ , and c) catalase and alkyl hydroperoxide reductase negative *E. coli*  $\Delta katGEahpCF$  in response to 30 to 60 J/cm<sup>2</sup> of CW-410 (250 mW/cm<sup>2</sup>). *E. coli*  $\Delta katGEahpCF$  experienced the greatest reduction in CFU. Measurements of ROS through HPF fluorescence of 60 J/cm<sup>2</sup> treated d) wild type *E. coli*, e)  $\Delta katGE$  mutant, and f)  $\Delta katGEahpCF$  reveal only the  $\Delta katGEahpCF$  mutant was found to exhibit higher ROS levels following light exposure. \*\*\*\*:  $p < 0.0001$ , \*\*\*:  $p < 0.001$ , \*\*:  $p < 0.01$ , ns = No Significance. ....21
- Figure 5: Catalase Photodeactivation Sensitizes Bacteria to Exogenous H<sub>2</sub>O<sub>2</sub>. When combined with 22 mM of H<sub>2</sub>O<sub>2</sub>, 15 J/cm<sup>2</sup> of 410 nm light resulted in a a) near 4-log reduction in CFU for MRSA and b) complete eradication of *P. aeruginosa* following 30 minutes of incubation. Data published in Dong et al., *JCI Insight.*, 2022.<sup>34</sup> .....23
- Figure 6: Impact of Blue Light on Catalase Deficient Bacteria. a) CFU measurements of catalase negative *E. faecalis* found light to have no effect on H<sub>2</sub>O<sub>2</sub> activity. b) CFU measurements of *E. coli* BW25113 and its catalase deficient mutants ( $\Delta ahpC$ ,  $\Delta katG$ ,  $\Delta katE$ ,  $\Delta katGE$ ) revealed that the catalase encoded by *katG* significant contributes to H<sub>2</sub>O<sub>2</sub> defense. Time killing curves of c) wild type *E. coli* BW25113, d) *E. coli*  $\Delta katG$ , and *E. coli*  $\Delta katGE$ . Samples all treated to ns-410. Data adapted from Dong et al., *JCI Insight.*, 2022.<sup>34</sup> .....24
- Figure 7: Catalase Rescue Salvages Light Treated *E. coli* from ROS Sensitivity. CFU/mL of blue light treated a-b) wild type *E. coli* BW25113 or the c-d) *E. coli*  $\Delta katGE:pBad\_katE$  rescue strain incubated in 2.2 mM of H<sub>2</sub>O<sub>2</sub> for 30 minutes

following a 4 hour incubation in the absence or presence of 1% arabinose in M9 media for 4 hours. Arabinose incubation has no effect on wild type activity, while the presence of arabinose and subsequent catalase expression significantly provides significant defense to the combined effects of blue light and H<sub>2</sub>O<sub>2</sub>. \*:  $p < 0.05$ . Data published in Dong et al., *JCI Insight.*, 2022.<sup>34</sup> .....27

Figure 8: Effects of Iron Chelators on Catalase Photodeactivation. a) By reacting with ferrous and ferric iron ions, H<sub>2</sub>O<sub>2</sub> exerts its toxic effects by further propagating formation of additional ROS sources in what is known as the Fenton Reaction. CFU measurements of *E. coli* BW25113 treated with 30 J/cm<sup>2</sup> of CW-410 (200 mW/cm<sup>2</sup>, 2.5 minutes) and 2.2 mM of H<sub>2</sub>O<sub>2</sub> in the b) absence of iron chelators, c) the presence of deferoxamine, or d) the presence of 2,2 bipyridyl reveal the presence of chelators has an only minor effect on light induced ROS sensitization. \*\*\*\*:  $p < 0.0001$ . .....28

Figure 9: Catalase Photodeactivation Sensitizes Bacteria to Antibiotics. CFU measurements of a) *E. coli* BW25113, b) *S. enterica* 2, or c) *S. enterica* 3 treated to blue light and incubated in the presence of the aminoglycoside tobramycin for 4 hours. Significant improvements in tobramycin activity observed. The same treatment applied to d) catalase negative *E. faecalis* was found to be ineffective. For the fluoroquinolone ciprofloxacin, 4 hours of antibiotic incubation following light treatment was found to improve the activity of the antibiotic against both log phase e) *P. aeruginosa* PAO-1 and f) *A. baumannii* 2. \*\*\*\*:  $p < 0.001$ , \*\*:  $p < 0.01$ . Data published in Dong et al., *JCI Insight.*, 2022.<sup>34</sup> .....29

Figure 10: Catalase Photodeactivation Improves Macrophage Killing Efficiency. A) CFU/mL of intracellular *P. aeruginosa* PAO-1 following two 60 J/cm<sup>2</sup> CW-410 treatments performed over the course of 12 hours. B) CFU/mL of macrophages treated with light treated PAO-1 in the presence or absence of the NOX2 inhibitor DPI. DPI neutralizes the effects of light treatment. C) HPF fluorescence ROS measurements of RAW 264.7 macrophage and untreated or light treated PAO-1. D) Survival percentage of uninfected RAW 264.7 macrophages with or without light exposure. All macrophage killing assays performed with a MOI = 20. \*\*\*\*:  $p < 0.0001$ , \*\*\*:  $p < 0.001$ , ns = No Significance. Data published in Dong et al., *JCI Insight.*, 2022.<sup>34</sup> .....31

Figure 11: Blue Light and Short Term, High Concentration H<sub>2</sub>O<sub>2</sub> Against Mammalian and Bacterial Cells. 75 J/cm<sup>2</sup> of CW-410 (250 mW/cm<sup>2</sup>, 5 minutes) and 0.1% H<sub>2</sub>O<sub>2</sub> (1 minute incubation) was applied to a) MTT assay with CHO cells and CFU measurements against both b) log phase MRSA and c) log phase *P. aeruginosa*. \*\*\*:  $p < 0.001$ , \*\*:  $p < 0.01$ , # = Below Detection Limit. Data published in Dong et al., *JCI Insight.*, 2022.<sup>34</sup> .....33

Figure 12: Catalase Photodeactivation in a *In Vivo* *P. aeruginosa* Infected Murine Abrasion Model. a) Treatment regimen of CW-410 light and H<sub>2</sub>O<sub>2</sub> for infected murine abrasion wounds. Mice received two treatments over 16 hours. Light

treatments consisted of delivery of 120 J/cm<sup>2</sup> of CW-410 (200 mW/cm<sup>2</sup>) while 0.5% H<sub>2</sub>O<sub>2</sub> was used for H<sub>2</sub>O<sub>2</sub> treatment. B) CFU/mL results of wound bioburden following light treatment. \*\*\*:  $p < 0.001$ , \*:  $p < 0.05$ . Scale bar = 100 μm. Data published in Dong et al., *JCI Insight.*, 2022.<sup>34</sup> .....35

Figure 13: Blue Light Induced Catalase Deactivation of *Candida* fungal cells. a) Catalase activity measurement of various *Candida* species treated to 30 J/cm<sup>2</sup> of 405 nm blue light. CFU/mL of *C. albicans* SC5314 treated to H<sub>2</sub>O<sub>2</sub> alongside either b) 30 J/cm<sup>2</sup> of blue light or c) 4 hours of incubation in 50 mM of catalase inhibiting AMT. \*\*\*:  $p < 0.001$ , \*\*:  $p < 0.01$ . Data published in Data published in Dong et al., *Advanced Science.*, 2022<sup>86</sup> .....45

Figure 14: Blue Light Suppresses *C. albicans* Hyphae Formation. Phase-contrast imaging of a) untreated and b) CW-405 (60 J/cm<sup>2</sup>) blue light treated *C. albicans* following 1 hour of incubation under hyphae inducing conditions. c) Average length of hyphae for untreated and light treated *C. albicans* measured from confocal images. d) Histogram distribution of average hyphae length for untreated and light treated *C. albicans*. \*\*\*\*:  $p < 0.0001$ . Data published in Jusuf et al., *Photochemistry and Photobiology*, 2022.<sup>85</sup> .....61

Figure 15: Hyphae Lengths of Catalase Deactivated *C. albicans*. a) Average length of hyphae for untreated and 50 mM incubated *C. albicans* measured from phase contrast images. b) Histogram distribution of average hyphae length for untreated and AMT treated *C. albicans*. c) Average length of hyphae for untreated and CW-405 (60 J/cm<sup>2</sup>) blue light treated catalase deficient *C. albicans*  $\Delta cat1$  following 1 hour of incubation under hyphae inducing conditions measured from phase contrast images. d) Histogram distribution of average hyphae length for untreated and light treated *C. albicans*  $\Delta cat1$ . \*\*\*\*:  $p < 0.0001$ , ns = No Significance. Data published in Jusuf et al., *Photochemistry and Photobiology*, 2022.<sup>85</sup> .....62

Figure 16: Blue Light Induced Hyphae Suppress Occurs Across Multiple *Candida* Strains. Phase contrast imaging of a) untreated and b) CW-405 (60 J/cm<sup>2</sup>) treated *C. dubliniensis* following 1.5 hours of incubation under hyphae inducing conditions. c) Average length of hyphae for untreated and light treated *C. dubliniensis* measured from confocal images. Phase contrast imaging of d) untreated and e) CW-405 (60 J/cm<sup>2</sup>) treated *C. tropicalis* following 3 hours of incubation under hyphae inducing conditions. f) Average length of hyphae for untreated and light treated *C. tropicalis* measured from confocal images. \*\*\*\*:  $p < 0.0001$ . Data published in Jusuf et al., *Photochemistry and Photobiology*, 2022.<sup>85</sup> .....64

Figure 17: Quantification of D<sub>2</sub>O Metabolic Incorporation can Detect Changes in Cellular Metabolism. a) Method of utilizing D<sub>2</sub>O to label proteins and lipids within cells. Stimulated Raman scattering imaging of *C. albicans* treated with 90% D<sub>2</sub>O for 1 hour under hyphae forming conditions reveals changes in general metabolism. b) Transmission imaging and c) C-D bond imaging at 2165 cm<sup>-1</sup> of untreated *C.*

*albicans*. d) Cross-phase transmission imaging and f) C-D bond imaging at  $2165\text{ cm}^{-1}$  of light treated *C. albicans* ( $60\text{ J/cm}^2$ ). g) Change in average single-cell mean C-D bond SRS intensity between untreated and light treated *C. albicans*. f) GC-MS normalized abundance peaks of fatty acids Palmitic Acid (16:0), Palmitoleic Acid (16:1), Stearic Acid (18:0), Oleic Acid (18:1), and Linoleic Acid (18:2) present within untreated and light treated *C. albicans* incubated under fatty acids. Peaks were normalized against a pentadecanoic acid (15:0) internal standard. \*\*\*\*\*:  $p < 0.0001$ . Data published in Jusuf et al., *Photochemistry and Photobiology*, 2022.<sup>85</sup>..65

Figure 18: Hyphae Growth of *C. albicans* Co-Cultured With Neutrophils. Both a) untreated and b) light treated ( $75\text{ J/cm}^2$ ) *C. albicans* were cultured in complete RPMI media at  $37\text{ }^\circ\text{C}$  for 4 hours and imaged under a confocal microscope. c) Average length of hyphae for untreated and light treated *C. albicans* within co-culture measured from confocal images. d) Histogram distribution of average hyphae length for untreated and light treated *C. albicans* within co-culture. \*\*\*\*\*:  $p < 0.0001$ . Data published in Jusuf et al., *Photochemistry and Photobiology*, 2022.<sup>85</sup>.....68

Figure 19: Blue Light and Short Term, High Concentration  $\text{H}_2\text{O}_2$  Against Mammalian and Fungal Cells. CFU/mL measurements of a) *Candida auris* 2 (AR-0382) treated with  $30\text{ J/cm}^2$  of CW-405 ( $200\text{ mW/cm}^2$ , 2.5 minutes) and  $0.1\%$   $\text{H}_2\text{O}_2$  (1 minute incubation). b) An MTT assay with CHO cells using the same conditions found no change in viability in response to the treatment. c) An additional MTT assay of CHO cells with higher light dosage ( $60\text{ J/cm}^2$ ) found higher light dosages to have no impact on mammalian cell viability. \*\*\*\*\*:  $p < 0.0001$ , \*:  $p < 0.05$ , ns = No Significance. Data adapted from Dong et al., *JCI Insight*, 2022<sup>34</sup> and Jusuf et al., *Photochemistry and Photobiology*, 2022<sup>85</sup>.....69

Figure 20: Catalase Photodeactivation and  $\text{H}_2\text{O}_2$  Synergistically Reduces *C. albicans* Bioburden Within a Murine Abrasion Model. a) Treatment regimen of blue light and  $\text{H}_2\text{O}_2$  for fungal infected murine abrasion wounds. b) *C. albicans* selective BiGGY agar plates of homogenized wound tissue following treatment regimen. c) CFU/mL of homogenized murine tissue following treatment regimen. d) PAS-stained histology slides of *C. albicans* infected mice following treatment regimen. Scalar bar:  $50\text{ }\mu\text{m}$ . Fungal colonization area was pointed by red arrows. \*\*:  $p < 0.01$ . Outlier was determined through whisker box plot analysis. Data published in Dong et al., *Advanced Science*, 2022.<sup>86</sup>.....71

Figure 21: Catalase deactivation and  $\text{H}_2\text{O}_2$  treatment within a EpiDerm skin scaffold model. (a) CFU of *C. albicans* infected EpiDerm scaffold following treatment and homogenization. PAS staining of (b) untreated skin, (c)  $\text{H}_2\text{O}_2$  treated, and (d) combination CW-405 and  $\text{H}_2\text{O}_2$  treated scaffold skin model. Combination treated skin exhibits significantly lower *Candida* bioburden and hyphae growth. Scale bar:  $100\text{ }\mu\text{m}$ . \*:  $p < 0.05$ .....73

- Figure 22: Catalase Photodeactivation on Non-*Candida* Fungal Strains. a) Application of 30 or 60 J/cm<sup>2</sup> of 405 nm blue light and 2.2 mM of H<sub>2</sub>O<sub>2</sub> was found to reduce the viability of *Aspergillus fumigatus*, a filamentous mold. b) Converting the viability to CFU measurements reveals that combining light treatment and H<sub>2</sub>O<sub>2</sub> results in the complete eradication of the filamentous mold. \*\*\*:  $p < 0.001$ , # = Below Detection Limit.....74
- Figure 23: Combination of catalase deactivating CW-405 and silver sulfadiazine results in synergistic interactions within model bacteria organism *E. coli* (BW25113). a) Checkerboard assay of *E. coli* exposed to varying dosages of CW-405 and silver sulfadiazine within tryptic soy broth. Treatment with 60 J/cm<sup>2</sup> of CW-405 and 8 µg/mL silver sulfadiazine results in a fractional inhibitory concentration index (FICI) of 0.375. FICI values below 0.5 indicate synergistic interactions. b) CFU measurements of bacterial population indicate combination of light and silver sulfadiazine resulted in complete eradication, further confirming the synergistic interactions. In contrast, light or silver sulfadiazine alone has little impact on the overall CFU. \*:  $p < 0.05$ , #: Below detection limit. Data published in Jusuf & Cheng, *Photobiomodulation, Photomedicine and Laser Surgery*, 2023<sup>147</sup>.....91
- Figure 24: CFU measurements of CW-405 (60 J/cm<sup>2</sup>) treated a) *P. aeruginosa* (PAO-1), and b) MRSA following incubation with silver sulfadiazine in PBS. Light or silver sulfadiazine alone has little impact on overall CFU, while the combination of the two agents results in complete eradication. In nutrient rich conditions, CFU measurements of CW-405 (60 J/cm<sup>2</sup>) treated c) *P. aeruginosa* (PAO-1), and d) MRSA following incubation with silver sulfadiazine in tryptic soy broth indicate that while higher dosages of silver sulfadiazine are required, improved performance with CW-405 still occurs. \*\*\*\*:  $p < 0.0001$ , \*\*:  $p < 0.01$ , \*:  $p < 0.05$ , #: Below detection limit. Data published in Jusuf & Cheng, *Photobiomodulation, Photomedicine and Laser Surgery*, 2023<sup>147</sup>.....92
- Figure 25: Mechanisms of CW-405 and silver sulfadiazine synergy. The combination of CW-405 (60 J/cm<sup>2</sup>) and low concentration silver sulfadiazine results in a) a 1-log reduction in wild type *E. coli* but b) no significant reduction in catalase deficient *E. coli*  $\Delta katGE$  mutants. Further investigation in the possible role of catalase in the synergy reveal that the addition of exogenous bovine catalase completely neutralizes the synergistic effects of CW-405 and silver sulfadiazine in both c) PAO-1 and d) MRSA. The impact of catalase deactivation on the ROS production of silver sulfadiazine was further explored through an ROS detecting HPF dye. When applying the combination treatment to e) PAO-1 and f) MRSA, HPF dye reveals significant increases in ROS florescence for the combination treated samples. \*\*\*\*:  $p < 0.0001$ , \*:  $p < 0.05$ , ns = No Significance, #: Below detection limit. Data published in Jusuf & Cheng, *Photobiomodulation, Photomedicine and Laser Surgery*, 2023<sup>147</sup>.....94

Figure 26: MRSA and PAO-1 infected murine abrasion wound models were used to evaluate the effectiveness of blue light and silver sulfadiazine combination treatment. a) 1 cm<sup>2</sup> abrasion wounds were generated on the dorsal flanks of BALB/c mice and infected with bacterial loads. b) When applying 1% silver sulfadiazine cream to infected wounds, it was ensured that the wound would be covered by the silver sulfadiazine cream. MRSA infected wounds treated with daily application sessions of CW-405 (120 J/cm<sup>2</sup>) and 1% silver sulfadiazine cream for 4 days were c) quantified via CFU plating on mannitol salt agar and d) found to exhibit minor average improvement from the combination treatment in comparison to the untreated wounds. In PAO-1 infected wounds, wounds were treated with CW-405 (120 J/cm<sup>2</sup>) and silver sulfadiazine cream twice in 24 hours and e) plated on cetrinide agar were f) found to improve the efficacy of PAO-1 significantly, with a near 2-log reduction in CFU population observed from the untreated group. In both murine models, silver sulfadiazine alone was found to be either ineffective in the case of PAO-1 infected wounds or beneficial to bacterial growth in the case of MRSA infected wounds. \*\*:  $p < 0.01$ , \*:  $p < 0.05$ . Data published in Jusuf & Cheng, *Photobiomodulation, Photomedicine and Laser Surgery*, 2023<sup>147</sup>.....96

## LIST OF ABBREVIATIONS

aBL .....	Antimicrobial Blue Light
AMT .....	3-Amino-1,2,4-triazole
ANSI.....	American National Standards Institute
ATCC.....	American Type Culture Collection
C-D .....	Carbon-Deuterium
CFU .....	Colony-Forming Units
CO <sub>2</sub> .....	Carbon Dioxide
cRPMI.....	Complete Roswell Park Memorial Institute Medium
CW-410/405 .....	Continuous-Wave 405 nm Blue Light
D <sub>2</sub> O .....	Deuterium Oxide
DMEM .....	Dulbecco's Modified Eagle Medium
FBS .....	Fetal Bovine Serum
H&E.....	Hematoxylin and Eosin
H <sub>2</sub> O <sub>2</sub> .....	Hydrogen Peroxide
IRB.....	Institutional Review Board
iRFP .....	Near-infrared Fluorescent Protein
LED .....	Light-Emitting Diode
MRSA .....	Methicillin-resistant <i>Staphylococcus aureus</i>
ns-410 .....	Nanosecond Pulsed 410 nm Blue Light
PAS.....	Periodic Acid–Schiff
PBS .....	Phosphate Buffered Saline

ROS .....	Reactive Oxygen Species
SRS .....	Stimulated Raman Spectroscopy
SSD.....	Silver Sulfadiazine
SSTI.....	Skin and Soft Tissue Infection
TSB.....	Tryptic Soy Broth
YPD .....	Yeast Extract Peptone Dextrose

## GLOSSARY

**Catalase:** A tetramer enzyme comprised of four iron-containing heme groups. Among the most common enzymes found in aerobic organisms, this enzyme is responsible for decomposing toxic hydrogen peroxide to water and oxygen. Found in both prokaryotic and eukaryotic organisms, this enzyme is primarily responsible for protecting cells from oxidative damage from either endogenous or exogenous reactive oxygen species.

**Porphyrin:** Heterocyclic macrocycle molecules comprised of four modified pyrrole rings connected by methine bonds to form an interconnected aromatic ring structure. Within the center “pocket” of the ring structure, porphyrins usually bind to metal ions.

Porphyrins with iron ions are often referred to as heme molecules, which acts as a essential cofactor in several metabolic proteins and plays an important role in cell signaling.

## CHAPTER ONE: Introduction

### Rise and Spread of Antibiotic Resistance

Following the isolation and mass production of penicillin in 1945, the subsequent few decades are often considered the “Golden Age” of antibiotic discovery. Despite the observed development of antibiotic resistance in bacterium, new novel classes of antibiotics were continuously being introduced that could combat and neutralize these resistance mechanisms<sup>1,2</sup>. However, since the late 1980’s, no new classes of antibiotics have been introduced, due in part to the higher regulatory standards as well as lower financial returns for pharmaceutical companies, resulting in fewer and fewer new antibacterial agents being approved and introduced into the market<sup>3,4</sup>. Combined with the heavy agricultural and healthcare overuse of antibiotics, this has led to the development and spread of antibiotic resistance within a wide variety of bacterial strains<sup>5-7</sup>. The situation is even worse for antifungal agents, as only four different classes of antifungal are currently commercially available, meaning that acquisition of multi-drug resistance could result in near untreatable fungal strains, as already observed within the pathogenic *Candida auris* strain<sup>8</sup>. As antibiotic and antifungal resistance continues to proliferate worldwide, the spread of multi-drug resistance is estimated to not only increase the mortality of infections for at-risk patients, but also induce a severe economic burden, increasing yearly global healthcare costs from \$300 billion to more than \$1 trillion by 2050<sup>9-11</sup>. Even today, in the US alone, resistant pathogens are estimated to be responsible for 99,000 deaths annually, increasing healthcare costs to up to \$29,000 for every patient with antibiotic resistant infections<sup>12,13</sup>. For skin and soft tissue infections (SSTI), the

spread of antibiotic resistance is especially concerning due to the potential of permitting the potential exchange of resistance genes to susceptible bacteria strains within the polymicrobial biofilm environment of skin infections, making infections much more difficult to treat<sup>14,15</sup>. For diabetic or immunocompromised individuals, these resistant pathogens hold an even greater threat to their well-being due to their weakened immune systems, rendering them much more dependent on antibiotic or antifungal agents<sup>16-18</sup>.

Despite these issues, the current most common method of treating drug resistant infections remains the continued usage of antibiotics, specifically the usage of “drugs of last resort” such as vancomycin for bacterial infections and amphotericin B for fungal infections. However, these drugs have already been found to be losing effectiveness in certain bacterial and fungal strains, highlighting the growing threat<sup>19-21</sup>. Alternative solutions, such as the development of antibiotic cocktails containing a combination of different antibiotics or the usage of antibiotic resistance inhibitors have been explored, but complications with increased costs, drug toxicity, and the potential creation of multi-drug resistant organisms has slowed the widespread adoption of these alternatives<sup>22-24</sup>. With the last remaining effective available antimicrobials gradually losing their potency, and the current direction of the pharmaceutical industry remaining focused on currently existing antibiotics and antifungal agents, there is an urgent need to develop new types of non-antibiotic reliant treatment methods for infections.

### **Phototherapy: Antimicrobial Blue Light**

Within the past few years, phototherapy has emerged as a reliable and non-drug reliant method of treating microbial infections. While the usage of light for the treatment of disease has been known since ancient times, it is only within the last century that phototherapy and photomedicine has seriously come into fruition thanks to the creation of artificial light sources<sup>25</sup>. Unlike traditional antibiotics, the usage of photons provides a non-drug reliant method of treating infections, reducing the likelihood of developing resistance to this treatment. In the realm of skin infections, while phototherapy has previously been used for the treatment of skin infections such as acne or herpes lesions, these treatments often rely on exogenous reactive oxygen species (ROS) producing photosensitizer agents like methyl blue to kill sources of the infection within the wound<sup>26</sup>. However, in the past few years, antimicrobial blue light (aBL) alone has been found to exert antimicrobial effects on a wide range of bacterial pathogens, viruses, biofilms, and fungi, emerging as a possible alternative to antibiotic and antifungal usage in the treatment of infections<sup>27,28</sup>. The discovery of aBL offers the possibility of a new non-drug reliant method of treatment patients suffering from drug-resistant infections, offering the potential ability to significantly improve a patient's quality of life, and allowing for a reduced risk of the infection.

While potential applications of aBL have been extensively explored and established against multiple microbes and pathogens, the actual mechanisms responsible for the antimicrobial nature of blue light remains controversial. The leading theory holds that endogenous porphyrins present within pathogens act as photosensitizers, reacting

with blue light and converting to an excited triplet state that produces reactive oxygen species (ROS), damaging the interior of the cell and resulting in cell death<sup>29-31</sup>. However, recent studies by the Ji-Xin Cheng Lab have found that blue light is capable of interacting with a variety of different molecules within bacteria, such as photolyzing the antioxidant staphyloxanthin or granadaene colored pigments present within *S. aureus* and *S. agalactiae* respectively.<sup>32,33</sup> This indicates that there may be a wide variety of photosensitive molecular targets present within bacteria that could contribute to the antimicrobial activity of blue light.

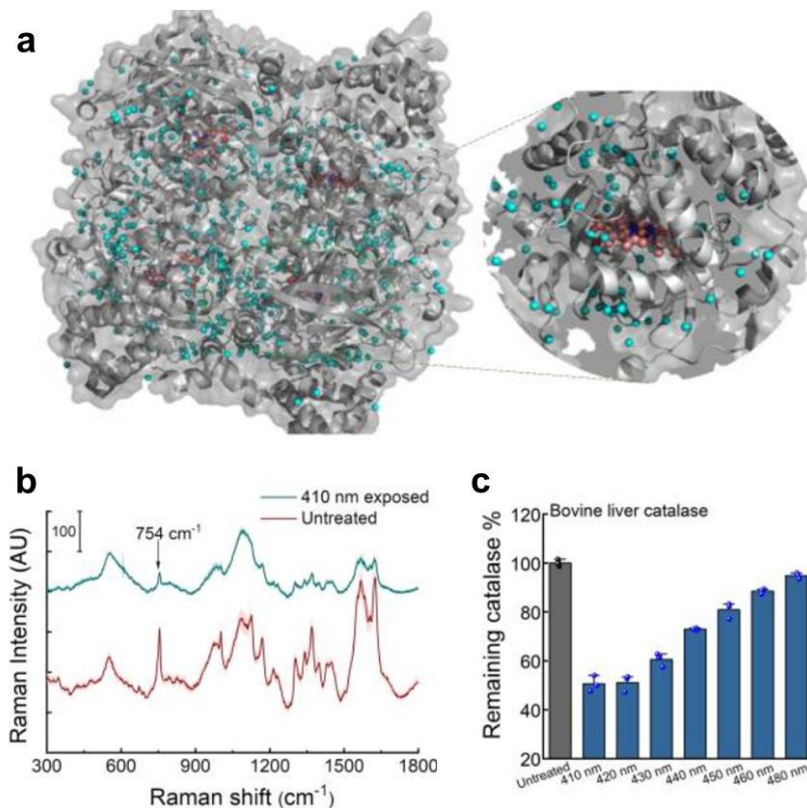


**Figure 1: Blue Light Disrupts Catalase Structure and Activity. a)** PyMOL simulation of *P. aeruginosa* catalase, highlighting heme subunits (red) within structure. **b)** Raman spectra of bovine liver catalase before and after exposure to 30 J/cm<sup>2</sup> of 410 nm light. The 754 cm<sup>-1</sup> catalase peak is highlighted. **c)** Remaining catalase activity of bovine liver catalase following exposure to varying wavelengths of blue light. Data published in Dong et al., *JCI Insight.*, 2022.<sup>34</sup>

Among the multitude of molecules and mechanisms present within pathogens to protect them from external threats, one of the most common defense molecules present within a broad range of both bacteria and fungi is the molecule known as catalase. As a tetramer antioxidant enzyme found in nearly all aerobic organisms (**Figure 1a**), catalase is primarily responsible for neutralizing toxic hydrogen peroxide ( $\text{H}_2\text{O}_2$ ) to  $\text{H}_2\text{O}$  and  $\text{O}_2$  with incredible efficiency, converting between 2.5 to 5 million moles of  $\text{H}_2\text{O}_2$  to water and oxygen per minute<sup>35-37</sup>. This molecule not only helps neutralize toxic ROS produced endogenously by the autoxidation of redox enzymes, but it also plays a key role in enhancing pathogen virulence by protecting pathogens from the host immune system<sup>38,39</sup>. Specifically, bacterial and fungal catalase can neutralize the ROS burst produced by immune cells like neutrophils and macrophages following phagocytosis, therefore enhancing survival, and providing evasion of the immune system<sup>40,41</sup>. In addition to antioxidant defense, catalase has also been found to contribute to the lipid metabolism in the peroxisomal  $\beta$ -oxidation pathway within eukaryotic cells, suggesting that the antioxidant enzyme contributes to significantly more metabolic processes than just simple ROS neutralization and defense<sup>42,43</sup>.

On a structural level, catalase consists of 4 iron containing porphyrin heme groups, which contributes to its observed absorbance peak between 405 and 410 nm<sup>44,45</sup>. Further investigation with Raman spectroscopy found that these porphyrin heme groups are responsible for the  $754\text{ cm}^{-1}$  characteristic peak observed in bovine liver catalase. Based on the known catalase absorbance, the Ji-Xin Cheng lab discovered that treatment with 410 nm light was found to exert significant structural changes in catalase, resulting

in a significant reduction in the porphyrin characteristic peak, indicating a dissociation of the heme ring from catalase (**Figure 1b**). Further specific wavelength tests performed by the Cheng lab have discovered that while blue light in general is capable of inactivating catalase, it is blue light specifically between 400 to 420 nm that displays the highest efficiency of catalase in vitro, reducing active catalase activity by roughly 50% (**Figure 1c**). These results demonstrate the potential applicability of catalase as a broad-spectrum target of phototherapy across a wide variety of pathogens.

Based on the ability of blue light to deactivate isolated catalase, as well as the significant role catalase plays in a variety of metabolic functions, we hypothesize that catalase deactivation plays a key role in the mechanism behind antimicrobial blue light, potential contributing to the accumulation of ROS and subsequent oxidative stress within microbes, as well as generating further downstream effects such as increasing ROS sensitization and disrupting lipid metabolism within bacterial and fungal strains. Furthermore, the catalase deactivating capabilities of blue light should be capable of improving the antimicrobial activity of ROS forming antimicrobials like aminoglycosides against drug resistant bacterial infections, providing a translational path to the usage of this technology within clinical settings. We hypothesize that not only is catalase deactivation a key mechanism within antimicrobial blue light against pathogens, but the synergy between catalase deactivating phototherapy and ROS producing antimicrobials should result in a significant improvement in the effectiveness and efficiency of these compounds in the treatment of skin infections, allowing for the usage of reduced amounts of antimicrobials or improved treatment times.

## **CHAPTER TWO: Antimicrobial Phototherapy Increases Bacterial ROS Sensitivity Via Catalase Deactivation**

The work and figures presented in this chapter was published in *JCI Insight* by the American Society for Clinical Investigation<sup>34</sup>. The CC-BY license permits use, distribution, and reproduction in any medium, provided the original work is properly cited and allows the commercial use of published articles.

### **Introduction**

#### *Bacterial Skin Infections*

Bacterial skin and soft tissue infections (SSTIs) have long been known as one of the most frequently encountered types of infections in both hospital and ambulatory settings, occurring at an incidence rate of 48.5 infections per 1000 patients-years in 2009, vastly outpacing other common bacterial infections like urinary tract infections or pneumonia<sup>46</sup>. However, it has only been in recent years that the rate of SSTIs have been found to be steadily increasing, rising nearly 40% between 2000 and 2012<sup>47</sup>. This rise in SSTIs has primarily been linked to the gram-positive *S. aureus* (catalase-positive), with the incidence of *S. aureus* SSTIs in the United States doubling from 57 to 117 cases per 100,000 people between 2001 and 2009 and exerting an annual economic cost of \$4.5 billion by 2010<sup>48,49</sup>. Antibiotic-resistant MRSA significantly contributes to these rising statistics, as the percentage of *S. aureus* isolates identified as MRSA increased from 13% in 1998 to 48% in 2009<sup>50</sup>. While *S. aureus* strains like MRSA remains among the most common sources of SSTIs, other pathogens like *P. aeruginosa* and *E. coli* have been

identified as the second and third most prevalent isolated species found in SSTIs across North America, Latin America, and Europe<sup>51</sup>. Similar to *S. aureus* and MRSA, antibiotic resistance has been found in both these bacterial species, with *E. coli* isolates displaying resistance to ampicillin, tetracycline, and fluoroquinolones while *P. aeruginosa* has been known to be naturally resistant to several common antibiotics and has been found to be capable of developing multi-drug or even pan-drug resistance<sup>52,53</sup>. With the heavy presence of antibiotic resistance observed among several bacterial pathogens found within skin infections, identifying novel methods to treat these skin infections less reliant on heavy antibiotic usage are sorely needed. Even today, the most common method of treating SSTIs remains the systematic delivery of broad-spectrum antibiotics through oral or intravenous methods, increasing the risk of potential resistance development and a less efficient delivery method compared to localized topical delivery<sup>54,55</sup>. Alternatively, finding methods to boost the immune system's ability to eradicate pathogens can provide another more natural method of eradicating pathogens from wounds without needing to significantly rely on traditional antibiotics<sup>56</sup>.

#### *Current Knowledge on the Effects of Antimicrobial Blue Light on Bacteria*

While the antimicrobial nature of visible light has been known for years, it is only within the past few years that the mechanisms responsible for the phenomenon have been seriously investigated. Prior studies have revealed how medically relevant nosocomial bacterial pathogens such as *P. aeruginosa* or *A. baumannii* could be inactivated following exposure to blue light<sup>57,58</sup>. Further studies have gone on to reveal how antimicrobial blue light (aBL) is also capable of inactivating periodontal, foodborne, waterborne, plant,

veterinary, and viral pathogens<sup>28</sup>. While the effectiveness of aBL has been confirmed to be dependent on a variety of factors, including the growth phase and environmental conditions, the precise mechanism responsible for the antimicrobial phenomenon of blue light remains understudied. Studies have indicated that blue light can disrupt the membrane integrity and affect membrane potential of pathogens<sup>59</sup>. However, the most common theory explaining the mechanism of aBL is from DNA damage induced by oxidative stress. Blue light is believed to excite natural endogenous porphyrins and flavins within microbial cells, resulting in the production of toxic ROS<sup>57,58,60</sup>. Some studies have explicitly attributed the endogenous coproporphyrin, a protoporphyrin IX precursor, to be the primary compound responsible for ROS production<sup>61</sup>. However, studies performed on both blue light susceptible and blue light resistant *Salmonella* strains have indicated no significant difference in the amount of endogenous coproporphyrin expressed between strains<sup>62</sup>, indicating the presence of porphyrin may not be the key factor responsible in the antimicrobial activity of blue light.

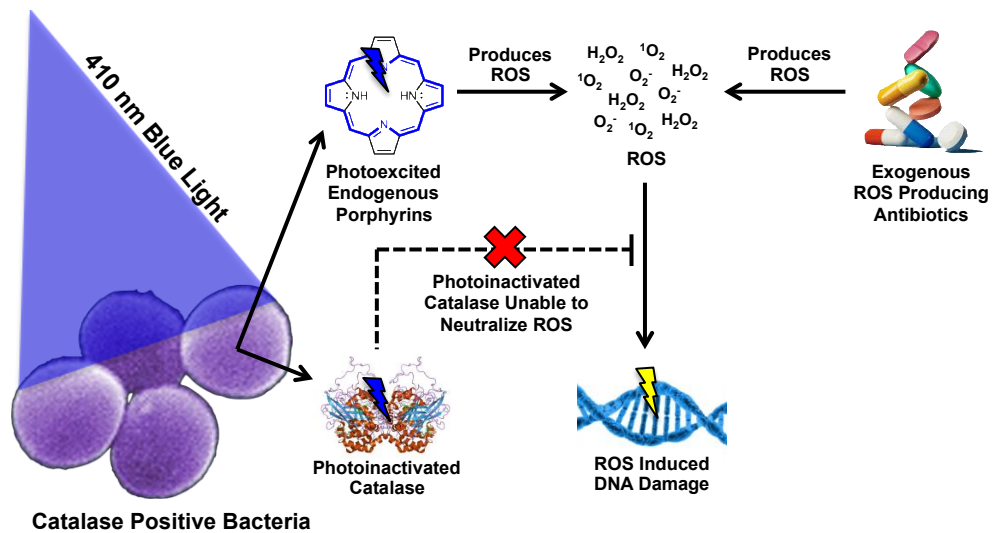


**Figure 2: Potential Contribution of Catalase to Antimicrobial Blue Light Activity.** As blue light is known to photoexcite endogenous porphyrins to produce toxic ROS, it is possible

**that the inactivation of catalase by blue light prevents the neutralization of ROS. This allows for both ROS formed by endogenous porphyrin excitation and ROS generated by exogenous sources to induced oxidative damage.**

This lack of clarity regarding how aBL impacts cell behavior hinders the potential widespread adoption of this technology for medical use and indicates that further knowledge into effects of aBL are sorely needed. The discovery that blue light can deactivate bacterial catalase may prove key in better understanding the specific mechanisms at work within the phenomenon. It is possible that the deactivation of antioxidants like catalase may increase bacterial sensitivity to the ROS produced by photoexcited endogenous porphyrins, therefore indicating that antioxidants molecules act as a key obstacle to the antimicrobial activity of blue light (**Figure 2**). This deactivation of catalase would also likely contribute to increased bacterial sensitivity to exogenous ROS sources like H<sub>2</sub>O<sub>2</sub>. Exploring the role of catalase and catalase deactivation in aBL, as well as how this modulates interactions with antimicrobial agents can generate improved understanding and clarity into aBL mechanisms, paving the way for future developments and innovations into its possible clinical applicability.

#### *Antimicrobial Blue Light Deactivates Bacterial Catalase*

Based on the ability for blue light to deactivate isolated bovine liver catalase, further investigation into the catalase deactivating capabilities of blue light discovered that aBL was able to inactivate the catalase present within bacteria, reducing catalase activity by over 60% in MRSA (**Figure 3a**) and 30% in *P. aeruginosa* (**Figure 3b**) in response to 15 J/cm<sup>2</sup> of 410 to 420 nm of nanosecond pulsed blue light.

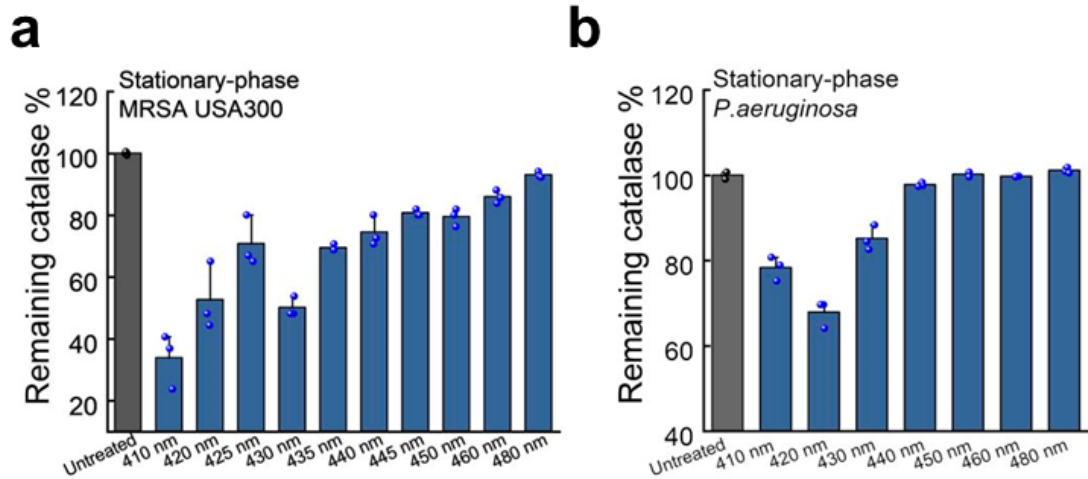


**Figure 3: Antimicrobial Blue Light Deactivates Active Catalase within Bacteria.** Under 15 J/cm<sup>2</sup> of blue light, 410 to 420 nm light significantly reduces the catalase activity found within both stationary phase a) MRSA and b) *P. aeruginosa*. Data published in Dong *et al.*, *JCI Insight.*, 2022.<sup>34</sup>

While these studies reveal that bacterial catalase can be deactivated by 410 to 420 nm blue light, it does little to confirm if the deactivation of bacterial catalase has a significant effect on the bacterial antioxidant defenses, given the high turnover efficiency of catalase and the fact that not all active catalase within bacteria appeared to be inactivated following light exposure. In addition, other antioxidant enzymes present within the bacteria, such as alkyl hydroperoxide reductase in *E. coli*, which is responsible for the neutralization of endogenously produced ROS formed within the bacterium<sup>63</sup>, would also potentially significantly contribute to ROS defenses. Additional investigation is also needed to see if catalase deactivation can synergize with more indirect sources of ROS. This includes sources like the ROS burst produced by host immune cells, or the ROS produced by conventional and common antibiotics like aminoglycosides or quinolones as part of their mechanism of action, which can help demonstrate the potential translatability of the technology<sup>64,65</sup>. Furthermore, by investigating the effects of ROS

producing antimicrobials on skin infections through animal models, it will be possible to determine the impact that blue light induced catalase deactivation has on the treatment of drug resistant infections within infected skin wounds and provide an important first step in demonstrating the translatability of this technology to actual clinical settings.

## **Methods and Materials**

### *Blue Light Source*

For nanosecond (ns) pulsed light, a tunable short pulsed Opolette HE 355 laser (OPOTEK) was used to apply light. This laser source applied light at a repetition rate of 20 Hz and a pulsed width of ~5 ns. Using a collimator and an optic fiber, the diameter of the beam was expanded to cover a 1 cm<sup>2</sup> area. Under these conditions, nanosecond pulsed light was primarily applied at power outputs between 35 to 50 mW/cm<sup>2</sup>. Future references to nanosecond pulsed blue light will be referred to as “ns-410”.

For continuous wave (CW) light, a mounted 405 nm LED (M405L4, ThorLabs) was attached to a modifiable collimation adapter (SM2F32-A, ThorLabs) and adjusted to focus the fluence region to a ~1 cm square area. Fluence was controlled through a T-Cube LED driver (LEDD1B, ThorLabs), allowing for a wide range of blue light power outputs between 0 and 400 mW/cm<sup>2</sup>. To follow the nanosecond pulsed light’s naming convention, future references to continuous wave 405 nm light will be referred to as “CW-410”.

### *Bacterial Strains and Cell Lines*

Wild type *E. coli* (MG1655) and its  $\Delta katGE$  and  $\Delta katGEahpCF$  (LC106) mutants were provided by Dr. James Imlay of the University of Illinois Urbana-Champaign in Urbana, Illinois, USA. Wild type *E. coli* (BW25113) and its *E. coli* mutants ( $\Delta ahpC$ ,  $\Delta katG$ ,  $\Delta katE$ ,  $\Delta katGE$ ) were obtained through Dr. Xilin Zhao of Rutgers University in New Brunswick, New Jersey, USA. *E. coli* (BW25113), MRSA (USA300), *P. aeruginosa* PAO-1 (ATCC 47085), *S. enterica* 2 (ATCC 700720), *S. enterica* 3 (ATCC 13076), *A. baumannii* 2 (ATCC BAA-747), and *E. faecalis* 1 (NR-31970) were obtained through Dr. Mohamed N. Seleem of Virginia Tech University in Blacksburg, Virginia, USA. Cell lines used in this study, such as the Chinese Hamster Ovary (CHO) cells and RAW 264.7 murine macrophages, were purchased directly from the ATCC.

### *Bacterial Preparation and Blue Light Treatment*

Bacterial samples were prepared first by incubating bacteria strains within TSB overnight within an overnight shaker at 37°C and 250 RPM. Bacteria was then centrifuged and resuspended in 1x PBS to an OD600 of 1.0. Following preparation, 10  $\mu$ L aliquots of suspension was placed on a glass coverslip and treated with varying dosages of either continuous wave (CW-410) or nanosecond pulsed blue light at wavelengths between 410 nm and 480 nm. Immediately after light exposure, treated aliquots were diluted with either 990  $\mu$ L of PBS or 990  $\mu$ L of PBS supplemented with various concentrations of H<sub>2</sub>O<sub>2</sub>. Samples were then incubated for up to 30 minutes before being serially diluted in a 96 well plate and then plated on agar plate for CFU counting. For time kill assays, *E. coli* BW25115 and its mutants ( $\Delta ahpC$ ,  $\Delta katG$ ,  $\Delta katE$ ,  $\Delta katGE$ )

were incubated for 2 hours, with 60  $\mu\text{L}$  aliquots of incubated sample removed at the 20-minute, 40-minute, 1-hour, 1.5-hour, and 2-hour time points for serial dilution and agar plating.

#### *ROS Measurement*

A hydroxyl radical and peroxyxynitrite sensor (HPF) dye (H36004, ThermoFisher Scientific) was used to measure ROS presence within light treated bacteria. Overnight cultured *E. Coli* MG1655 and its mutants ( $\Delta katGE$  and  $\Delta katGEahpCF$ ) were resuspended in PBS to an OD600 of 1.0. From here, a 10  $\mu\text{L}$  aliquot was treated to up to 30 or 60  $\text{J}/\text{cm}^2$  of CW-410 (250  $\text{mW}/\text{cm}^2$ ). Immediately following light exposure, the sample was diluted in 40  $\mu\text{L}$  of PBS and then combined with 200  $\mu\text{L}$  of 5  $\mu\text{M}$  HPF solution, generating a final HPF concentration of 4  $\mu\text{M}$ . This sample was then allowed to incubate at 37°C for 45 minutes, before 75  $\mu\text{L}$  of HPF suspension was transferred to a 96-well plate and fluorescence ( $n = 3$ ) was quantified at an excitation/emission setting of 485/520 nm.

#### *Bacterial Transformation and Catalase Rescue*

An *E. Coli* DH5 $\alpha$  strain containing an arabinose regulated pBAD-HPII (katE catalase) plasmid (AddGene, 105839) was used alongside a GeneJET Plasmid Miniprep Kit (ThermoFisher Scientific, K0503) to isolate the catalase expressing plasmid. Using a TransformAid Bacterial Transformation Kit (ThermoFisher Scientific, K2711), the pBAD-HPII plasmid was inserted into the catalase knockout mutant *E. Coli*  $\Delta katGE$ , transforming the strain into the catalase rescue strain *E. Coli*  $\Delta katGE:pBad\_katE$ . From

here, both wild type *E. Coli* (BW25113) and *E. Coli*  $\Delta katGE:pBad\_katE$  were cultured at 37°C to log phase and then resuspended in PBS. A 10 uL droplet was treated to CW-410 (30 J/cm<sup>2</sup>), diluted within M9 minimal media containing 1% arabinose, and then incubated for 4 hours at 37°C. After incubation, the incubated sample was exposed to 2.2 mM of H<sub>2</sub>O<sub>2</sub> for 30 minutes before the sample as serially diluted and plated. The resulting CFU results were used to compare the phenotypic response.

#### *Iron Chelator Application*

To determine if the iron present within deactivated catalase contributed to increased ROS sensitization following blue light exposure, light treated stationary phase *E. coli* was treated to the iron chelators deferoxamine (D9533, Sigma Aldrich) or 2,2, Bipyridyl (D216305, Sigma Aldrich). *E. coli* BW25113 was prepared as previously described above and a 20  $\mu$ L aliquot was treated to 30 J/cm<sup>2</sup> of CW-410. After exposure, aliquots were diluted within 1980  $\mu$ L of PBS and incubated alongside 2 mM of either Fe<sup>3+</sup> binding deferoxamine or Fe<sup>2+</sup> binding 2,2, bipyridyl for 30 minutes at 37°C. After chelator incubation, 2.2 mM of H<sub>2</sub>O<sub>2</sub> was added to samples and incubated for 30 minutes at 37°C before samples were diluted and plated on agar plates for CFU counting.

#### *Antibiotic Treatment of Light Treated Bacteria*

For each antibiotic tested, bacteria were usually precultured in antibiotics prior to light exposure and subsequent incubation. For each bacterial strain tested, strains were cultured overnight in TSB. After culturing, 1 mL of bacteria solution was centrifuged and resuspended in 1 mL of fresh TSB media supplemented with either 10  $\mu$ g/mL of

tobramycin (T4014, Sigma Aldrich) or 0.1 µg/mL of ciprofloxacin (17850, Sigma Aldrich). After preculturing was complete, the preculture solution was centrifuged and resuspended in PBS. A 10 µL suspension droplet was then treated to 18 J/cm<sup>2</sup> of ns-410. The treated aliquot was then diluted in 990 µL of TSB alongside either 2 µg/mL of tobramycin or 0.1 µg/mL of ciprofloxacin and incubated at 37°C for up to 6 hours.

#### *Catalase Deactivation of Bacteria-Macrophage Co-Culture*

RAW 264.7 macrophages were resuspended in DMEM and placed in a 96 well plate at a concentration of  $5 \times 10^5$  cells per well. Following overnight incubation and adherence, macrophage media was replaced with fresh DMEM. Log phase *P. aeruginosa* PAO-1 was prepared and resuspended in PBS to an OD<sub>600</sub> of 1.25, and a 10 µL bacterial aliquot containing  $1 \times 10^7$  cells was added to each macrophage containing well and allowed to naturally incubate and undergo phagocytosis at 37°C for 1 hour, creating a multiplicity of infection (MOI) of 20. After phagocytosis, media was replaced with DMEM supplemented with 10% FBS and 50 µg/mL gentamicin and then incubated for an additional hour to kill extracellular bacteria. After incubation, the media was removed, and cells were washed twice with PBS before being treated to CW-410 (60 J/cm<sup>2</sup>). The remaining PBS was then removed, replaced with DMEM with 10% FBS, and then incubated for 3 hours at 37°C. Once the 3-hour incubation was complete, the cells were once again washed with PBS, treated to CW-410 (60 J/cm<sup>2</sup>), and then incubated in DMEM supplemented with 10% FBS for 6 hours. Following the final 6 hour incubation, cells were washed with DMEM containing 50 µg/mL gentamicin and lysed with 0.1%

Triton X. Lysed macrophage cells were then serially diluted and plated on agar plates. CFU enumeration was used to quantify the killing efficiency of macrophages.

To determine if it was the ROS burst produced by macrophages responsible for the enhanced killing efficiency of macrophages, macrophages within a 96 well plate were once again prepared as previously described. Following overnight incubation, macrophage media was replaced with fresh DMEM containing 20  $\mu\text{M}$  of diphenyleneiodonium chloride (Sigma Aldrich, D2926), or DPI, a known inhibitor of the NOX enzymes responsible for the ROS burst in macrophages. Following 1 hour of DPI pre-incubation, a 10  $\mu\text{L}$  aliquot containing  $1 \times 10^7$  log phase *P. aeruginosa* PAO-1 was treated with CW-410 (60  $\text{J}/\text{cm}^2$ ) and added to the macrophage wells (MOI = 20). Following 2 hours of incubation under 37°C, the macrophages were washed with PBS and then incubated for 1 hour in DMEM with 10% FBS and 200  $\mu\text{g}/\text{mL}$  gentamicin. After incubation, the media was removed, washed with PBS, lysed with 0.1% Triton-X, serially diluted, and then plated on agar plates.

For ROS measurements of macrophages treated with light treated bacteria, RAW 264.7 macrophages were prepared in a 96 well plate in the process previously described. After overnight incubation and adherence, log phase PAO-1 was prepared and resuspended in PBS to an OD600 of 1.25. A 50  $\mu\text{L}$  aliquot was treated with CW-410 (60  $\text{J}/\text{cm}^2$ ) and mixed with 950  $\mu\text{L}$  of pre-warmed DMEM, creating a bacterial concentration of  $5 \times 10^7$  CFU/mL. Old DMEM media was then removed from macrophage media and then replaced with 200  $\mu\text{L}$  of bacterial suspension ( $\sim 1 \times 10^7$  CFU), generating a MOI of

20. Macrophages were incubated in the bacteria infected DMEM for 1 hour at 37°C and then incubated in DMEM with 10% FBS and 50 µg/mL gentamicin for another hour to kill extracellular bacteria. Following incubation, macrophages were washed with pre-warmed PBS and each well was treated to 100 µL of an Intracellular H<sub>2</sub>O<sub>2</sub> Assay Kit (Sigma Aldrich, MAK164) for 1 hour at 37°C. After probe incubation, the cells were washed, and the media was replaced with 100 µL of PBS. The resulting fluorescence was measured using a plate reader at an excitation wavelength of 490 nm and an emission wavelength of 525 nm.

#### *Mammalian Cell Toxicity*

To assess the potential toxicity of 410 nm blue light against RAW 264.67 macrophages or CHO cells, an MTT assay was used to measure the change in viability in response to light treatment. Cells were cultured in DMEM with 10% FBS to a 90% confluence. Once cells had reached a high enough confluence, cells were detached via trypsin, counted, and diluted in DMEM to a concentration of  $1 \times 10^6$  cells/mL. 100 µL of suspension was then transferred to a 96-well plate, applying  $1 \times 10^5$  cells per well. An additional 100 µL of DMEM was added to each well before the plate was incubated overnight at 37°C and 5% CO<sub>2</sub> to allow cells to attach to the bottom of the wells. The next day, DMEM was removed and replaced with pre-warmed PBS before being treated to 75 J/cm<sup>2</sup> of CW-410 (250 mW/cm<sup>2</sup>). For the H<sub>2</sub>O<sub>2</sub> treatment, 0.1% H<sub>2</sub>O<sub>2</sub> resuspended in DMEM was added to the H<sub>2</sub>O<sub>2</sub> treatment groups for 1 minute. After treatment, H<sub>2</sub>O<sub>2</sub> containing media was removed and all wells, including the non-H<sub>2</sub>O<sub>2</sub> treated groups,

were washed twice with PBS to remove all traces of the ROS source and maintain experimental consistency. After treatment, the PBS was removed and replaced with fresh, pre-warmed DMEM and allowed to incubate overnight at 37°C and 5% CO<sub>2</sub> to allow for stress recovery. The following day, a cell viability assay was performed based on established protocols utilizing MTT (M6494; Life Technologies). The resulting MTT absorbance values were quantified through a plate reader at 590 nm. Groups were treated in replicates of n = 4.

#### *In Vivo Bacterial Infection Murine Model*

Twenty 6–7-week-old, female, BALB/c mice (Jackson Laboratories, 000651) were anesthetized via isoflurane and abrasion wound was formed by scrapping a #15 sterile scalpel against the skin. A 10 µL aliquot containing 10<sup>8</sup> CFU of log-phase *P. aeruginosa* PAO-1 was directly applied and evenly spread across the wound with the pipette tip. After application, the mice were returned to their cages for 30 to 60 minutes to allow the mice to recover from the surgery and to allow for the bacteria infection to properly establish. The mice were then divided into 4 groups: Untreated, CW-410 Treated, H<sub>2</sub>O<sub>2</sub> treated, and CW-410 with H<sub>2</sub>O<sub>2</sub> treated, each group consisting of 5 mice (n = 5). CW-410 was applied by placing infected wounds below the 200 mW/cm<sup>2</sup> (In line with ANSI standards) CW-410 light source and treated wounds to a total of 120 J/cm<sup>2</sup>. H<sub>2</sub>O<sub>2</sub> treatment consisted of applying a 10 µL droplet of 0.5% H<sub>2</sub>O<sub>2</sub> onto the wound and evenly spreading the droplet across the wound. The H<sub>2</sub>O<sub>2</sub> was allowed to naturally dry. Combination treatment consisted of the application of blue light treatment immediately followed by the H<sub>2</sub>O<sub>2</sub> treatment. Mice were treated twice over a 15-hour time span.

Treatment was applied 3 and 15 hours after initial infection. 1 hour after the second treatment, the mice were euthanized and the infected tissue was surgically removed, homogenized, and serially diluted in 2 mL of PBS. CFU measurements were conducted on *P. aeruginosa*-specific ceftrimide agar plates (22470, Sigma Aldrich).

The potential phototoxicity of this light treatment on healthy skin was quantified by applying the same two time light and H<sub>2</sub>O<sub>2</sub> treatment on non-wounded regions of the skin of the combination treated mice. During the wound collection, this skin region was surgically removed and fixed in 10% buffered formalin alongside intact healthy skin samples from untreated mice. Formalin-fixed samples were processed by the Boston University Experimental Pathology Laboratory Service Core for H&E staining. The resulting histology slides were visualized by a microscope under a 60× objective.

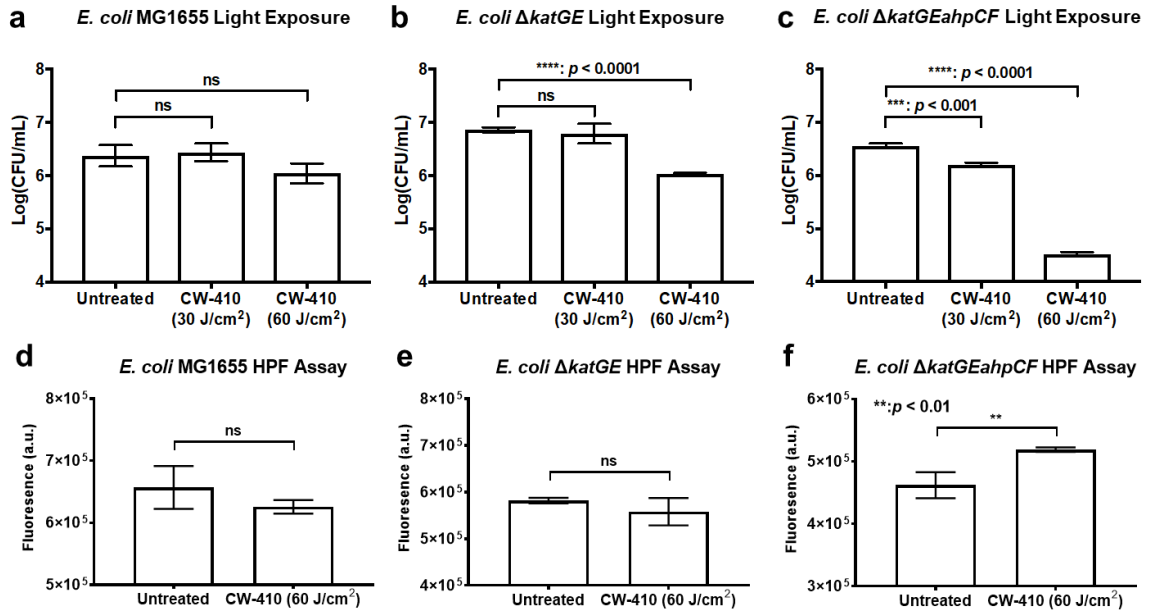
#### *Statistical Analysis*

Statistical analysis was conducted via Student's 2-tailed unpaired *t* test (2 groups) and 1-way ANOVA (3 or more groups). Significance was set at *P*-values < 0.05.

#### *Study Approval*

Mouse abrasion model experimentation was approved by the Boston University Animal Care and Use Committee and was in accordance with NIH guidelines.

## Results

*Antioxidant Enzyme Removal and Blue Light Antimicrobial Activity*

**Figure 4: CFU and ROS of Light Treated *E. coli* Mutants.** CFU measurements of a) wild type *E. coli* MG1655, b) catalase deficient *E. coli*  $\Delta katGE$ , and c) catalase and alkyl hydroperoxide reductase negative *E. coli*  $\Delta katGEahpCF$  in response to 30 to 60 J/cm<sup>2</sup> of CW-410 (250 mW/cm<sup>2</sup>). *E. coli*  $\Delta katGEahpCF$  experienced the greatest reduction in CFU. Measurements of ROS through HPF fluorescence of 60 J/cm<sup>2</sup> treated d) wild type *E. coli*, e)  $\Delta katGE$  mutant, and f)  $\Delta katGEahpCF$  reveal only the  $\Delta katGEahpCF$  mutant was found to exhibit higher ROS levels following light exposure. \*\*\*\*:  $p < 0.0001$ , \*\*\*:  $p < 0.001$ , \*\*:  $p < 0.01$ , ns = No Significance.

The impact of blue light alone on the viability of bacteria was primarily tested through the model bacterium *E. coli*. *E. coli* is understood to express two different types of catalase under the genes *katG* and *katE*<sup>66</sup>. In addition to these two catalases, *E. coli* also expresses the alkyl hydroperoxide reductase *ahpCF* that is primarily responsible for neutralizing endogenously produced ROS<sup>63</sup>. To evaluate the impact of these antioxidant enzymes on the antimicrobial activity of blue light, CFU measurements were performed on wild type *E. coli* (MG1655), its double catalase removed mutant  $\Delta katGE$ , and its

catalase and alkyl hydroperoxide reductase removed mutant *ΔkatGEahpCF*. After 30 to 60 J/cm<sup>2</sup> of CW-410 (250 mW/cm<sup>2</sup>) exposure, wild type *E. coli* experienced no change in CFU population (**Figure 4a**), the catalase deficient *E. coli ΔkatGE* experienced a 1-log reduction in CFU after 60 J/cm<sup>2</sup> of CW-410 (**Figure 4b**), and the CFU of catalase and reductase deficient *E. coli ΔkatGEahpCF* was reduced by 0.5-log and 2-log in response to 30 and 60 J/cm<sup>2</sup> of CW-410 respectively (**Figure 4c**). The increased sensitivity to aBL alone under the *ΔkatGE* and *ΔkatGEahpCF* confirms that antioxidant molecules provide resistance to any ROS naturally produced by blue light alone.

Based on the lower tolerance of the catalase and reductase mutants to blue light alone, the ROS present within the bacteria immediately after exposure was used to obtain a rough estimate of potential changes in ROS levels within the cell population. After 60 J/cm<sup>2</sup> of CW-410 exposure, there was no significant difference in HPF fluorescence levels between the wild type *E. coli* MG1655 (**Figure 4d**) and the *ΔkatGE* mutant (**Figure 4e**) detected. However, the fluorescence of light treated *ΔkatGEahpCF* increased significantly following light treatment (**Figure 4f**), indicating increased presence of ROS present within the catalase and reductase deficient mutant strain. The increased detected ROS levels indicates that the accumulation of ROS solely from light exposure requires the removal or absence of antioxidant molecules, and the presence of these enzymes actively suppresses the killing efficiency of blue light alone.

*Catalase Photodeactivation Sensitizes Bacteria to Exogenous H<sub>2</sub>O<sub>2</sub>*

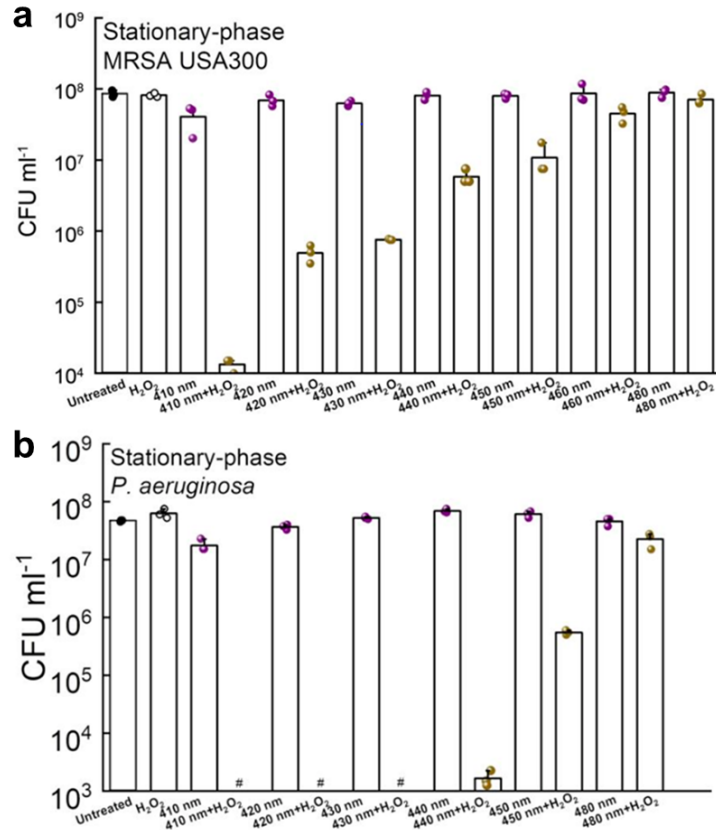


**Figure 5: Catalase Photodeactivation Sensitizes Bacteria to Exogenous H<sub>2</sub>O<sub>2</sub>.** When combined with 22 mM of H<sub>2</sub>O<sub>2</sub>, 15 J/cm<sup>2</sup> of 410 nm light resulted in a a) near 4-log reduction in CFU for MRSA and b) complete eradication of *P. aeruginosa* following 30 minutes of incubation. Data published in Dong et al., *JCI Insight.*, 2022.<sup>34</sup>

To determine if catalase photodeactivation had an impact on the sensitivity of bacteria to exogenous ROS sources, gram-positive and gram-negative bacterial strains were treated to a wide variety of different blue light wavelengths followed by incubation within 22 mM of H<sub>2</sub>O<sub>2</sub> for 30 minutes. When combined with a direct exogenous ROS source like H<sub>2</sub>O<sub>2</sub>, blue light was found to significantly enhance the antimicrobial activity of H<sub>2</sub>O<sub>2</sub>, reducing the quantity of colony-forming units of MRSA by as much as 4-log (**Figure 5a**) and resulting in the complete eradication of *P. aeruginosa* (**Figure 5b**).

Between MRSA and *P. aeruginosa*, 410 nm blue light exhibited the greatest ROS

sensitization among the various wavelengths tested, although *P. aeruginosa* ROS sensitization was found to occur in a wide variety of blue light wavelengths. The wavelengths able to induce the greatest increase in H<sub>2</sub>O<sub>2</sub> efficiency was also found to correlate with the wavelengths able to induce the greatest decrease in catalase activity, with 410 to 420 nm exhibiting the greatest bacterial catalase inactivation and ROS sensitization while 480 nm light exhibited no effect on either bacterial catalase deactivation or bacterial ROS sensitization. This correlation between catalase inactivation and ROS sensitization therefore points to catalase as a primary target of blue light.

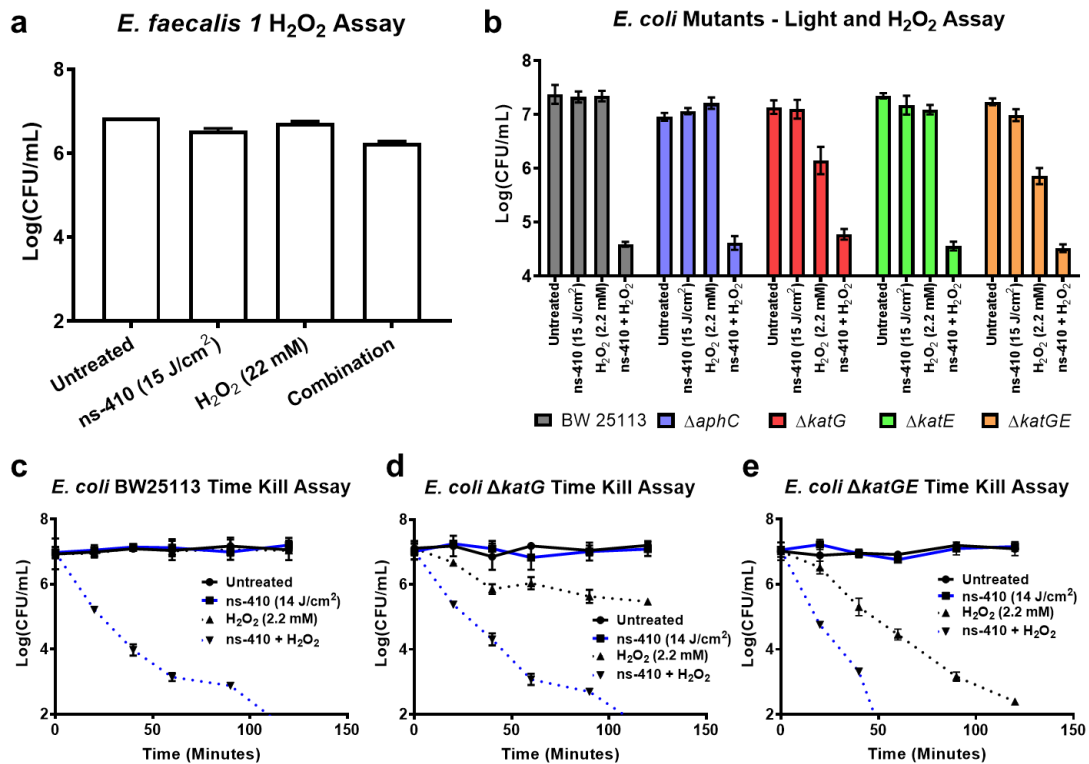


**Figure 6: Impact of Blue Light on Catalase Deficient Bacteria.** a) CFU measurements of catalase negative *E. faecalis* found light to have no effect on H<sub>2</sub>O<sub>2</sub> activity. b) CFU measurements of *E. coli* BW25113 and its catalase deficient mutants (*AahpC*, *AtatG*, *AtatE*, *AtatGE*) revealed that the catalase encoded by *katG* significant contributes to H<sub>2</sub>O<sub>2</sub> defense. Time killing curves of c) wild type *E. coli* BW25113, d) *E. coli* *AtatG*, and *E. coli* *AtatGE*. Samples all treated to ns-410. Data adapted from Dong et al., *JCI Insight.*, 2022.<sup>34</sup>

While these results indicate the ability for blue light to sensitize bacteria to H<sub>2</sub>O<sub>2</sub>, further evidence is needed to confirm the internal deactivation of catalase as the primary driver of this ROS sensitizing phenomenon. To better investigate the role of catalase in light induced ROS sensitization, the catalase negative bacterial strain *E. faecalis* was treated with 15 J/cm<sup>2</sup> of 410 nm light and incubated within 22 mM of H<sub>2</sub>O<sub>2</sub> for 30 minutes. CFU results of the treatment found the combination treatment to reduce the CFU of the light treated bacteria by less than 0.5-log, failing to show the improved H<sub>2</sub>O<sub>2</sub> activity observed in the catalase positive strains (**Figure 6a**).

In addition to testing catalase deficient bacterial strains, the impact of blue light on a variety of *E. coli* antioxidant mutants was evaluated. A treatment of 15 J/cm<sup>2</sup> of ns-410 and 2.2 mM H<sub>2</sub>O<sub>2</sub> was performed on *E. coli* BW25113, its single catalase knockout mutants  $\Delta katG$  and  $\Delta katE$ , its double catalase knockout mutant  $\Delta katGE$ , and its alkyl hydroperoxide reductase knockout mutant  $\Delta ahpC$ . (**Figure 6b**) From the CFU measurements, the wild type,  $\Delta ahpC$ , and  $\Delta katE$  strains behaved identically, all expressing a roughly 2.5-log reduction in CFU from the combination treatment with minimal responses from the individual treatments. While both  $\Delta katG$  and  $\Delta katGE$  expressed similar 2.5-log reductions under combination treatment, they were also found to be significantly more sensitive to H<sub>2</sub>O<sub>2</sub> alone, experiencing a roughly 1-log reduction.

The effects of blue light on these two mutants ( $\Delta katG$  and  $\Delta katGE$ ) were examined in more detail through a time kill assay alongside the wild type. After two hours, complete eradication of the wild type *E. coli* BW25113 was observed in the ns-410 and H<sub>2</sub>O<sub>2</sub> treated group while individual treatments had no impact on viability whatsoever

(**Figure 6c**). Catalase-deficient *E. coli*  $\Delta katG$  and *E. coli*  $\Delta katGE$  were much more sensitive to H<sub>2</sub>O<sub>2</sub> than the wild type strain (**Figure 6d and 6e**). In addition, the time kill curve exhibited by *E. coli*  $\Delta katGE$  under H<sub>2</sub>O<sub>2</sub> demonstrated similarities to the wild-type *E. coli* BW25113 exposed to ns-410 plus H<sub>2</sub>O<sub>2</sub>, indicating that it was catalase was indeed the primary target of 410 nm light. However, the observation of more effective killing of the double catalase knockout mutant by the combination treatment than the H<sub>2</sub>O<sub>2</sub> treatment alone indicates that catalase may not be the only antioxidant molecule photosensitive to 410 nm light.

To fully confirm the catalase deactivation hypothesis, a catalase rescue experiment was performed using the catalase deficient *E. coli*  $\Delta katGE$  transformed with a pBad-HPII plasmid to form the rescue strain *E. coli*  $\Delta katGE:pBad\_katE$ . Under this rescue strain, the expression of catalase could be promoted by the presence of arabinose. Following creation of this rescue strain, both wild type *E. coli* BW25113 and the rescue strain were cultured to log phase and then treated to 30 J/cm<sup>2</sup> of 410 nm blue light. After exposure, the bacteria were incubated within M9 media supplemented with 1% arabinose for 4 hours at 37°C to allow time for catalase expression. After incubation, bacterial suspensions were treated to 2.2 mM of H<sub>2</sub>O<sub>2</sub> for 30 minutes before the CFU was quantified.

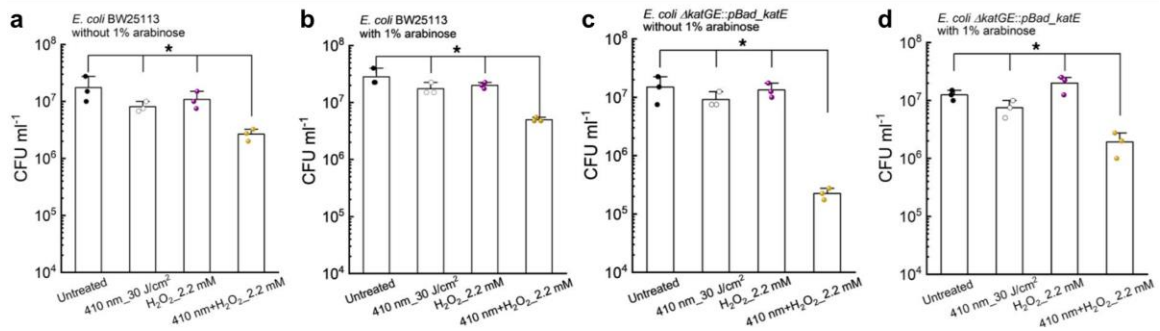


**Figure 7: Catalase Rescue Salvages Light Treated *E. coli* from ROS Sensitivity.** CFU/mL of blue light treated a-b) wild type *E. coli* BW25113 or the c-d) *E. coli*  $\Delta katGE:pBad\_katE$  rescue strain incubated in 2.2 mM of H<sub>2</sub>O<sub>2</sub> for 30 minutes following a 4 hour incubation in the absence or presence of 1% arabinose in M9 media for 4 hours. Arabinose incubation has no effect on wild type activity, while the presence of arabinose and subsequent catalase expression significantly provides significant defense to the combined effects of blue light and H<sub>2</sub>O<sub>2</sub>. \*:  $p < 0.05$ . Data published in Dong et al., *JCI Insight.*, 2022.<sup>34</sup>

As expected, arabinose had no observable impact on the CFU reducing effects of combination treatment on the wild type *E. coli* BW25113 (**Figure 7a and 7b**). For the *E. coli*  $\Delta katGE:pBad\_katE$  rescue strain incubated alongside arabinose, a 1-log CFU/mL reduction in the combination treatment was observed (**Figure 7c**), while the rescue strain without arabinose expressed a higher 2-log CFU/mL reduction (**Figure 7d**), indicating that catalase gene salvaging can rescue catalase deficient *E. coli*  $\Delta katGE$  from H<sub>2</sub>O<sub>2</sub> induced oxidative stress, and further suggests that catalase is the primary target of 410 nm antimicrobial blue light.

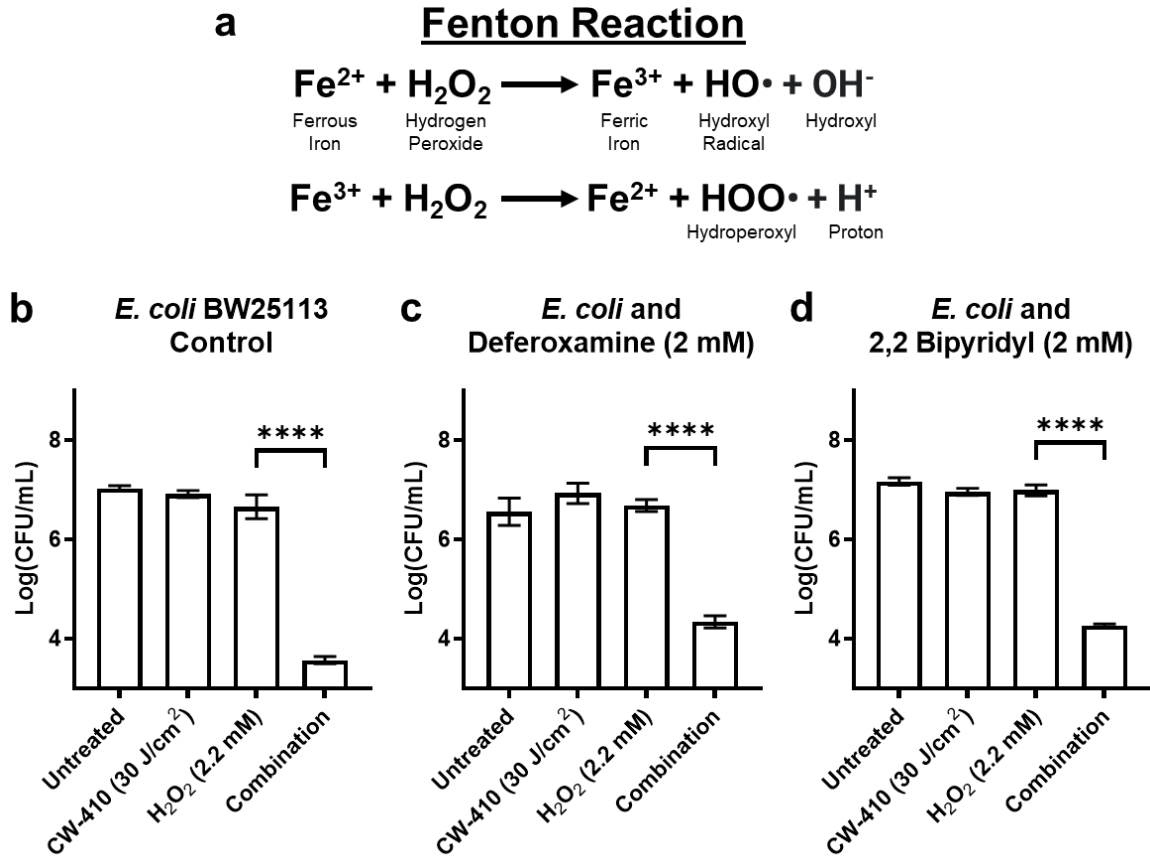


**Figure 8: Effects of Iron Chelators on Catalase Photodeactivation.** a) By reacting with ferrous and ferric iron ions,  $\text{H}_2\text{O}_2$  exerts its toxic effects by further propagating formation of additional ROS sources in what is known as the Fenton Reaction. CFU measurements of *E. coli* BW25113 treated with  $30 \text{ J/cm}^2$  of CW-410 ( $200 \text{ mW/cm}^2$ , 2.5 minutes) and  $2.2 \text{ mM}$  of  $\text{H}_2\text{O}_2$  in the b) absence of iron chelators, c) the presence of deferoxamine, or d) the presence of 2,2 bipyridyl reveal the presence of chelators has an only minor effect on light induced ROS sensitization. \*\*\*\*:  $p < 0.0001$ .

While the blue light induced deactivation of catalase was clearly observed based on catalase activity measurements, one question regarding the impact of the presence of the deactivated catalase within the bacteria remained in terms of the potential availability of free iron from the deactivated catalase possibly contributing to increased ROS sensitization by acting as a source of iron for use in the Fenton reaction, where iron ions like  $\text{Fe}^{3+}$  or  $\text{Fe}^{2+}$  and  $\text{H}_2\text{O}_2$  react together to form additional ROS molecules like hydroxide ( $\text{OH}^-$ ) and hydroxyl radicals (**Figure 8a**). To investigate this, iron chelators

were incubated with light treated *E. coli* before being treated with 2.2 mM of H<sub>2</sub>O<sub>2</sub>. Untreated *E. coli* was found to experience a 3.5-log reduction in CFU/mL under combination treatment in line with previous results (**Figure 8b**). Combination treatment of *E. coli* in the presence of Fe<sup>3+</sup> binding deferoxamine (**Figure 8c**) or Fe<sup>2+</sup> binding 2,2, bipyridyl (**Figure 8d**) resulted in a 2.5 to 3-log reduction in CFU/mL, at most reducing the effectiveness of combination treatment by 1-log. The minimal of effect of iron chelators indicates that the free iron present within the environment following light and H<sub>2</sub>O<sub>2</sub> treatment does not significantly contribute to the enhanced ROS sensitization.

### Catalase Deactivation and Antibiotic Potentiation

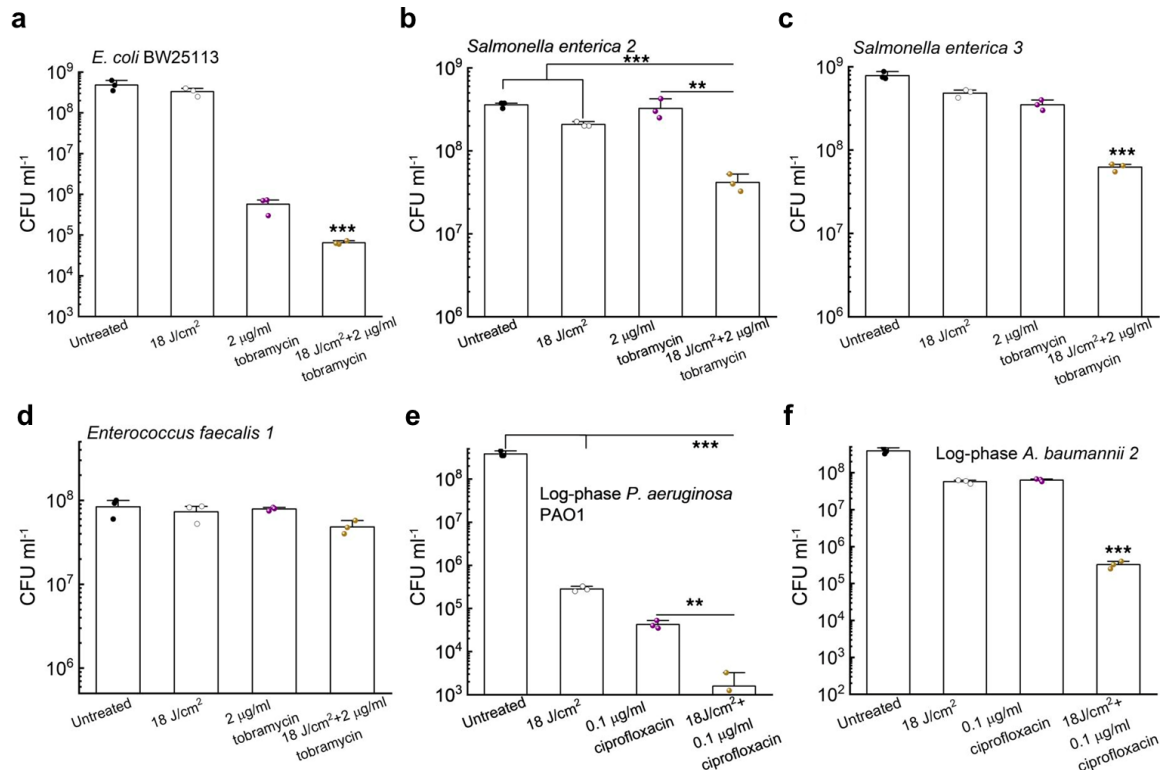


**Figure 9: Catalase Photodeactivation Sensitizes Bacteria to Antibiotics.** CFU measurements of a) *E. coli* BW25113, b) *S. enterica* 2, or c) *S. enterica* 3 treated to blue light and incubated in the presence of the aminoglycoside tobramycin for 4 hours. Significant improvements in tobramycin activity observed. The same treatment applied to d) catalase negative *E. faecalis*

was found to be ineffective. For the fluoroquinolone ciprofloxacin, 4 hours of antibiotic incubation following light treatment was found to improve the activity of the antibiotic against both log phase e) *P. aeruginosa* PAO-1 and f) *A. baumannii* 2. \*\*\*:  $p < 0.001$ , \*\*:  $p < 0.01$ . Data published in Dong et al., *JCI Insight.*, 2022.<sup>34</sup>

Studies on the mechanism of action of traditional antibiotics indicate that antibiotic classes like  $\beta$ -lactam, aminoglycoside, fluoroquinolones all capable of trigger significant intracellular ROS generation through the hyperactivation of the citric acid cycle<sup>67</sup>. Thus, the viability of combining catalase deactivating blue light with antibiotics was explored through the use of the ROS producing aminoglycoside tobramycin<sup>68</sup> and fluoroquinolone ciprofloxacin<sup>69</sup>. In the case of tobramycin, the addition of catalase deactivating blue slightly improved the effectiveness of the antibiotic against catalase positive *E. coli* (**Figure 9a**) and *S. enterica* (**Figure 9b and 9c**) by roughly 1-log. In contrast, light and antibiotic treatment on catalase negative *E. faecalis* resulted in no enhancement of tobramycin activity (**Figure 9d**). In the case of ciprofloxacin, the addition of light with 0.1  $\mu\text{g/mL}$  of ciprofloxacin resulted in a near 1-log improvement ciprofloxacin activity against log phase *P. aeruginosa* (**Figure 9e**) and a 2-log improvement in ciprofloxacin activity against log phase *A. baumannii* (**Figure 9f**). Taken together, the results suggest that blue light induced catalase deactivation can increase the antimicrobial effectiveness of indirect exogenous ROS sources like antibiotics.

## Catalase Deactivation and Immune Cells

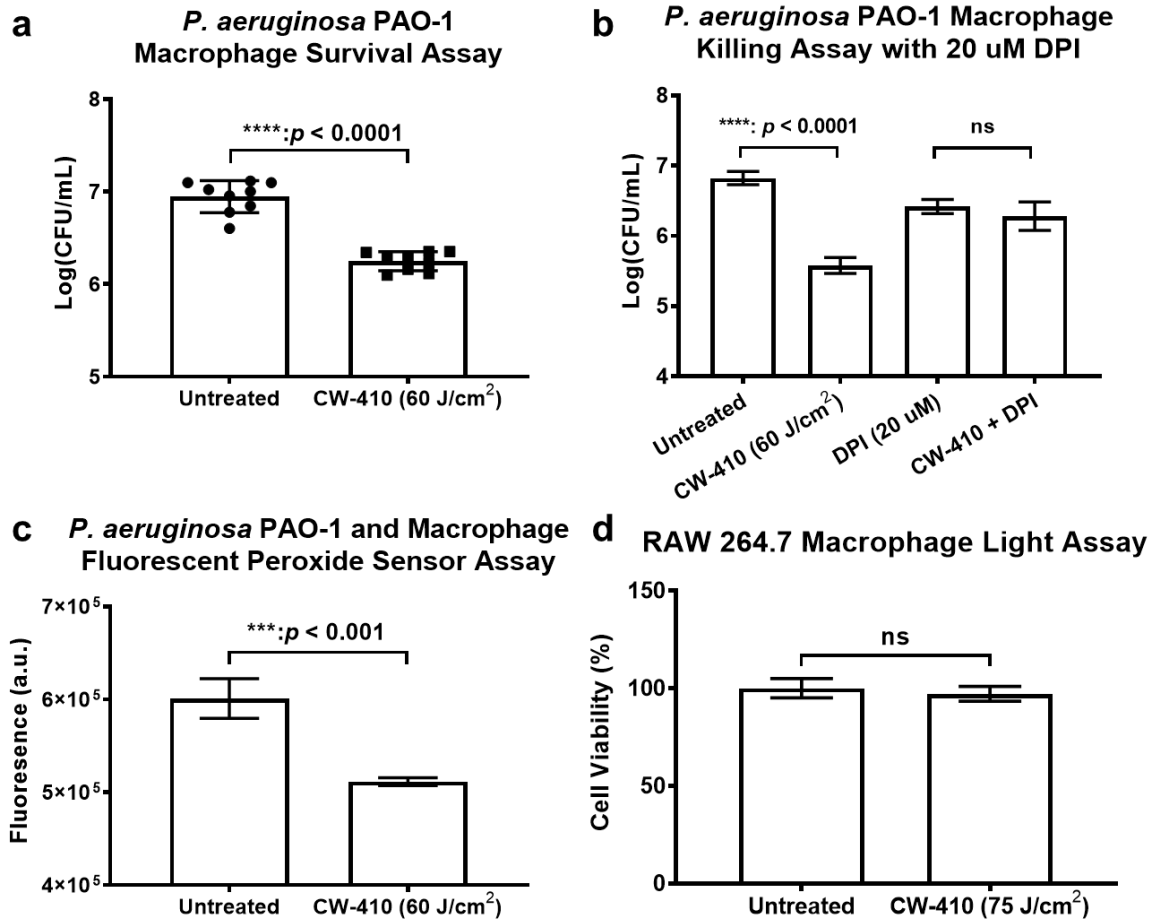


**Figure 10: Catalase Photodeactivation Improves Macrophage Killing Efficiency.** A) CFU/mL of intracellular *P. aeruginosa* PAO-1 following two 60 J/cm<sup>2</sup> CW-410 treatments performed over the course of 12 hours. B) CFU/mL of macrophages treated with light treated PAO-1 in the presence or absence of the NOX2 inhibitor DPI. DPI neutralizes the effects of light treatment. C) HPF fluorescence ROS measurements of RAW 264.7 macrophage and untreated or light treated PAO-1. D) Survival percentage of uninfected RAW 264.7 macrophages with or without light exposure. All macrophage killing assays performed with a MOI = 20. \*\*\*\*:  $p < 0.0001$ , \*\*\*:  $p < 0.001$ , ns = No Significance. Data published in Dong et al., *JCI Insight.*, 2022.<sup>34</sup>

While catalase deactivation was capable of sensitizing bacteria indirect sources of ROS like antibiotics, one of the key questions remaining in regards catalase inactivated bacteria was its interactions with the host immune system. The ROS burst produced by NADPH oxidase (NOX2) proteins within macrophages and neutrophils is known to

expose engulfed pathogens to ROS. Thus, studies were conducted on *P. aeruginosa* PAO-1 under the effects of RAW 264.7 macrophage phagocytosis. Treatment of blue light following macrophage internalization of *P. aeruginosa* was found to result in a significantly lower intercellular bacterial bioburden than the untreated sample, indicating greater killing efficiency of the macrophages (**Figure 10a**).

To confirm that it is the ROS burst specifically that is responsible for the improved killing efficiency of light treated bacteria observed in macrophages, a NOX2 inhibitor, diphenyleneiodonium chloride (DPI) was added to an infection co-culture. DPI is a known inhibitor of NOX, and can actively suppress NOX2 activity by binding to its heme and flavin cofactors, therefore suppressing the ROS burst produced by macrophages<sup>70</sup>. Macrophages treated with light treated PAO-1 in the absence of DPI were found to exhibit a more than 1-log improvement in CFU/mL reduction in terms of improved macrophage killing efficiency, exhibiting similar results to the macrophage co-cultures treated post-infection (**Figure 10b**). However, in the presence of ROS burst inhibiting DPI, the improved killing efficiency provided by light treatment was completely neutralized, demonstrating that the ROS burst is critical for the elimination of intracellular bacteria and that blue light treatment specifically improves the effectiveness of this ROS burst against bacteria.

To further examine the ROS presence within the macrophage co-culture, a fluorescent peroxide sensor was used to investigate the modulation in the amount of ROS produced by macrophages that have engulfed light treated *P. aeruginosa* (**Figure 10c**). Fluorescence measurements indicate a significant decrease of ROS produced by

macrophages that have engulfed light treated cells, indicating that catalases deactivated bacteria stimulates lower ROS production from macrophages, potentially due to their lower virulence and greater susceptibility to even low concentrations of ROS. Furthermore, application of 410 nm light directly to RAW 264.7 murine macrophages was found to have no significant impact on the overall viability of non-infected macrophages, indicating that potential damage to the immune cells alone was minimal (**Figure 10d**). Taken together, the following data suggests that that catalase deactivating, 410 nm blue light can improve the ability for the host immune system to eradicate intercellular bacteria, establishing the translatability of this technology to potentially synergize with host immune systems.

*Bacterial Catalase Deactivation Mammalian Translation*

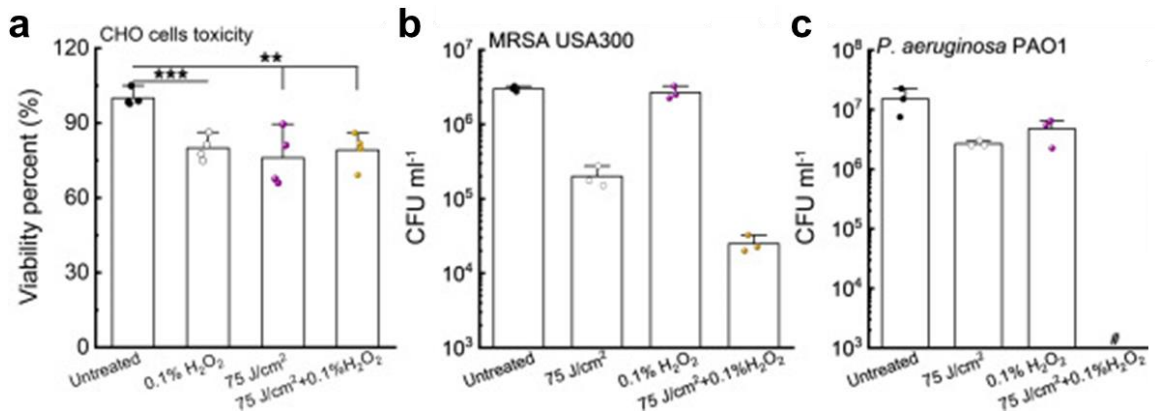


**Figure 11: Blue Light and Short Term, High Concentration H<sub>2</sub>O<sub>2</sub> Against Mammalian and Bacterial Cells.** 75 J/cm<sup>2</sup> of CW-410 (250 mW/cm<sup>2</sup>, 5 minutes) and 0.1% H<sub>2</sub>O<sub>2</sub> (1 minute incubation) was applied to a) MTT assay with CHO cells and CFU measurements against both b) log phase MRSA and c) log phase *P. aeruginosa*. \*\*\*:  $p < 0.001$ , \*\*:  $p < 0.01$ , # = Below Detection Limit. Data published in Dong et al., *JCI Insight.*, 2022.<sup>34</sup>

To further determine the potential translatability of this ROS sensitizing technology towards infections, the effectiveness of antimicrobial blue light with short-term exposure to higher concentration H<sub>2</sub>O<sub>2</sub> was quantified on growth phase gram-

positive and gram-negative bacteria strains. In addition, the potential toxicity of the treatment was evaluated through a MTT assay on CHO cells. Since most medical H<sub>2</sub>O<sub>2</sub> formulations used for disinfection purposes commonly range between 0.1% and 3% concentrations, a 0.1% concentration was used, equivalent to a molarity of 29.3 mM<sup>71</sup>. Based on the MTT assay, CHO cells retained a viability of 80% following treatment to the combination of 75 J/cm<sup>2</sup> of CW-410 and 1 minute exposure to 0.1% H<sub>2</sub>O<sub>2</sub> (**Figure 11a**). This combination treated viability was the same as the viability observed in the individual light or H<sub>2</sub>O<sub>2</sub>, indicating that mammalian cells fail to experience the same synergy observed previously in bacterial strains. Applying the same treatment conditions to log phase MRSA (**Figure 11b**), and *P. aeruginosa* (**Figure 11c**), found that the addition of blue light improved the effectiveness of H<sub>2</sub>O<sub>2</sub> against MRSA and allowed for complete eradication against both *P. aeruginosa*. Unlike the stationary phase bacteria, the log phase strains were also found to be more sensitive to the 410 nm light alone, with MRSA and *P. aeruginosa* experiencing a 1-log CFU reduction. This increased sensitivity of log phase bacteria may be due to differences in catalase expression depending on the growth state. Based on the results, *P. aeruginosa* appears to exhibit high sensitivity for the combination treatment and was selected as the pathogen to be tested within an *in vivo* abrasion model to further determine translatability within *in vivo* conditions.

### In Vivo Bacterial Catalase Deactivation Murine Model

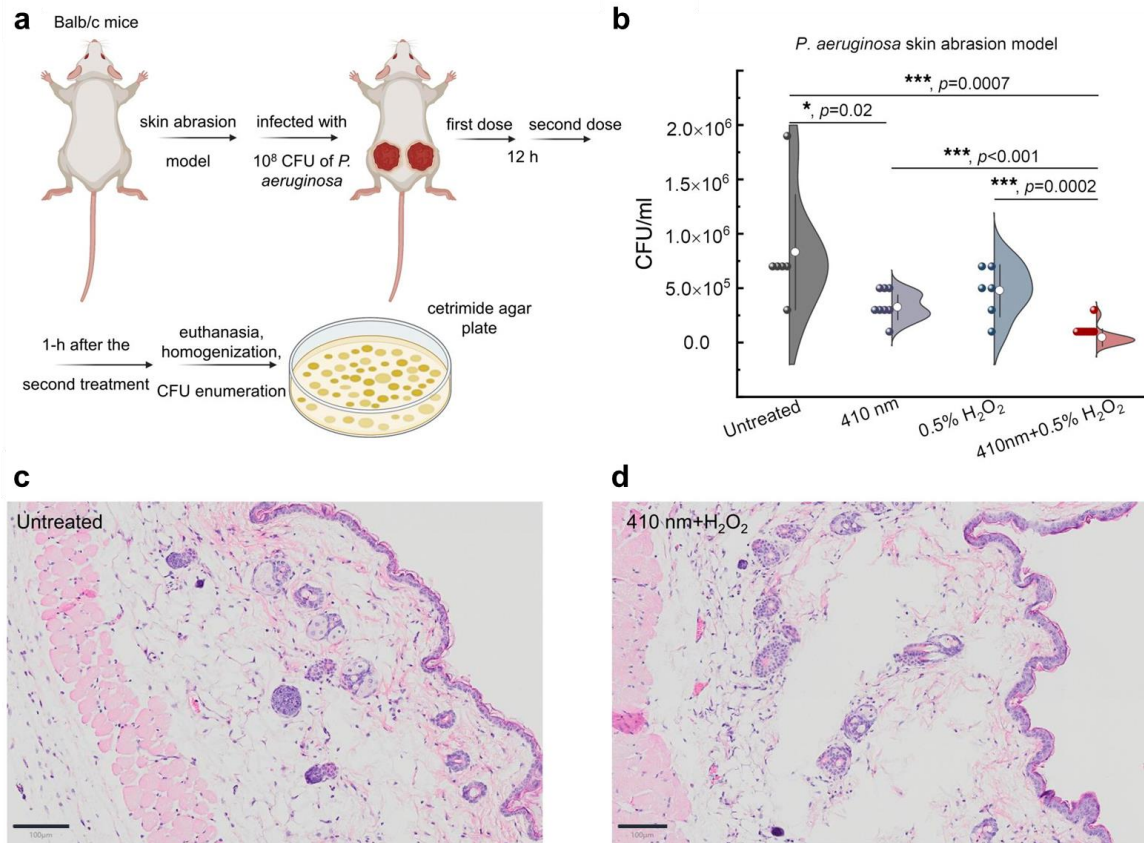


**Figure 12: Catalase Photodeactivation in a *In Vivo P. aeruginosa* Infected Murine Abrasion Model.** a) Treatment regimen of CW-410 light and H<sub>2</sub>O<sub>2</sub> for infected murine abrasion wounds. Mice received two treatments over 16 hours. Light treatments consisted of delivery of 120 J/cm<sup>2</sup> of CW-410 (200 mW/cm<sup>2</sup>) while 0.5% H<sub>2</sub>O<sub>2</sub> was used for H<sub>2</sub>O<sub>2</sub> treatment. b) CFU/mL results of wound bioburden following light treatment. \*\*\*:  $p < 0.001$ , \*:  $p < 0.05$ . Scale bar = 100  $\mu$ m. Data published in Dong et al., *JCI Insight.*, 2022.<sup>34</sup>

To evaluate the potential translatability of this technology, a murine *P. aeruginosa* PAO-1 infected abrasion model was used to determine the viability of this treatment against *in vivo* bacterial skin infections, based on an established abrasion model by Dai et al<sup>72</sup>. Abrasion wounds were infected with 10<sup>8</sup> CFU of log phase PAO-1 and treated mice received wound treatments consisting of either 120 J/cm<sup>2</sup> of CW-410 exposure, application of 0.5% H<sub>2</sub>O<sub>2</sub>, or a combination of the light and H<sub>2</sub>O<sub>2</sub> treatment.

Mice received a total of two treatments within the course of 16 hours, after which the mice were euthanized and the wounds were extracted, homogenized, and quantified for bacterial bioburden (**Figure 12a**). Based on the resulting CFU measurements, untreated mice retained a PAO-1 CFU load of roughly  $10^6$  CFU/mL. While 0.5% of H<sub>2</sub>O<sub>2</sub> alone had no significant impact on the bacterial population, the application of 410 nm light alone significantly reduced the average bacterial load by around 60%. In addition, for the combination treated groups, the combined treatment improved the antimicrobial activity of H<sub>2</sub>O<sub>2</sub> against PAO-1 infected wounds by roughly 1-log (**Figure 12b**). To determine if the light and H<sub>2</sub>O<sub>2</sub> had a toxic effect on the skin, untreated and combination treated regions of unwounded skin were analyzed through hematoxylin and eosin (H&E) staining. No significant difference in epidermis, dermis, and subcutaneous tissue was observed between the untreated (**Figure 12c**) and combination treated (**Figure 12d**) regions of the skin.

### Discussion and Conclusion

Through exploration of the effects of blue light alone on a model *E. coli* MG1655 bacteria model, it was discovered that while wild type *E. coli* could easily tolerate up to 60 J/cm<sup>2</sup> in CW-410 treatment, the same dosage resulted in a significant reduction in bacterial population for the catalase deficient  $\Delta katGE$  mutant. In addition, removal of an additional antioxidant enzyme known as alkyl hydroperoxide reductase (ahpCF) from the catalase deficient mutant was found to significantly increase the antimicrobial activity of blue light by nearly 1.5-log. These results indicate that while blue light alone is indeed capable of producing ROS within the bacteria internally, the presence of antioxidant

enzymes can neutralize any ROS that would have developed from the photoexcited endogenous porphyrins. This is supported by ROS measurements indicating that ROS levels were only observed to increase once both catalase and the alkyl hydroperoxide reductase was removed in the *ΔkatGEahpCF* mutant. While the same increase in ROS levels wasn't observed under the catalases negative mutant, it is likely that the alkyl hydroperoxide reductase was able to compensate for the loss of catalase, as the molecule is specifically noted to neutralize endogenously produce H<sub>2</sub>O<sub>2</sub>, although it is much less efficient at neutralizing ROS and can be easily saturated compared to catalase<sup>63</sup>. Thus, while the results are consistent with studies that indicate that aBL produces intracellular ROS, our data shows that antioxidant enzymes can provide resistance against the toxic effects of aBL at lower dosages. The antimicrobial activity of aBL observed at higher dosages can likely be partially attributed to the ROS produced by the endogenous porphyrins eventually accumulating to the point where they overcome the existing antioxidant defense system, especially with the ongoing deactivation of catalase that is likely occurring over the duration of the light treatment.

While the data demonstrates the importance that antioxidant enzymes like catalase play in aBL, additional research on the downstream effects of this blue light exposure on bacteria revealed that not only does aBL exposure increase bacterial sensitivity to exogenous H<sub>2</sub>O<sub>2</sub> among catalase positive bacterial strains like MRSA or *P. aeruginosa*, but it is the specific deactivation of catalase that is primarily responsible for this increased sensitization. Tests on catalase negative bacteria strains like *E. faecalis* exhibit no increased ROS sensitization from light treatment, indicating catalase alone contributes

significantly to sensitization. In addition, tests on catalase deficient *E. coli* mutants indicated that 410 nm blue light is capable of inactivating different types of catalase, whether it be the monofunctional *katE* catalase or the bifunctional *katG* catalase-peroxidase<sup>73,74</sup>. Time-killing assays of wild type *E. coli* and *E. coli*  $\Delta katGE$  revealed the killing efficiency of H<sub>2</sub>O<sub>2</sub> to be near identical between the 410 nm treated wild type *E. coli* and the untreated *E. coli*  $\Delta katGE$ , and catalase gene complementation further indicated that the arabinose triggered catalase recovery was able to provide protection against H<sub>2</sub>O<sub>2</sub> induced oxidative stress following light exposure. This confirms that catalase acts as a primary target of 410 nm blue light and its deactivation is significantly responsible for the increased ROS sensitization caused by blue light. Interestingly, more effective killing of the 410 nm treated double catalase knockout mutant was observed under H<sub>2</sub>O<sub>2</sub> exposure, suggesting that other blue light photosensitive antioxidant molecular targets exist within bacterial pathogens.

H<sub>2</sub>O<sub>2</sub> is known to be heavily dependent on the availability of iron to properly form additional types of ROS like hydroxide (OH<sup>-</sup>) and hydroxyl radicals<sup>75</sup>. Since catalase specifically contains bound ferric iron ions to react with H<sub>2</sub>O<sub>2</sub>, and Raman analysis indicated that the catalase porphyrin heme structure is structurally damaged by blue light exposure, it was theorized that the potential free iron ions released would contribute to the observed increased ROS sensitization, as H<sub>2</sub>O<sub>2</sub> alone can degrade heme molecules and release the iron ions within, amplifying their toxic effects<sup>76</sup>. Thus, the contribution of potentially free iron ions from deactivated catalase under light and H<sub>2</sub>O<sub>2</sub> treatment was explored through iron chelators, a known inhibitor of the Fenton reaction<sup>77</sup>.

Interestingly, the iron chelators only had a minor effect on light induced ROS sensitization, and the combination of light and H<sub>2</sub>O<sub>2</sub> was still able to reduce the *E. coli* population by 99.9%, indicating that the free iron ions present within the bacterial environment are only a small contributor to the increased ROS sensitization observed, and that H<sub>2</sub>O<sub>2</sub>-Fenton reactions with other iron bound substrates or iron-independent, low H<sub>2</sub>O<sub>2</sub> concentration induced DNA damage are more likely to be responsible for the increased ROS sensitivity<sup>78</sup>. Regardless, while it appears that the iron originating from deactivated catalase does not appear to significantly contribute to the increased ROS sensitivity, the minor contribution of free iron observed, assuming it originates from deactivated catalase, would fall in line with how heme molecules can enhance ROS activity, similar to how the toxicity of H<sub>2</sub>O<sub>2</sub> is enhanced by hemoglobin<sup>79</sup>. While the Raman data and previous studies on heme and H<sub>2</sub>O<sub>2</sub> interactions indirectly imply the release of free iron ions from the deactivated catalase, further experiments can be done in the future to directly confirm changes in the concentration of free iron ions present within light treated microbes, such as elemental analysis with atomic emission spectroscopy.

While the mechanistic interactions of blue light induced ROS sensitivity and catalase deactivation had been investigated, to demonstrate the potential translatability of this technology to medical settings, the impact of catalase deactivating blue light was explored under more clinically relevant agents and conditions. Catalase deactivating blue light was not only found to improve the efficiency of ROS producing antibiotics like tobramycin and ciprofloxacin against catalase positive bacteria, but catalase deactivation was found to specifically enhance the ROS burst produced by macrophages, enhancing

the killing efficiency of immune cells to kill phagocytosed bacteria. Studies have indicated that bacterial catalase protects bacteria from the ROS burst produced by the immune cells, therefore promoting survival and proliferation within the phagocytotic vacuoles<sup>80,81</sup>. The improved killing efficiency of macrophages under catalase deactivating blue light *in vitro* provided an excellent basis to further explore the effect of blue light and H<sub>2</sub>O<sub>2</sub> within an *in vivo* model. Before exploring this model, the impact of short term, high concentration H<sub>2</sub>O<sub>2</sub> and blue light was explored on both mammalian CHO cells and log phase bacteria to potentially minimize the length of exogenous ROS exposure time needed to exert significant improved antimicrobial activity. While both log phase MRSA and *P. aeruginosa* were found to be more sensitive to blue light alone, only *P. aeruginosa* experienced complete eradication when 0.1% H<sub>2</sub>O<sub>2</sub> was added, potentially due to the antioxidant staphyloxanthin pigment found in MRSA providing greater ROS resistance<sup>32</sup>. However, in the mammalian CHO cell MTT assay, while slightly lower 80% viability was observed for all treatment groups, combination treatment failed to exhibit the same increased H<sub>2</sub>O<sub>2</sub> efficiency observed in bacteria. This can be attributed to the significantly greater surface to volume ratio of the average 1 μm<sup>3</sup> bacterial cell versus the 1000 to 10000 μm<sup>3</sup> human eukaryotic cell, resulting in a much more potent response to H<sub>2</sub>O<sub>2</sub> by the bacteria<sup>82</sup>.

Based on the mammalian cell tests, a combination of short-term, high concentration H<sub>2</sub>O<sub>2</sub> and blue light was applied to an *in vivo* bacterial abrasion murine model. Application of blue light alone was not only able to reduce the bacterial load present within the infected wounds, but the catalase photodeactivation was also able to

significantly enhance the activity of  $\text{H}_2\text{O}_2$  even within the wound environment. The 200  $\text{mW}/\text{cm}^2$  power setting that the blue light was applied at also falls within the ANSI safety limits regarding 400 to 700 nm laser light exposure to skin, ensuring that the conditions applied to the model could theoretically be translated to a human model, further demonstrating the translatability of this technology<sup>83</sup>. These results demonstrate the potential viability of utilizing catalase deactivating blue light to treat infected wounds and represent the first step of translating this technology toward a clinical setting.

Overall, by exploring the relationship between aBL and catalase deactivation, not only was it discovered that antioxidants like catalase significantly contribute to the neutralization of endogenously produced ROS caused by blue light alone, but aBL was found to induce significant ROS sensitization by specifically targeting catalase. In addition, it was found that free iron ions, potentially generated by the degradation of the catalase heme molecules in reaction to both light and  $\text{H}_2\text{O}_2$ , are only a minor contributor to the increased antimicrobial activity of  $\text{H}_2\text{O}_2$ , indicating that the bulk of ROS sensitization is likely due to ROS interactions with iron bound substrates or iron-independent oxidative damage. In determining the translatability of this technology, blue light was found to not only sensitize bacteria to antibiotics and the host immune system, but it also was found to remain effective even within an *in vivo* wound environment, potentially providing a non-drug reliant method of sensitizing catalase positive, drug resistant pathogens to conventional antibiotics. Despite these findings, there are still questions remaining about the interactions between bacteria and aBL that can be explored in future works, such as determining if known photosensitive molecules, such as the blue

light sensitive cytochrome c, could contribute to increased ROS sensitivity observed in light treated catalase deficient *E. coli*<sup>84</sup>. Additional investigations can also be done on the specific structural breakdown of catalase induced by blue light. Taken together, the following work further details the relationship between bacterial catalase deactivation and aBL and demonstrates the potential utilization of this technology to fight drug resistant infections.

## **CHAPTER THREE: Antimicrobial Phototherapy Reduces Fungal Virulence within *In Vitro* and *In Vivo* Environments**

The work and figures presented in this chapter was published in Photochemistry and Photobiology<sup>85</sup>. Reprinted with permission from John Wiley and Sons. Copyright by 2022 American Society for Photobiology. DOI: 10.1111/php.13719

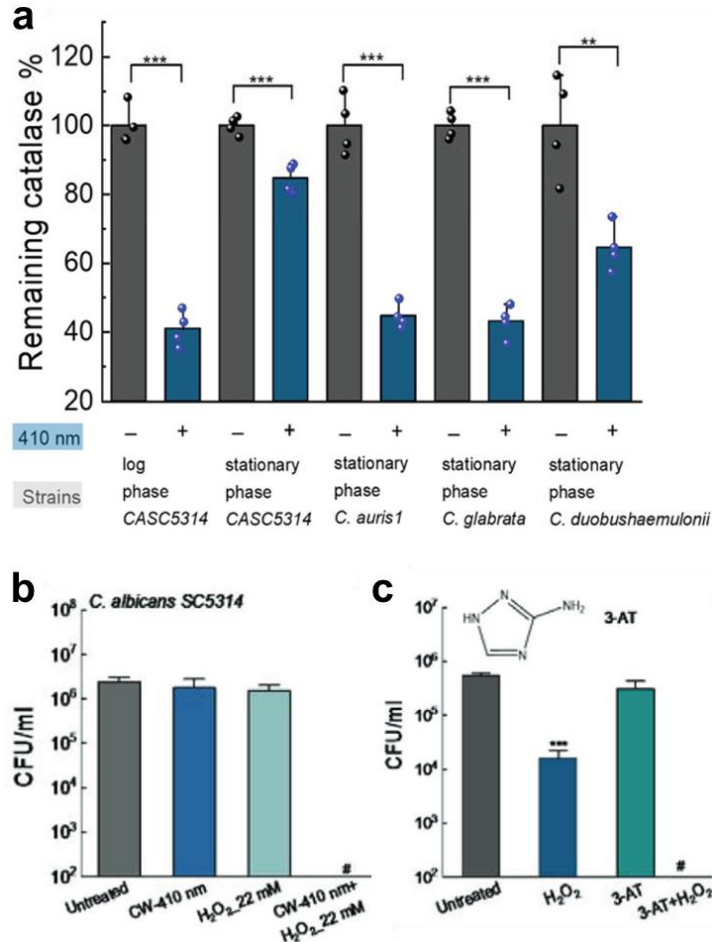
Data and figures presented in this chapter were published in Advanced Science<sup>86</sup>. The CC-BY license permits use, distribution, and reproduction in any medium, provided the original work is properly cited and allows the commercial use of published articles.

### **Introduction**

#### *Fungal Skin Infections*

Like bacterial infections, fungal pathogens have also emerged in recent years as a severe global health risk and are estimated to be responsible for over 150 million cases of severe infections and 1.7 million deaths annually<sup>87</sup>. One key factor contributing to the rise of fungal infections is the growing population of vulnerable patients, such as the elderly, immunocompromised, and recently hospitalized<sup>88</sup>. In the United States, the *Candida* fungal strain is estimated to be the fourth most common cause of bloodstream infections, and *Candida albicans* alone is estimated to be responsible for 50% to 70% of all candidiasis cases<sup>89,90</sup>. Other fungal strains, such as mold species like *Aspergillus* or *Trichophyton*, have also significantly contribute to spreading fungal infections, whether it be through cutaneous or general skin infections<sup>91-93</sup>. These dermal infections have been found to be steadily rising over the past 30 years, especially among immunocompromised patients<sup>94</sup>. Dermal and cutaneous infections are especially noteworthy due to how they

can provide an possible entryway into the bloodstream, resulting in the potential development of invasive candidiasis<sup>95</sup>. This overall increase in fungal infections has been further complicated by the growing development of antifungal resistance to all currently available classes of antifungal drugs (polyenes, azoles, allylamines and echinocandins), driven in part by the agricultural industry's overuse of antifungal chemicals and the pharmaceutical industry's current focus on refining existing bacterial antibiotics<sup>96,97</sup>. The rise of antifungal resistance can be best seen in the *Candida* fungal species with the emergence of azole resistant *Candida* species alongside multidrug-resistant *C. auris*<sup>98,99</sup>. The development of *Candida* resistance is especially concerning due to its capability of rendering fungal bloodstream infections more deadly and difficult treat. Based on the rising trends of *Candida* infections and the growing risk of emergent antifungal resistance, there exists a critical need for a non-antifungal reliant method of treating *Candida* infections.

Catalase Deactivation and *Candida*

**Figure 13: Blue Light Induced Catalase Deactivation of *Candida* fungal cells.** a) Catalase activity measurement of various *Candida* species treated to 30 J/cm<sup>2</sup> of 405 nm blue light. CFU/mL of *C. albicans* SC5314 treated to H<sub>2</sub>O<sub>2</sub> alongside either b) 30 J/cm<sup>2</sup> of blue light or c) 4 hours of incubation in 50 mM of catalase inhibiting AMT. \*\*\*:  $p < 0.001$ , \*\*:  $p < 0.01$ . Data published in Dong et al., *Advanced Science*, 2022<sup>86</sup>

Previous studies conducted by the Cheng lab have revealed that, like bacterial species, the catalase present within *Candida* fungi can be sensitized with aBL. Experiments performed on multiple *Candida* strains reveal that 405 to 410 nm blue light can inactivate the active catalase present within various *Candida* fungi strains (**Figure 13a**). Subsequent tests also found aBL treated *Candida albicans* exhibited similar trends of increased ROS sensitization as previously observed in bacterial cells, with complete

eradication of stationary phase *C. albicans* observed following light and H<sub>2</sub>O<sub>2</sub> treatment (**Figure 13b**). Additional usage of the chemical catalase inhibitor 3-amino-1,2,4-triazole (AMT) revealed that chemical deactivation of catalase results in an identical phenotypic response to H<sub>2</sub>O<sub>2</sub> as 410 nm light treatment (**Figure 13c**), demonstrating the inactivation of internal catalase as the driving force of ROS sensitization in *C. albicans*. Further tests would go on to indicate the ability for blue light to improve the antimicrobial activity of antifungal agents like amphotericin B and micafungin against a variety of different *Candida* strains<sup>86</sup>.

However, while increased ROS sensitization is clearly observed across multiple *Candida* fungal strains, several questions remain regarding the application of catalase deactivating blue light to fungi. These questions include the need to further investigate the downstream effects of light induced catalase deactivation on the significantly more complex eukaryotic fungal cells, its overall applicability and translation within *in vivo* models, and determining if this technology is applicable to non-*Candida* fungal strains.

### *Fungal Hyphae Development*

Like most pathogens, fungi express a wide variety of mechanisms that allow them to increase their virulence and resist attempts by the body's natural host immune response to eradicate them. Two of the more notable virulence factors include the expression of catalase as well as the ability to transition between a yeast form and filamentous hyphae form, commonly referred to as dimorphism<sup>100,101</sup>. The first virulence factor, catalase, is one of the most common enzymes expressed within aerobic fungal organisms and protects cells from oxidative damage by converting H<sub>2</sub>O<sub>2</sub> to oxygen and water<sup>102</sup>. Like

with bacteria, catalase contributes to fungal virulence by protecting phagocytosed fungi from the ROS burst produced by immune cells like neutrophils<sup>103</sup>. With the presence of catalase, phagocytosed fungi can survive the initial ROS burst produced by immune cells and provide the survived pathogen with more opportunities to establish infections within a host<sup>100,104</sup>. These survival capabilities within a phagocytosed environment can therefore enable an additional second virulence factor in the form of hyphae formation. While fungal molds like *Aspergillus* or *Trichophyton* only replicate by producing networks of tubular branching filamentous hyphae, *C. albicans* and other select strains of *Candida* are unique in its dimorphic ability to grow as either a unicellular budding yeast form or a filamentous hyphae form<sup>105,106</sup>. This dimorphism plays a key role in the virulence of *C. albicans*, as hyphae filaments can utilize the mechanical force exerted by polarized hyphae growth to penetrate deeper into epithelial cells and escape from macrophages or neutrophils following phagocytosis<sup>107-109</sup>. In addition, hyphae formation also contributes to the formation of biofilms, further complicating treatment options of fungal skin infections<sup>110</sup>. While there exist numerous stimuli capable of stimulating hyphae development in *C. albicans* like temperature, serum presence, and pH, the actual morphological transition from yeast to hyphae form has been found to be significantly impacted by lipid biogenesis, with disruptions in sterol or sphingolipid biosynthesis resulting in impaired hyphae growth and polarization<sup>111</sup>. Additionally, it has also been found that transition to the hyphae form results in increases in unsaturated fatty acids, indicating that lipogenesis plays a key role in hyphae development<sup>112</sup>.

Interestingly, studies have found that both catalase and hyphae development are

related, as *C. albicans* grown on hyphae inducing media have been found to exhibit increased catalase activity. In addition, *C. albicans* with double catalase gene disruptions demonstrated suppressed hyphae development<sup>113</sup>. This phenomenon can potentially be explained by how *C. albicans* are known to produce significant amount of ROS during their transition to a hyphal state<sup>114,115</sup>. This aspect, coupled with the fact that extracellular H<sub>2</sub>O<sub>2</sub> is capable of inducing hyphae formation, indicates that ROS presence plays a potential signaling role in hyphae development<sup>116</sup>. Catalase has also been found to play a role in certain aspects of lipid metabolism, such as within the fatty acid  $\beta$ -oxidation pathway in peroxisomes<sup>43</sup>. Literature indicates that catalase is also used to protect proteins within the lipid metabolism pathway from damage, as ROS accumulation has been found to result in damage to key proteins involved in yeast lipid metabolism, such as fatty acid synthase<sup>117</sup>. Given the previously discussed importance of lipid production in hyphae development, it is possible that the deactivation of catalase could indirectly disrupt the lipid metabolism and suppress formation of hyphae. Thus, deactivation of catalase can provide a potential avenue of reducing virulence and infectivity of *C. albicans*, lowering the risk of invasive infection and improving the ability for the immune system to successfully kill of engulfed fungi. However, due to the toxic nature of most chemical catalase inhibitors like potassium cyanide and 3-amino-1,2,4-triazole (AMT), alternative solutions to induce catalase deactivation are needed<sup>118,119</sup>. Given the relationship between catalase, hyphae development, and lipid metabolism, we hypothesize that exposure to blue light can suppress the formation and development of hyphae in *Candida* species through disruption of lipid metabolism. By utilizing light to

inhibit hyphae formation, we can reduce the survival and invasion capabilities of *C. albicans*, therefore providing a non-antifungal reliant method of treating fungal infections.

Overall, this chapter aims to explore the downstream effects of catalase deactivation on the hyphae forming capabilities of *Candida* cells, as well as the translatability of aBL in treating *C. albicans* infections within *in vivo* settings, and its applicability to non-*Candida* fungal strains to demonstrate the translative potential of this technology.

## **Methods and Materials**

### *Blue Light Source*

A mounted 405 nm LED (M405L4, ThorLabs) was attached to a modifiable collimation adapter (SM2F32-A, ThorLabs) and adjusted to focus the fluence region to a ~1 cm square area. Fluence was controlled through a T-Cube LED driver (LEDD1B, ThorLabs), allowing for a wide range of blue light power outputs between 0 and 400 mW/cm<sup>2</sup>.

### *Fungal Strains and Cell lines*

Wild type *Candida albicans* Berkhout (SC5314) was purchased from the American Type Culture Collection (ATCC). Catalase-deficient *Candida albicans* 2089 ( $\Delta cat1$ ) was obtained from Dr. Alistair Brown at University of Exeter. Far-red fluorescent protein-expressing SC5314 (iRFP *C. albicans*) was acquired from the Mansour Lab<sup>120</sup>. Other dimorphic *Candida* strains, including *Candida tropicalis* and *Candida dubliniensis* were obtained from clinical isolates following biosafety committee and institutional review

board (IRB) approval. *Candida auris* 2 (AR-0382) and *Aspergillus fumigatus* (Strain 293) was provided by Dr. Michael K. Mansour at the Massachusetts General Hospital. For mammalian cells, human neutrophils were isolated from whole blood obtained from healthy donor volunteers consented under a Massachusetts General Hospital IRB-approved protocol.

#### *Fungal Preparation and Catalase Deactivation Phototherapy*

*Candida* strains were cultured overnight in yeast extract peptone dextrose (YPD) media at 30°C within either a shaking (200 RPM) or rotating incubator. Following overnight growth, fungi were resuspended in 1x PBS and quantified through a Luna Automated Cell Counter (L10001, Logos Biosystems). For light induced catalase deactivation, *Candida* was diluted to a cell density of  $5 \times 10^7$  CFU/mL, after which a 10  $\mu$ L aliquot of fungal suspension was placed on a glass coverslip and exposed to 60 J/cm<sup>2</sup> of 405 nm light (200 mW/cm<sup>2</sup>, 5 Minutes). After light treatment, the aliquot was transferred to 1 mL of complete RPMI 1640 (cRPMI, containing 10% fetal bovine serum (FBS) and 1% penicillin and streptomycin) and vortexed for 10 seconds. The fungal suspension was transferred to a glass bottom dish and incubated at 37°C with 5% CO<sub>2</sub> for between 1 to 3 hours. For chemically induced catalase inactivation, *Candida* was diluted to a cell density of  $5 \times 10^7$  CFU/mL and incubated in PBS containing 50 mM of 3-Amino-1,2,4-triazole, or AMT (Sigma Aldrich, 45324) for 4 hours at 30°C alongside a non-AMT treated control. After incubation, 10  $\mu$ L of the treated fungal suspension was transferred to 1 mL of cRPMI supplemented with 50 mM of AMT and incubated for 1 hour at 37°C with 5% CO<sub>2</sub> for 1 hour. Following incubation, the glass bottom dishes were removed and

centrifuged at 500 G for 30 seconds. The cRPMI media was removed and the fungi were washed with PBS. Following washing, dishes were centrifuged, the PBS was removed, and the adherent fungal cells were fixed in 10% buffered formalin.

For *Candida auris* tests, fungal samples were prepared in the same process as other *Candida* strains described above, only cells were resuspended in PBS at a concentration of  $1 \times 10^8$  CFU/mL. A 10  $\mu$ L aliquot was exposed to 30 J/cm<sup>2</sup> of blue light and then immediately diluted within 990  $\mu$ L of PBS. Light treated *Candida* was treated to 0.1% H<sub>2</sub>O<sub>2</sub> for 1 minute before being immediately serially diluted in a 96-well plate and plated on YPD agar plates for CFU quantification and counting.

For testing of *Aspergillus fumigatus*, a PrestoBlue viability assay was used to evaluate the response of the filamentous fungi to blue light and H<sub>2</sub>O<sub>2</sub>. *Aspergillus fumigatus* was cultured within sabouraud dextrose broth for 2 weeks. *Aspergillus* culture was then resuspended and diluted within PBS, and a cell counter was used to obtain a spore density of  $5 \times 10^7$  spores/mL. Following spore collection, a 20  $\mu$ L aliquot was subjected to either 30 J/cm<sup>2</sup> or 60 J/cm<sup>2</sup> of CW-405 in the process previously described. After treatment, the droplet was diluted within 1980  $\mu$ L of PBS. In a 96-well plate, 100  $\mu$ L of untreated or light treated spore suspension was deposited, and 2.2 mM of H<sub>2</sub>O<sub>2</sub> were added to wells. In a separate group, well sets containing  $10^8$ ,  $10^7$ ,  $10^6$ ,  $10^5$ , and  $10^4$  spores were established. Fungal cells were incubated at 30°C for 2 hours before all wells were supplemented with 90  $\mu$ L of sabouraud dextrose broth and 10  $\mu$ L of PrestoBlue reagent. The plate was then transferred to a plate reader set at 30°C and the fluorescence was quantified over the course of 48 hours at the excitation/emission of 560/590 nm.

Following measurement, the fluorescence of the different initial populations of *A. fumigatus* was used to generate a calibration curve to convert fluorescence to CFU/mL measurements.

#### *Neutrophil Isolation and Co-Culture*

Neutrophils were isolated from the blood of healthy volunteers in the process described by Mansour et al. under an approved IRB protocol<sup>121</sup>. To summarize, centrifugation was used to isolate the buffy coat layer from whole blood, after which the neutrophils were isolated from the layer via an EasySep Direct Human Neutrophil Isolation Kit (STEMCELL Technologies). The isolated neutrophils were washed and quantified with an acridine orange/propidium iodide dye through a cell counter. Purified neutrophils were then resuspended in cRPMI at a cell density of  $2.5 \times 10^5$  cells/mL.

For the *Candida* and neutrophil co-culture, iRFP *C. albicans* was cultured overnight in YPD media. iRFP *C. albicans* was washed in PBS and diluted to a final concentration of  $1.25 \times 10^8$  CFU/mL. A 5  $\mu$ L aliquot of iRFP *C. albicans* was exposed to a total of 75 J/cm<sup>2</sup> of 405 nm light (250 mW/cm<sup>2</sup>, 5 minutes) and then mixed in 45  $\mu$ L of 1 x PBS to obtain a fungal cell density of  $1.25 \times 10^7$  CFU/mL. From this stock, 2  $\mu$ L of fungal dilution was mixed with 200  $\mu$ L of neutrophil stock in an Eppendorf tube. After vortexing the tube, samples were transferred to a chambered #1.5 German cover-glass system. The system was centrifuged at 500 G for 30 seconds and then incubated for 4 hours at 37°C with 5% CO<sub>2</sub>. Following incubation, cRPMI media was removed and the co-culture was stained with Sytox Green for 15 minutes. After staining, the chamber was spun down at 2000 G for 5 minutes and then fixed in 10% buffered formalin.

### *Confocal and Phase Contrast Imaging*

Imaging of *Candida* hyphae was performed through either confocal imaging or phase contrast imaging. Confocal brightfield and fluorescence imaging was performed through a FV3000 Confocal Laser Scanning Microscope (Olympus) under a 60x Oil Objective. Sytox GREEN dye was detected at 488 nm excitation under a PMT voltage of 450 V and a 10% ND filter, with an emission detection range from 500 to 540 nm. iRFP dye was measured through 640 nm excitation with a PMT voltage of 750 nm and a 20% ND filter, with an emission range between 650 and 750 nm. For the phase contrast imaging, images were acquired under an IX81 Inverted Microscope (Olympus) under a 40x objective. A 1951 USAF calibration slide was used to determine the resolution of phase contrast images. Hyphae lengths were measured and quantified through ImageJ.

### *D<sub>2</sub>O Metabolism Stimulated Raman Spectroscopy Imaging*

In order to determine the impact of light induced catalase deactivation on hyphae growth, the rate of *de novo* lipid synthesis was indirectly quantified through the carbon-deuterium (C-D) bonds formed during incubation within a D<sub>2</sub>O containing media in a imaging procedure detailed by Meng et al<sup>122</sup>. Stimulated Raman scattering (SRS) imaging was used to quantify the amount of C-D bonds formed within untreated and light treated cells. D<sub>2</sub>O containing complete media was prepared by dissolving 0.5 g of YPD broth powder in 10 mL of D<sub>2</sub>O. The resulting solution was then sterilized by filtration using a 0.2 mm filter. 9 mL of the YPD/D<sub>2</sub>O media was mixed with 1 mL of FBS, generating a serum containing YPD solution in 90% D<sub>2</sub>O. *Candida* preparation and light induced catalase deactivation were performed as described earlier, only instead of cRPMI, the YPD/D<sub>2</sub>O

media was used instead. The resulting *C. albicans* was incubated at 37 °C with 5% CO<sub>2</sub> for 1 hour, after which the samples were washed with PBS and fixed in 10% buffered formalin.

To capture the stimulated Raman spectroscopy (SRS) signal, a femtosecond (fs) pulsed InSight DeepSee laser (Spectra-Physics) with a repetition rate of 80 MHz was utilized. The dual output of this system was utilized as the pump and Stokes beam. The Stokes beam was modulated through an acousto-optical modulator (AOM, 1205-C, Isomet) at 2.4 MHz. To allow for a tunable beating frequency, the pump beam was chirped with five 15 cm SF57 glass rods, while the Stokes beam was chirped with six glass rods (Schott). This chirping process increased the pulse durations of the beams to 2 ps. These beams were then sent into a custom laser scanning microscope with a 2D galvo mirror. The beams were focused on the sample using a 60x water objective (NA = 1.2, Olympus) and an oil condenser (NA = 1.4, Olympus) was used to collect signal. Once the beams have passed through the sample stage, the Stokes beam was filtered out and the pump beam was measured via a photodiode. A lock-in amplifier was then used to extract the stimulated Raman signal. In order to directly quantify the C-D vibrational signal originating from the D<sub>2</sub>O treated cells, the pump beam was set at 20 mW before the microscope and centered at a 849 nm wavelength, while the Stokes beam was set at 270 mW and centered at 1040 nm. A 200X200 pixel image was acquired using a pixel dwell time of 50 ms. SRS images were processed and analyzed through ImageJ.

*Gas Chromatography – Mass Spectroscopy*

To confirm the inhibition of fatty acids within light treated *C. albicans*, gas chromatography – mass spectroscopy (GC-MS) was used to quantify the changes in saturated and unsaturated fatty acids for untreated and light treated *C. albicans* in hyphae inducing conditions. Free fatty acids were extracted from fungi using a modified version of the Bligh and Dyer fatty acid extraction and derivatization method utilizing ethyl acetate substitutes for chloroform<sup>123</sup>. In summary, overnight cultured *C. albicans* was resuspended in PBS and then numerous aliquots of fungal suspension was exposed to 60 J/cm<sup>2</sup> of 405 nm light (200 mW/cm<sup>2</sup>, 5 minutes). Both untreated and light treated *C. albicans* were diluted to the same OD660 absorbance of 1.570, correlating to a cell density of  $5 \times 10^7$  cells/mL. 800  $\mu$ L ( $4 \times 10^7$  CFU/mL) of suspension was then centrifuged and resuspended in 2 mL of RPMI supplemented with 10% FBS, after which samples were allowed to incubate for 1 hour at 37 °C within a 2 mL Eppendorf tube. Following incubation, cells were centrifuged and washed twice in PBS, after which the *C. albicans* was resuspended in 400  $\mu$ L of PBS.

Extraction of the free fatty acids was performed by adding 50  $\mu$ L of 10% NaCl, 50  $\mu$ L of glacial acetic acid (Sigma Aldrich, AX0073), and 200  $\mu$ L of ethyl acetate (Sigma Aldrich, 270504) alongside around 350  $\mu$ L of 0.5 mm glass beads to reach an overall total volume of around 1 mL. For an internal standard, 1  $\mu$ L of 10 mg/mL pentadecanoic acid (Sigma Aldrich, P6125) was added to all samples. Samples were sonicated for 30 minutes, after which tubes were vortexed and then centrifuged for 10 minutes at 12000 G. Once centrifugation was complete, 100  $\mu$ L of the organic phase (top

layer of supernatant) was mixed with 870  $\mu\text{L}$  of methanol and 30  $\mu\text{L}$  of 12 M HCl within a 2 mL Eppendorf tube. Samples were vortexed and then incubated at 50  $^{\circ}\text{C}$  for 1 hour to undergo derivatization process. Following derivatization, samples were allowed to cool and 500  $\mu\text{L}$  of sterile water and 500  $\mu\text{L}$  of hexane (Sigma Aldrich, 270504) was added to the tube. Samples were vortexed and allowed to settle, after which 250  $\mu\text{L}$  of the top layer hexane was combined with 250  $\mu\text{L}$  of ethyl acetate within a GC-MS vial.

GC-MS measurements were conducted using an Agilent GC-MS 6890N (Agilent Technologies, USA) instrument. Utilizing a 1 $\mu\text{L}$  injection volume, samples were applied through a splitless helium inlet under a heater temperature of 250 C, a 7.91 psi pressure, and a total flow of 4.8 mL/min. Measurements were acquired under an Agilent 222-5532LTM column with capillary dimensions of 30 m by 250  $\mu\text{m}$  by 0.25  $\mu\text{m}$  nominally. Helium gas was flowed in under a 7.91 psi pressure at a flow rate of 0.6 mL/min and an average velocity of 17 cm/s. Oven temperatures were initially set at 50 C and ramped up to a maximum temperature of 325 C at a rate of 5 C/min for an overall runtime of 59 minutes.

#### *Mammalian Cell Toxicity*

A MTT assay was used to determine the toxicity of the blue light against mammalian CHO cells under *in vitro* settings. CHO cells were cultured in DMEM with 10% FBS until confluent and then removed through trypsin treatment, quantified with a cell counter and then resuspended in DMEM to a cell density of  $1 \times 10^6$  cell/mL. Wells in a 96-well plate were then supplemented with  $10^5$  CHO cells by adding 100  $\mu\text{L}$  of cell suspended media. Cells were allowed to adhere to the well bottom overnight at 37 $^{\circ}\text{C}$  with 5%  $\text{CO}_2$ .

Following adherence, DMEM media were removed *via* a vacuum tube, and the cells were washed twice with PBS. Following washing, 150  $\mu\text{L}$  of PBS was added to each well, after which cells were exposed to 30  $\text{J}/\text{cm}^2$  of blue light (200  $\text{mW}/\text{cm}^2$ , 5 min). After light exposure, PBS was removed and replaced with serum-free DMEM. For CHO cells treated with  $\text{H}_2\text{O}_2$ , cells were instead treated with pre-warmed DMEM supplemented with 0.1%  $\text{H}_2\text{O}_2$ . Following 1 minute of exposure, DMEM/ $\text{H}_2\text{O}_2$  media was removed from the wells and the cells were washed twice with PBS to remove any trace remains of  $\text{H}_2\text{O}_2$  before finally being replaced with serum-free DMEM. To maintain consistency, the non- $\text{H}_2\text{O}_2$  treated wells were also washed. To better quantify the effects of higher dosages of blue light (60  $\text{J}/\text{cm}^2$ ), a separate tolerance was performed in the process described above, only wells were filled with serum-free DMEM immediately following light treatment, with no washing to minimize cell detachment. CHO cells were then incubated at 37°C with 5%  $\text{CO}_2$  for 24 h to allow for remaining cells to recover from potential treatment-induced stress. After the recovery period had ended, the DMEM was removed, and 100  $\mu\text{L}$  of fresh DMEM was added to each well alongside 10  $\mu\text{L}$  of 5 mg/mL MTT (M6494; Life Technologies). Cells were incubated at 37°C with 5%  $\text{CO}_2$  for 4 h, after which the MTT/DMEM solution was removed and 100  $\mu\text{L}$  of filtered DMSO was mixed in and allowed to sit for 30 min to dissolve the crystalized formazan. The resulting dissolved formazan was quantified *via* absorbance measurements at 570 nm. This assay was performed in replicates of  $n = 4$ .

*In Vivo Candida Infection Murine Model*

Animal studies were approved by the Institutional Animal Care and Use Committee (IACUC) at Boston University and were performed in the Animal Science Center (ASC) in the Charles River Campus (CRC). For CFU and histology studies, a fungal abrasion model used by Dai et al was used. A total of 20 7-week-old balb/c mice (Jackson Laboratories, USA) were acquired, and two 1 cm by 1 cm abrasion wounds were generated on the back of each shaved mice using a #15 scalpel. Following wound generation, a 10  $\mu$ L droplet of log phase *C. albicans* containing a total fungal load of  $2 \times 10^6$  CFU was placed and evenly distributed over every wound with a pipette tip. The mice were then returned to their cage habitat for 3 hours to allow for surgery recovery and infection establishment. Following recovery, the mice wounds were separated into 4 groups: Untreated, blue light treated, H<sub>2</sub>O<sub>2</sub> treatment, and combination treatment, each consisting of 5 mice or a total of n = 10 wounds. Light was applied by treating wounds to a total of a total of 120 J/cm<sup>2</sup> of blue light (200 mW/cm<sup>2</sup>). Light treatment consisted of 2 5-minute light treatment sessions with a 5-minute break between sessions to allow for recovery. H<sub>2</sub>O<sub>2</sub> treatment consisted of application of 10  $\mu$ L of 0.5% H<sub>2</sub>O<sub>2</sub> directly to infected wounds until the droplet air evaporated. Combination treatment was performed by applying light treatment immediately followed by H<sub>2</sub>O<sub>2</sub> treatment. A total of 2 treatments were applied, one 3 hours after initial infection and another treatment 15 hours later. 2 Hours following the second light treatment, mice were euthanized, and half of the tissue was harvested and fixed in 10% buffered formalin, while the other half was homogenized in PBS and plated on *C. albicans*-specific BiGGY agar plates (73608,

Sigma-Aldrich). Histology samples were submitted to the Boston University Experimental Pathology Laboratory Service Core for processing and periodic acid-Schiff (PAS) staining. Histology slides were visualized under a VS120 Virtual Slide Scanner (Olympus).

#### *Ex Vivo Candida Infection Human Model*

In addition to murine abrasion wounds, EpiDerm Skin Scaffolds (EPI-202, Mattek) were used to evaluate the impact of catalase deactivation on *C. albicans* cutaneous infections within a human *ex vivo* model. EpiDerm Skin Scaffolds mimic human skin, acting as a highly differentiated 3D tissue model consisting of human-derived epidermal keratinocytes. These tissue inserts can be used to stimulate the human epidermis and dermis. For the 8 inserts infected, half were left untreated while the other half were treated with combination treatment. Using a #15 scalpel, 2 cutaneous abrasions were applied to the surface, after which a 20  $\mu$ L aliquot of PBS containing  $2 \times 10^6$  CFU of overnight cultured *C. albicans* SC5314 was placed on the surface of the skin and incubated for 4 hours at 37°C with 5% CO<sub>2</sub>. Following incubation, the surface of the skin was gently washed with PBS to remove excess *Candida* and treated to a combination of 120 J/cm<sup>2</sup> of CW-405 (200 mW/cm<sup>2</sup>) and 0.5% H<sub>2</sub>O<sub>2</sub>. Light application methodology was the same as within the *in vivo* model. After an additional two hours of incubation at 37°C with 5% CO<sub>2</sub>, EpiDerm membranes were either homogenized (n = 3) in PBS or fixed in formalin (n =1) for PAS staining. CFU measurements were performed on BiGGY agar plates while histology samples were submitted to the Boston University

Experimental Pathology Laboratory Service Core for processing and PAS staining.

Histology slides were visualized under a VS120 Virtual Slide Scanner.

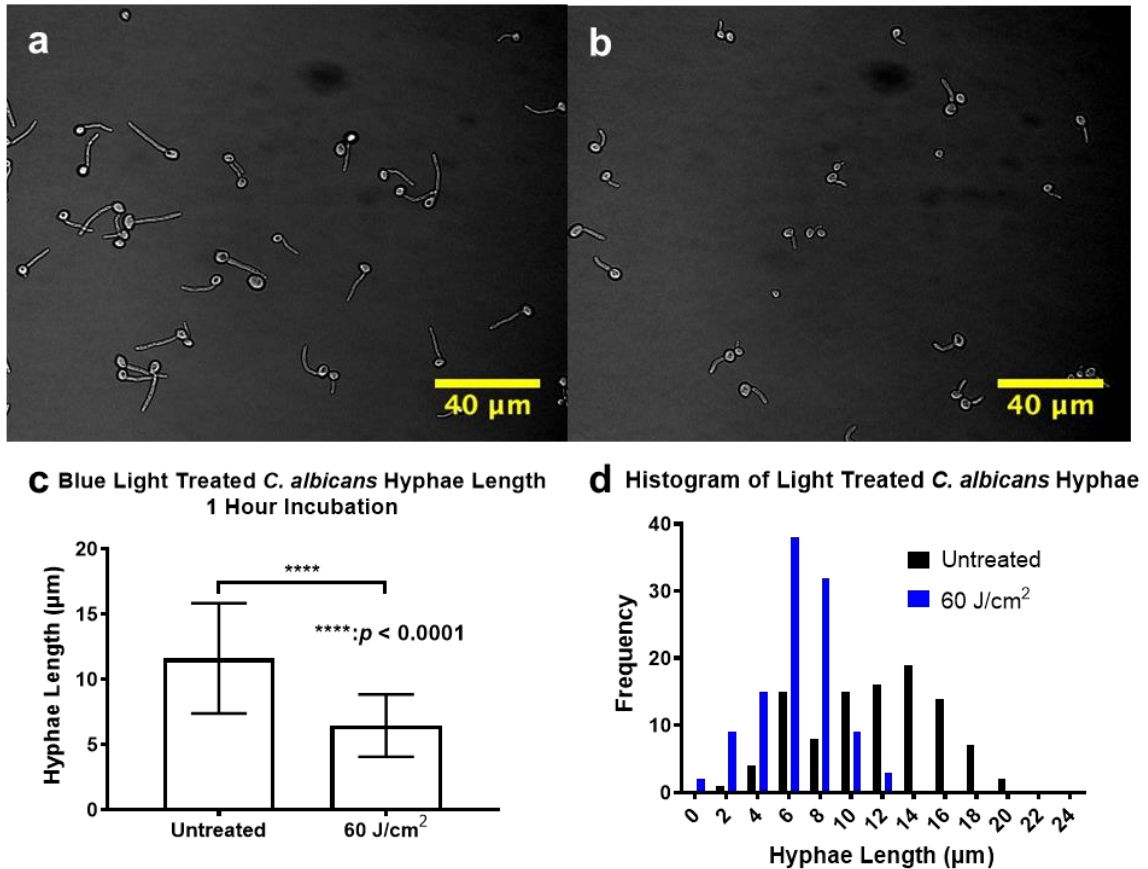
#### *Statistical Analysis*

Statistical analysis was performed through Student's unpaired *t*-tests conducted through PRISM 9. Significance was set at *P*-values < 0.05.

#### *Study Approval*

Animal studies were approved by the Institutional Animal Care and Use Committee (IACUC) at Boston University and were performed in the Animal Science Center (ASC) in the Charles River Campus (CRC) under approved protocol PROTO201800535. The blood drawing process for neutrophil extraction was approved by the Massachusetts General Hospital Institutional Review Board under approved protocol number 2019P002840.

## Results

*Blue Light Treatment and Catalase Deactivation in Candida Species*

**Figure 14: Blue Light Suppresses *C. albicans* Hyphae Formation.** Phase-contrast imaging of a) untreated and b) CW-405 (60 J/cm<sup>2</sup>) blue light treated *C. albicans* following 1 hour of incubation under hyphae inducing conditions. c) Average length of hyphae for untreated and light treated *C. albicans* measured from confocal images. d) Histogram distribution of average hyphae length for untreated and light treated *C. albicans*. \*\*\*\*:  $p < 0.0001$ . Data published in Jusuf et al., *Photochemistry and Photobiology*, 2022.<sup>85</sup>

Following 1 hour of incubation in hyphae forming conditions, untreated *C. albicans* were found to exhibit strong hyphae development (**Figure 14a**) while blue light treated *C. albicans* exhibited significantly reduced hyphae growth (**Figure 14b**). Measurements of hyphae lengths reveal that untreated *C. albicans* (n = 101) exhibited an average hyphae length of  $11.62 \pm 4.22 \mu\text{m}$ , while light treated *C. albicans* (n = 108)

demonstrated an average hyphae length of  $6.47 \pm 2.39 \mu\text{m}$ , correlating to an average hyphae length decrease of 44.3% (**Figure 14c**). Additional histogram plotting of hyphae lengths reveals that around 72% of untreated hyphae were over  $10 \mu\text{m}$  (**Figure 14d**). In contrast, only 11% of light-treated cells exhibited hyphae lengths over  $10 \mu\text{m}$ .

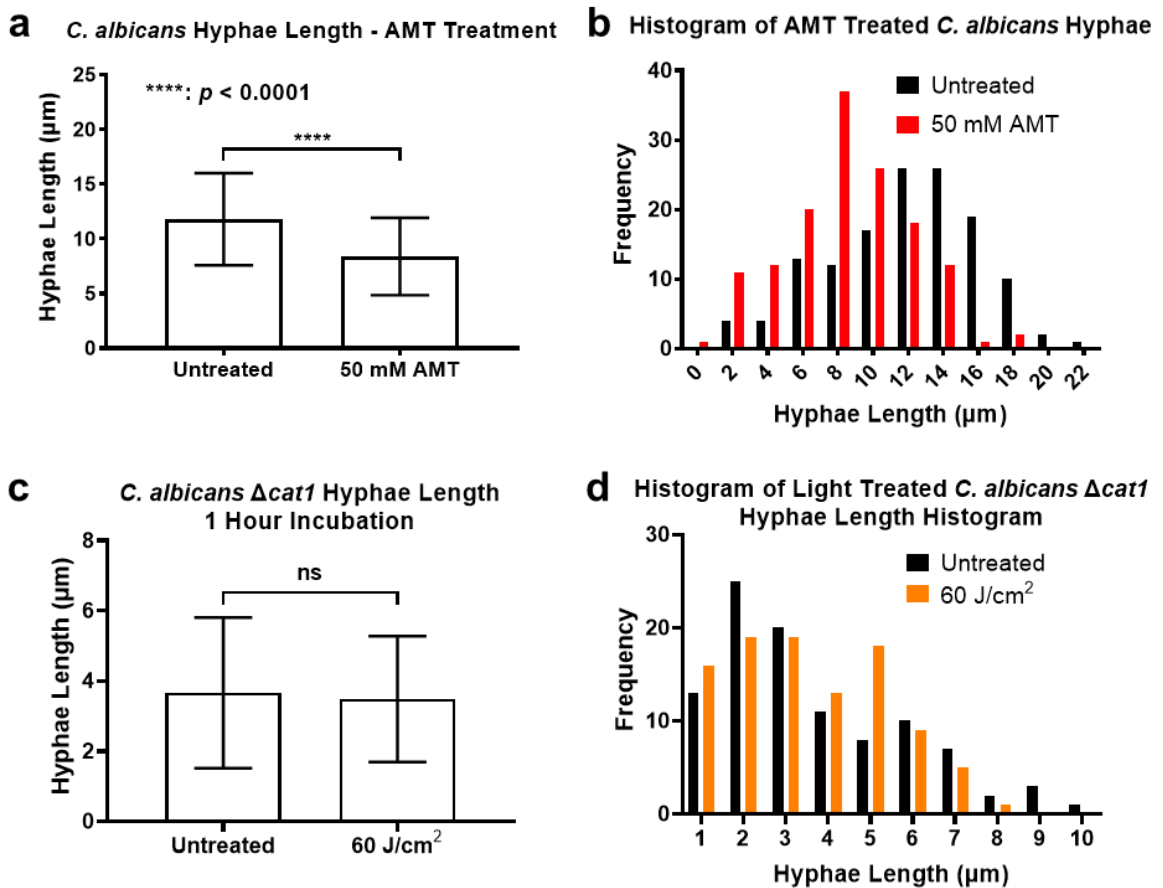


**Figure 15: Hyphae Lengths of Catalase Deactivated *C. albicans*.** a) Average length of hyphae for untreated and 50 mM incubated *C. albicans* measured from phase contrast images. b) Histogram distribution of average hyphae length for untreated and AMT treated *C. albicans*. c) Average length of hyphae for untreated and CW-405 (60 J/cm<sup>2</sup>) blue light treated catalase deficient *C. albicans*  $\Delta\text{cat1}$  following 1 hour of incubation under hyphae inducing conditions measured from phase contrast images. d) Histogram distribution of average hyphae length for untreated and light treated *C. albicans*  $\Delta\text{cat1}$ . \*\*\*\*:  $p < 0.0001$ , ns = No Significance. Data published in Jusuf et al., *Photochemistry and Photobiology*, 2022.<sup>85</sup>

To confirm that catalase deactivation was responsible for this phenomenon, tests were performed on both chemically and genetically catalase inactivated *C. albicans*. For

chemical deactivation, *C. albicans* was incubated in 50 mM of catalase inhibitor AMT. Non-AMT treated *C. albicans* hyphae (n = 134) were found to exhibit an average hyphae length of  $11.8 \pm 4.2 \mu\text{m}$ , while AMT treated *C. albicans* hyphae (n = 140) exhibited an average hyphae length of  $8.4 \pm 3.5 \mu\text{m}$  (**Figure 15a**). Histogram data of hyphae lengths indicates that 75% of measured untreated cells had hyphae lengths over  $10 \mu\text{m}$ , while AMT treated *C. albicans* had 42% of light treated cells exhibit hyphae lengths over  $10 \mu\text{m}$  (**Figure 15b**). The role of catalase in hyphae growth was also further examined by applying blue light to catalase deficient *C. albicans*  $\Delta\text{cat1}$  strain. While many cells in both the untreated and light treated groups exhibited no hyphae growth at all, measurements of detected hyphae found that untreated *C. albicans*  $\Delta\text{cat1}$  (n = 100) expressed an average hyphae length of  $3.7 \pm 2.1 \mu\text{m}$ , while light treated *C. albicans*  $\Delta\text{cat1}$  (n = 100) expressed an average hyphae length of  $3.5 \pm 1.8 \mu\text{m}$  (**Figure 15c**). Histogram data of the catalase deficient mutant indicates that untreated *C. albicans*  $\Delta\text{cat1}$  only showed slightly longer hyphae lengths, with 23% of untreated mutant hyphae measuring greater than  $6 \mu\text{m}$  compared to 15% of the light treated mutant hyphae. (**Figure 15d**) However, the vast majority of *C. albicans*  $\Delta\text{cat1}$  hyphae in both treatment groups remained below  $4 \mu\text{m}$ , accounting for 69% of untreated hyphae and 67% of the light treated hyphae.

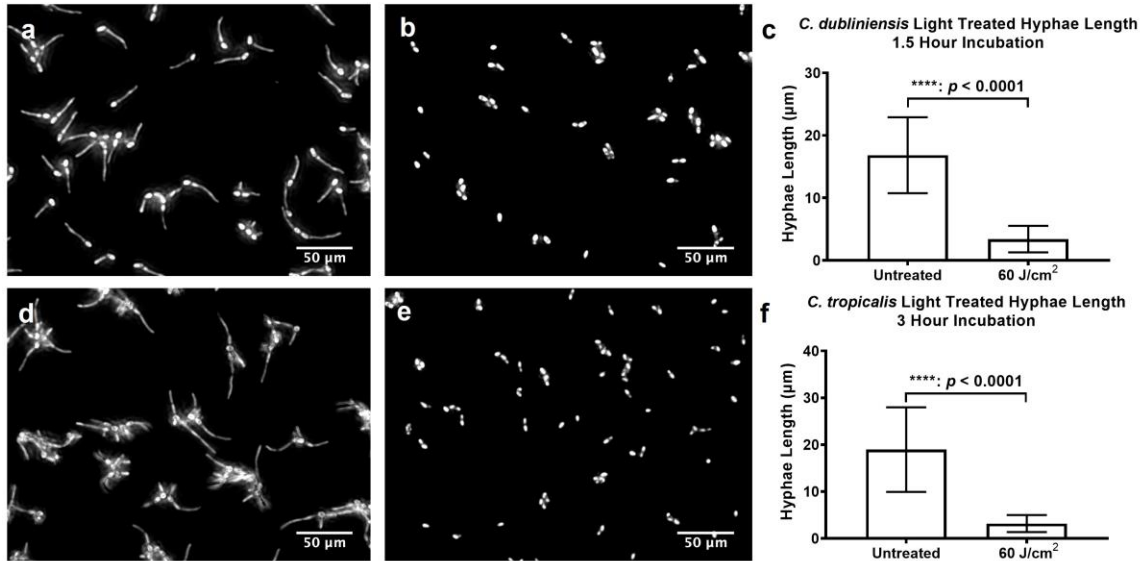
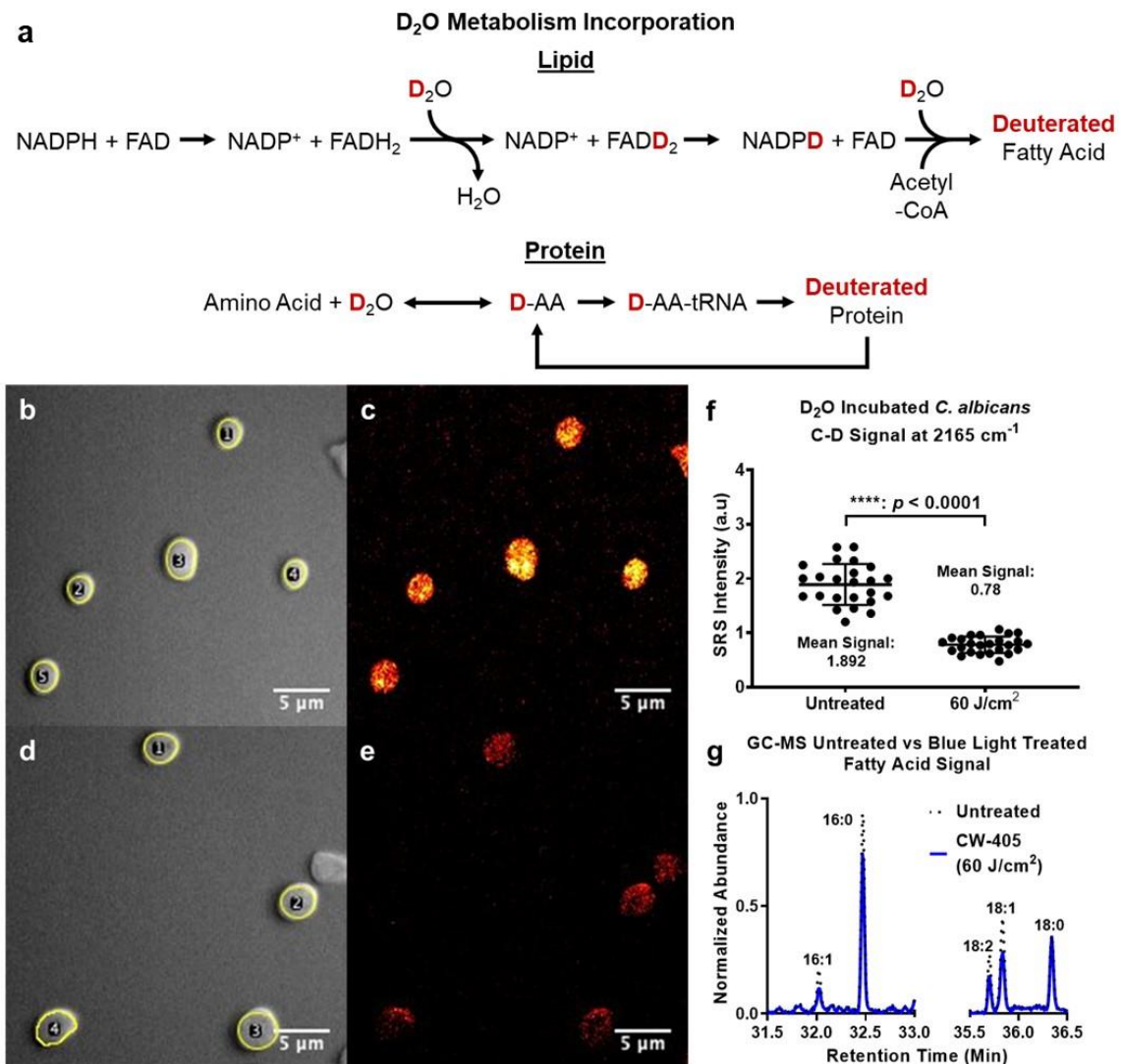


**Figure 16: Blue Light Induced Hyphae Suppress Occurs Across Multiple Candida Strains.** Phase contrast imaging of a) untreated and b) CW-405 (60 J/cm<sup>2</sup>) treated *C. dubliniensis* following 1.5 hours of incubation under hyphae inducing conditions. c) Average length of hyphae for untreated and light treated *C. dubliniensis* measured from confocal images. Phase contrast imaging of d) untreated and e) CW-405 (60 J/cm<sup>2</sup>) treated *C. tropicalis* following 3 hours of incubation under hyphae inducing conditions. f) Average length of hyphae for untreated and light treated *C. tropicalis* measured from confocal images. \*\*\*\*:  $p < 0.0001$ . Data published in Jusuf et al., *Photochemistry and Photobiology*, 2022.<sup>85</sup>

While *C. albicans* is the most prominent *Candida* species capable of transitioning to a hyphae form, other *Candida* species exhibit similar dimorphism, such as *C. dubliniensis* and *C. tropicalis*. Following incubation at 37°C with 5% CO<sub>2</sub> in complete RPMI for 1.5 hours, untreated *C. dubliniensis* hyphae (n = 50) (**Figure 16a**) was found to exhibit hyphae lengths of 16.8 ± 6.0 µm, while light treated *C. dubliniensis* hyphae (n = 50) (**Figure 16b**) exhibited average hyphae lengths of 3.4 ± 2.1 µm (**Figure 16c**). Similarly, *C. tropicalis* incubated in hyphae forming conditions for 3 hours were found to exhibit similar reductions in hyphae formation following light exposure. Untreated *C. tropicalis* hyphae (n = 50) (**Figure 16d**) was found to exhibit hyphae lengths of 18.9 ± 8.9 µm, while light treated *C. tropicalis* hyphae (n = 50) (**Figure 16e**) exhibited average

hyphae lengths of  $3.2 \pm 1.8 \mu\text{m}$  (**Figure 16f**). These results indicate the hyphae suppressing abilities of aBL are not exclusive to only *C. albicans* and are broadly applicable to a wide range of hyphae forming *Candida* pathogens.

*Fungal Metabolism of Catalase Deactivated C. albicans*

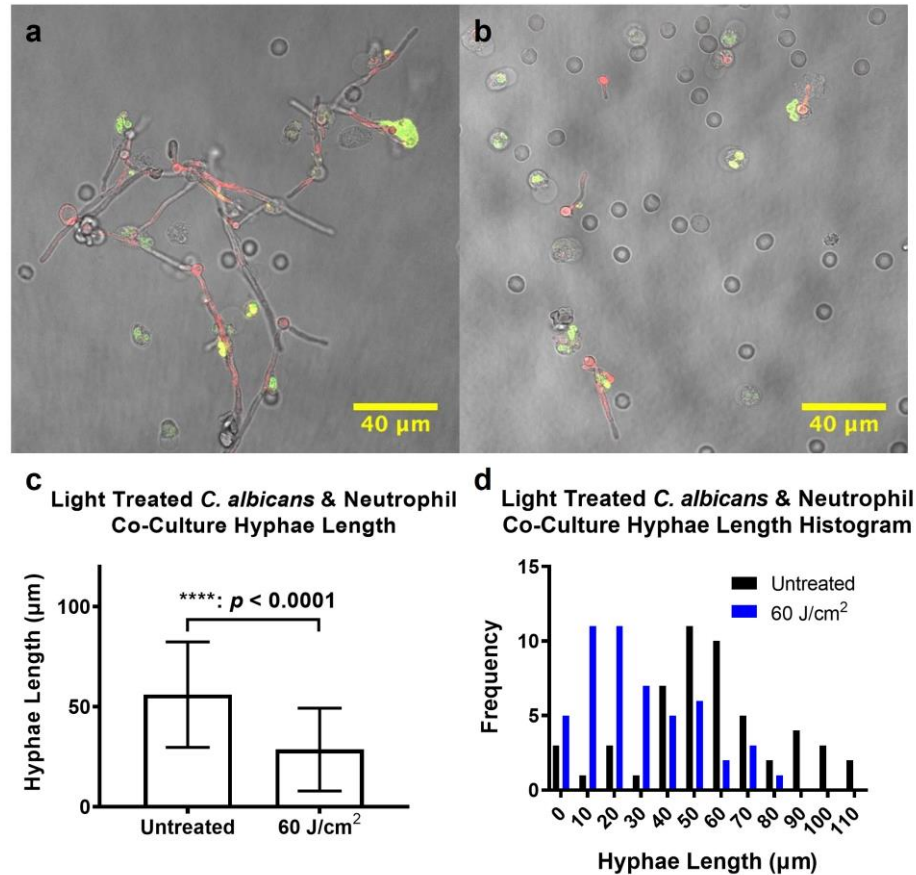


**Figure 17: Quantification of D<sub>2</sub>O Metabolic Incorporation can Detect Changes in Cellular Metabolism.** a) Method of utilizing D<sub>2</sub>O to label proteins and lipids within cells. Stimulated Raman scattering imaging of *C. albicans* treated with 90% D<sub>2</sub>O for 1 hour under hyphae forming conditions reveals changes in general metabolism. b) Transmission imaging and c) C-D bond imaging at 2165 cm<sup>-1</sup> of untreated *C. albicans*. d) Cross-phase transmission imaging and f) C-D bond imaging at 2165 cm<sup>-1</sup> of light treated *C. albicans* (60 J/cm<sup>2</sup>). g)

**Change in average single-cell mean C-D bond SRS intensity between untreated and light treated *C. albicans*. f) GC-MS normalized abundance peaks of fatty acids Palmitic Acid (16:0), Palmitoleic Acid (16:1), Stearic Acid (18:0), Oleic Acid (18:1), and Linoleic Acid (18:2) present within untreated and light treated *C. albicans* incubated under fatty acids. Peaks were normalized against a pentadecanoic acid (15:0) internal standard. \*\*\*\*:  $p < 0.0001$ . Data published in Jusuf et al., *Photochemistry and Photobiology*, 2022.<sup>85</sup>**

To visualize the intracellular metabolic activity and quantify changes in metabolism at a single cell level, SRS C-D imaging was used to quantify the incorporation of D<sub>2</sub>O into biomass under hyphae forming conditions with and without light treatment. In the presence of D<sub>2</sub>O, NADPH undergoes rapid enzyme-catalyzed exchange between the hydrogen atom in NADPH and the deuterium isotope, forming NADPD. (**Figure 17a**) Since production of new fatty acids are dependent on NADPH, replacement of NADPH with NADPD allows for the incorporation of deuterium into fatty acids, generating the C-D bond that can be quantified through vibrational SRS imaging at the 2165 cm<sup>-1</sup> wavenumber<sup>122,124,125</sup>. While newly synthesized proteins are also labeled through D<sub>2</sub>O metabolism, the presence of D<sub>2</sub>O labeled fatty acids can be confirmed by the presence of high intensity lipid droplets, which are a key method of storing newly produced fatty acids<sup>126</sup>. Significant changes in the presence and intensity of these lipid droplets can be used to evaluate changes in lipid metabolism. Individual non-light treated *C. albicans* (n = 24) incubated in 90% D<sub>2</sub>O and hyphae forming conditions for 1 hour (**Figure 17b**) were found to exhibit strong C-D signal (**Figure 17c**). In contrast, individual light treated *C. albicans* (n = 25) (**Figure 17d**) were found to exhibit minimal C-D signals across the entirety of the cell body (**Figure 17e**). Quantification of the average C-D SRS signal values for the D<sub>2</sub>O treated cells found individual light treated *C. albicans* to experience a 58.8% decrease in C-D signal intensity (**Figure 17f**). In

addition, high intensity C-D signal within the untreated cells were found to exhibit small intracellular lipid droplets with high SRS intensities, while the remaining part of the yeasts cells often yielded lower intensities, mostly contributed by the protein signals. These high intensity lipid droplets were completely absent in the light treated fungi cells, indicating a significant disruption in the lipid production. The SRS C-D imaging results confirmed that the *de novo* lipogenesis is significantly inhibited under light treatment in *C. albicans*. Additional usage of GC-MS to quantify changes in lipid contents indicated that, following normalization of free fatty acid peaks via a pentadecanoic acid internal standard, significant decreases in peak heights corresponding to saturated palmitic acid as well as the unsaturated fatty acids palmitoleic acid, oleic acid, and linoleic acid were directly observed. (**Figure 17g**) Additional implementation of blank peak area subtraction and internal standard normalization would further reveal greater decreases in both saturated and unsaturated fatty acids. Decreases of 78.2% and 74.9% were observed in palmitic acid and stearic acid, respectively. Meanwhile, unsaturated fatty acids palmitoleic, oleic, and linoleic acids decreased by 25.7%, 23.6%, and 31.2%, respectively. These results act as further confirmation regarding the overall decrease in fatty acid metabolism observed within hyphae-producing conditions following light induced catalase deactivation.

*C. albicans* and Neutrophil Co-Culture

**Figure 18: Hyphae Growth of *C. albicans* Co-Cultured with Neutrophils.** Both a) untreated and b) light treated ( $75 \text{ J/cm}^2$ ) *C. albicans* were cultured in complete RPMI media at  $37^\circ \text{C}$  for 4 hours and imaged under a confocal microscope. c) Average length of hyphae for untreated and light treated *C. albicans* within co-culture measured from confocal images. d) Histogram distribution of average hyphae length for untreated and light treated *C. albicans* within co-culture. \*\*\*\*:  $p < 0.0001$ . Data published in Jusuf et al., *Photochemistry and Photobiology*, 2022.<sup>85</sup>

To determine if light induced catalase inactivation would also impact hyphae development in the presence of innate immune cells, light-treated *C. albicans* were incubated alongside harvested neutrophils in a multiplicity of infection (MOI) of 1:20. Confocal imaging of neutrophil co-cultured *C. albicans* found untreated *C. albicans* able to easily escape from neutrophil capture through hyphae formation (**Figure 18a**). In contrast, light-treated *C. albicans* exhibited significant reductions in overall hyphae

growth and development (**Figure 18b**). Measurements of average hyphae lengths in the untreated co-culture ( $n = 51$ ) were found to be  $56.1 \pm 26.1 \mu\text{m}$ , while light treated fungi ( $n = 52$ ) in the co-culture experienced reduced hyphae growth by around 49% to  $28.6 \pm 20.4 \mu\text{m}$  (**Figure 18c**). Further investigations into overall hyphae length reveal that around 13% of untreated hyphae within the co-culture were less than  $20 \mu\text{m}$  in length, in contrast to the 53% of light treated hyphae (**Figure 18d**). The inhibition of hyphae growth in light treated fungi remained extremely statistically significant in both the solo-culture and co-culture conditions, with a 44% decrease in hyphae length observed in the light treated solo-culture while a 49% decrease in hyphae length was observed in the neutrophil co-culture. The presence of the neutrophils appeared to suppress hyphae growth by an additional 5% and may indicate that neutrophils can positively contribute to the inhibition of hyphae development alongside light treatment.

#### Fungal Catalase Deactivation Mammalian Translation

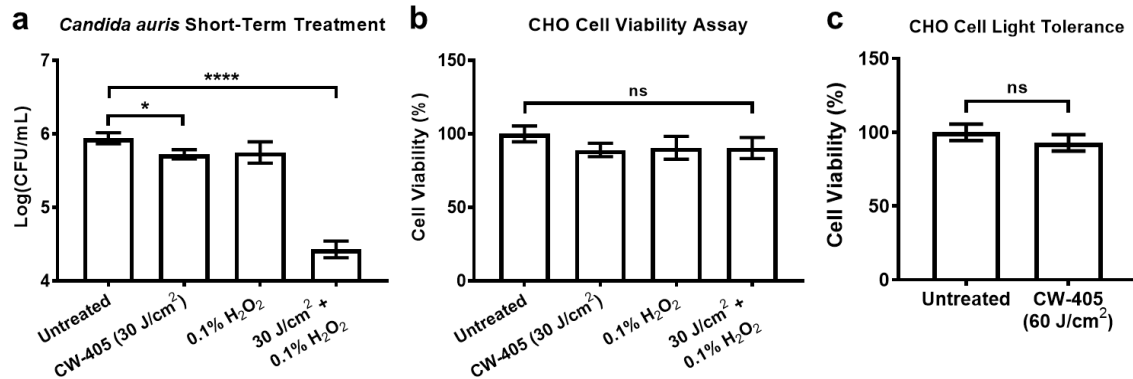


**Figure 19: Blue Light and Short Term, High Concentration H<sub>2</sub>O<sub>2</sub> Against Mammalian and Fungal Cells.** CFU/mL measurements of a) *Candida auris* 2 (AR-0382) treated with 30 J/cm<sup>2</sup> of CW-405 (200 mW/cm<sup>2</sup>, 2.5 minutes) and 0.1% H<sub>2</sub>O<sub>2</sub> (1 minute incubation). b) An MTT assay with CHO cells using the same conditions found no change in viability in response to the treatment. c) An additional MTT assay of CHO cells with higher light dosage (60 J/cm<sup>2</sup>) found higher light dosages to have no impact on mammalian cell viability. \*\*\*\*:  $p < 0.0001$ , \*:  $p < 0.05$ , ns = No Significance. Data adapted from Dong et al., *JCI Insight*, 2022<sup>34</sup> and Jusuf et al., *Photochemistry and Photobiology*, 2022<sup>85</sup>.

While the downstream effects of blue light induced catalase deactivation results in a disruption of the hyphae forming capabilities of *Candida* strains, to take advantage of this phenomenon, as well as the light induced ROS sensitization previously observed in fungal cells, the mammalian cell tolerance and toxicity of this treatment will need to be first quantified. As such, like previous bacterial studies, the effectiveness of blue light with short-term, higher concentration H<sub>2</sub>O<sub>2</sub> was measured on a multidrug resistant *Candida auris* strain followed by MTT viability assays with mammalian CHO cells. For *C. auris*, while treatments of 30 J/cm<sup>2</sup> of aBL and 1 minute exposure to 0.1% H<sub>2</sub>O<sub>2</sub> had minimal to no effect on the CFU/mL of *C. auris* individually, in combination the treatment resulted in a near 95% reduction in CFU/mL (**Figure 19a**). When this same treatment was applied to CHO cells in an MTT assay, both the individual treatments as well as the combination treatment was found to have no effect on the overall viability of the CHO cells (**Figure 19b**), indicating that the mammalian cells were easily able to tolerate the combination treatment, as well as confirming that unlike fungal cells, mammalian cells were capable of tolerating H<sub>2</sub>O<sub>2</sub> for short durations even with the potential deactivation of their own catalase. Furthermore, when applying the same 60 J/cm<sup>2</sup> blue light dosages used to induce hyphae suppression in dimorphic *Candida* strains, CHO cells exhibited no toxicity to the light dosage (**Figure 19c**). The ability for mammalian cells to not only tolerate the ROS sensitization and exogenous H<sub>2</sub>O<sub>2</sub> treatment that would be toxic to even multidrug resistant fungal strains, as well as its ability to tolerate dosages of light that can cause hyphae suppression in fungi, offers a promising indication of the technology's viability within in vivo systems and

environments.

### *In Vivo Fungal Murine Models*

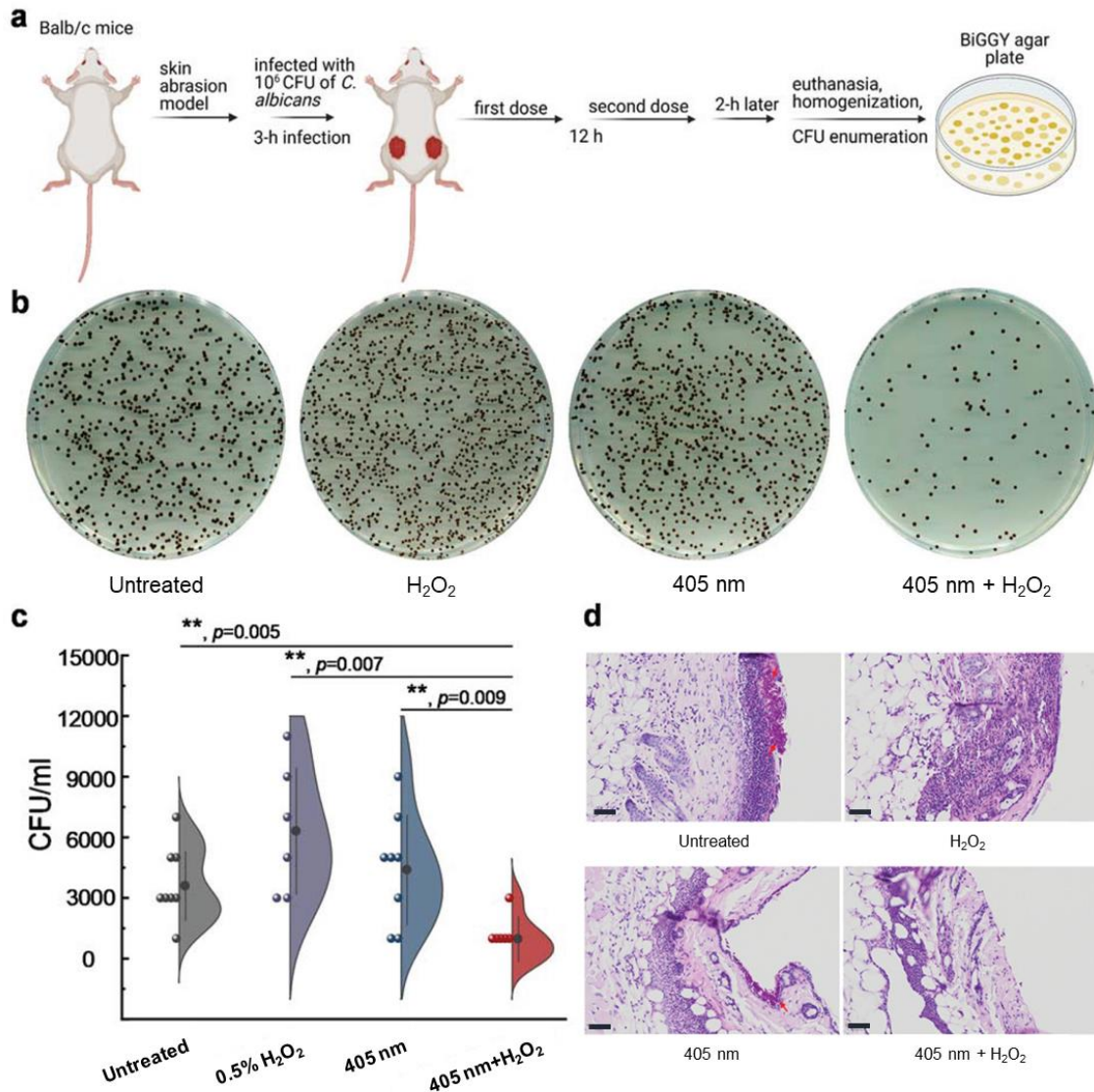


**Figure 20: Catalase Photodeactivation and  $H_2O_2$  Synergistically Reduces *C. albicans* Bioburden Within a Murine Abrasion Model.** a) Treatment regimen of blue light and  $H_2O_2$  for fungal infected murine abrasion wounds. b) *C. albicans* selective BiGGY agar plates of homogenized wound tissue following treatment regimen. c) CFU/mL of homogenized murine tissue following treatment regimen. d) PAS-stained histology slides of *C. albicans* infected mice following treatment regimen. Scalar bar: 50  $\mu$ m. Fungal colonization area was pointed by red arrows.  $**$ :  $p < 0.01$ . Outlier was determined through whisker box plot analysis. Data published in Dong et al., *Advanced Science*, 2022.<sup>86</sup>

Following the establishment of the importance of the ability for light induced catalase deactivation to suppress hyphae development within *Candida* infections, tests were conducted on a *in vivo* *C. albicans* infected murine abrasion wound model previously established by Hamblin et al. specifically suited for phototherapy<sup>127</sup>. Not only was the goal to examine the effects of aBL on hyphae formation within a wound environment, but it was also intended to determine whether the light induced *Candida* ROS sensitization previously observed *in vitro* would also be applicable *in vivo*. 3 hours following the initial generation of the infected abrasion wounds, the fungal wounds were treated with either 120 J/cm<sup>2</sup> of CW-405, 0.5% H<sub>2</sub>O<sub>2</sub>, or a combination of the two. The second treatment was applied 12 hours following the first treatment, and 2 hours after the second treatment, mice were euthanized and the infected wounds were harvested, homogenized, and plated for CFU quantification (**Figure 20a**). CFU quantification on *C. albicans* selective BiGGY agar plates immediately indicate that the combination treatment resulted in a significant reduction in overall fungal bioburden (**Figure 20b**), and further quantification of the CFU/mL of *C. albicans* additionally reveals that the combination treatment resulted in the greatest reduction in fungal CFU load compared to the other treatment groups (**Figure 20c**). While these results indicate the effective ROS sensitization of *C. albicans* within the *in vivo* wound environment, additional histological studies performed through H&E staining of infected wounds after the two-treatment regimen reveal that while strong hyphae growth can be observed in the untreated wound, aBL treatment significantly suppresses hyphae development, similar to the *in vitro* observations (**Figure 20d**). Furthermore, the histology of combination treated wounds

revealed a reduction of *C. albicans* presence on the skin, correlating with the CFU measurements.

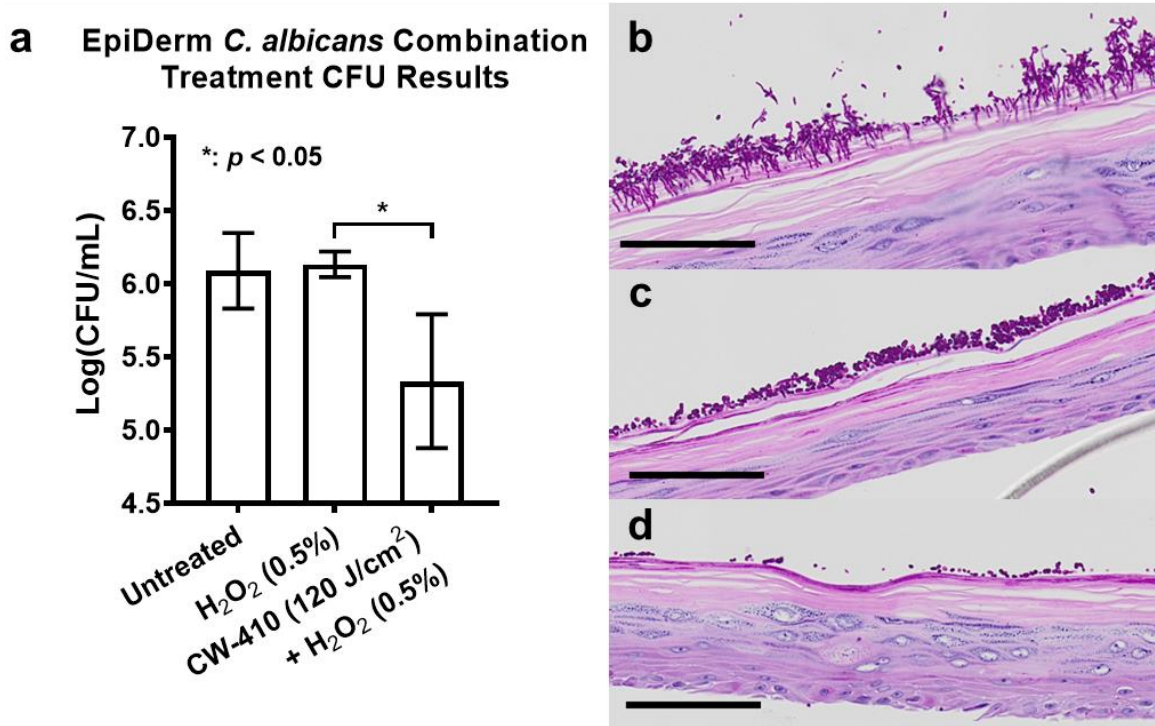


**Figure 21: Catalase deactivation and H<sub>2</sub>O<sub>2</sub> treatment within a EpiDerm skin scaffold model. (a) CFU of *C. albicans* infected EpiDerm scaffold following treatment and homogenization. PAS staining of (b) untreated skin, (c) H<sub>2</sub>O<sub>2</sub> treated, and (d) combination CW-405 and H<sub>2</sub>O<sub>2</sub> treated scaffold skin model. Combination treated skin exhibits significantly lower *Candida* bioburden and hyphae growth. Scale bar: 100 μm. \*:  $p < 0.05$ .**

To further examine the potential translatability of this technology, an preliminary *ex vivo* infection model was used to evaluate the effects of this combination treatment on human skin infections through the usage of an EpiDerm Skin Scaffold 3D tissue insert. These EpiDerm Skin Scaffolds have previously been used to evaluate the fungal dermatophyte infection process and how it interacts with the epidermal layers of artificial human skin<sup>128</sup>. These scaffolds can be used to further determine the translatability of the

blue light technology on a more human like skin environment. From CFU measurements, combination treatment was found to demonstrate a near 1-log CFU reduction in *Candida* bioburden from the untreated or H<sub>2</sub>O<sub>2</sub> treated group. (**Figure 21a**) In addition, histological staining of tissue inserts reveal that while untreated skin scaffolds exhibit the same large scale hyphae formation and skin colonization (**Figure 21b**), the implementation of just H<sub>2</sub>O<sub>2</sub> treatment resulted in reduced hyphae formation but high remaining surface colonization (**Figure 21c**). In contrast, both light and H<sub>2</sub>O<sub>2</sub> treatment results in the no observable hyphae formation and reduced fungal skin colonization (**Figure 21d**), correlating not only with the CFU measurements, but also mimicking the results observed previously within the *in vivo* murine model.

### Catalase Deactivation on Non-Candida Fungi

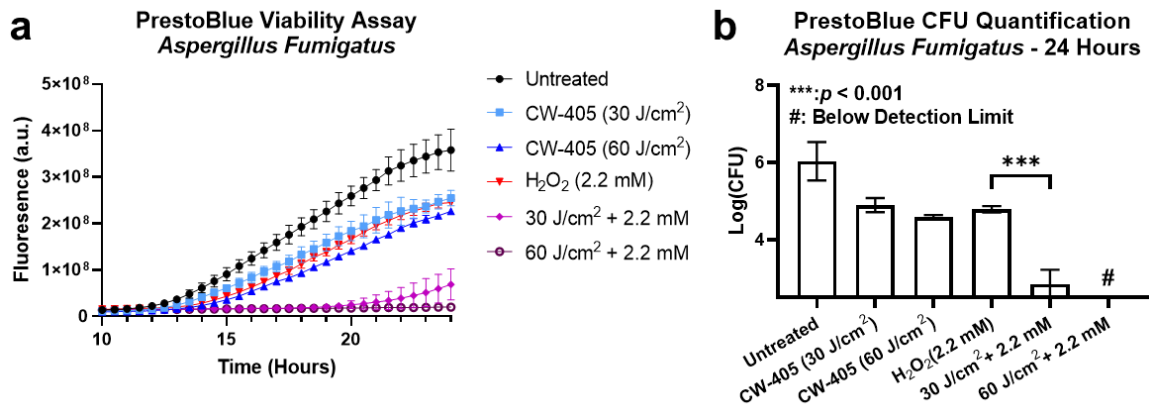


**Figure 22: Catalase Photodeactivation on Non-Candida Fungal Strains.** a) Application of 30 or 60 J/cm<sup>2</sup> of 405 nm blue light and 2.2 mM of H<sub>2</sub>O<sub>2</sub> was found to reduce the viability of *Aspergillus fumigatus*, a filamentous mold. b) Converting the viability to CFU measurements reveals that combining light treatment and H<sub>2</sub>O<sub>2</sub> results in the complete eradication of the filamentous mold. \*\*\*: p < 0.001, # = Below Detection Limit.

While extensive investigation has been performed on the interactions of catalase deactivation on *Candida* fungal species, to further develop the potential translatability of

this technology, the viability of phototherapy on non-*Candida* species is necessary. Investigations on the impact of aBL on the filamentous mold *Aspergillus fumigatus* indicates that light alone can reduce the overall viability of *A. fumigatus* to a similar degree to H<sub>2</sub>O<sub>2</sub> alone (**Figure 22a**). After 24 hours of incubation, CFU measurements of solo treatments of 30 J/cm<sup>2</sup> of CW-405 or 2.2 mM H<sub>2</sub>O<sub>2</sub> only reduced the overall CFU population by 1-log, while 60 J/cm<sup>2</sup> of exposure resulted in a 1.5-log reduction. However, when combined, 30 J/cm<sup>2</sup> and H<sub>2</sub>O<sub>2</sub> reduced CFU by 3-log, while 60 J/cm<sup>2</sup> and H<sub>2</sub>O<sub>2</sub> appeared to completely eradicate all *Aspergillus* spores (**Figure 22b**).

### Discussion and Conclusion

The ability for blue light to inactivate catalase has been previously observed by the Cheng Lab in various *Candida* strains. While decreased hyphae lengths were observed for light treated *C. albicans* incubated in the presence of RAW 264.7 macrophages, this phenomenon was not explored further in depth since the primary focus of the study was on fungal ROS sensitization<sup>86</sup>. Examining this phenomenon in greater detail, additional experiments conducted on the hyphae forming ability of *C. albicans* following treatment with catalase inactivating aBL reveal that this hyphae reducing phenomenon occurs independently of immune cell presence, reducing hyphae lengths by 44.3%. The contribution of catalase deactivation to the inhibition of hyphae formation was further supported by the similar inhibition patterns observed within *C. albicans* hyphae incubated within 50 mM of the chemical catalase inhibitor AMT, resulting in a 28.8% reduction in average hyphae lengths. Previous studies have revealed that disruption of the catalase gene can suppress hyphae development in hyphae inducing

conditions<sup>113</sup> and while both light-induced and chemical-induced catalase inhibition is capable of inactivating the catalase currently present within the fungi cells, the significantly shorter hyphae observed indicate that new catalase can still be developed during the culturing process. This indicates that the effects of hyphae inhibiting effects of catalase deactivation are only temporary, as the lack of catalase gene disruption ensures the fungi will eventually be able to recover the catalase it initially lost. The importance of catalase in the hyphae production process was further supported by the significantly inhibited hyphae production observed in the catalase deficient *C. albicans*  $\Delta cat1$  mutants, where the average length of untreated mutant hyphae was 68.1% lower the untreated hyphae of their wild type strain. The suppressed hyphae development observed in untreated  $\Delta cat1$  mutants is consistent with the lowered pathogenicity and survival capabilities of catalase deficient *C. albicans* mutants within murine infection models, as the loss of catalase would render fungal cells more susceptible to the ROS burst produced by immune cells and the suppressed hyphae development would prevent the fungi from escaping immune cell phagocytosis through hyphal penetration<sup>104,108,129</sup>. Furthermore, blue light alone had no significant effect on the inhibited hyphae development of *C. albicans*  $\Delta cat1$ , with light treated mutants only exhibiting a 4.8% reduction average hyphae length. The lack of significant change between the untreated and light treated mutants indicate that the ROS produced by the aBL alone is not enough to significantly damage the interior cell mechanisms, and that additional sources of ROS are necessary to fully suppress hyphae growth. The fact that hyphae growth was observed at all in the catalase deficient mutants can be likely attributed to the presence of alternative

antioxidant proteins such as thiol specific antioxidant, *TSAI*, which could exert similar antioxidant activity at a much lower effectiveness than catalase<sup>116</sup>. Regardless, the significantly greater hyphae inhibition observed within the light treated wild type *Candida* strain and the absence of significant inhibition between the untreated and light treated catalase deficient mutants not only confirms the importance of catalase in the development and propagation of hyphae, but it also indicates that it is the specific removal of catalase from the *C. albicans* and its cascading downstream effects that is primarily responsible for the hyphae suppressing effects of light treatment.

Similar trends of hyphae inhibition were observed across multiple hyphae forming *Candida* species like *C. dubliniensis* and *C. tropicalis*. This indicates that the hyphae inhibiting effect of blue light is due to a specific disruption in the hyphae forming mechanism of fungi, and not due to specific interactions exclusive to *C. albicans*. While the presence of shorter hyphae in the light treated *C. albicans* indicates that light treatment damages neither the key genes involved in hyphae production like *UME6* or *EEDI* nor the environmental pathways responsible for detecting hyphae inducing environmental conditions<sup>107</sup>, the inhibited growth observed points to a potential disruption in the polarized growth of hyphae. As previously discussed, catalase has a close association with lipid metabolism, and studies have indicated that polarized hyphal growth is partly driven by the formation of sterol and sphingolipid-rich lipid rafts at the tips of hyphae growths<sup>130</sup>. Inhibition in either sterol or sphingolipid biosynthesis via chemical inhibitors has been found to result in lowered membrane polarization and hyphae growth in treated *C. albicans*, demonstrating the vital role that lipid metabolism

plays in the development of hyphae<sup>111</sup>. Sphingolipids in general have also been found to contribute to nearly 30% of the lipid membrane in yeast cells<sup>131</sup>, indicating that sphingolipid production is a necessary component of plasma membranes, which are heavily extended during hyphae formation. Given the significant role lipid metabolism plays in hyphae development, aspects of lipid metabolism altered through light treatment were assayed on a single cell level through D<sub>2</sub>O metabolism analysis and on a bulk level through mass spectroscopy, focusing primarily on the production of free fatty acids. In eukaryotic organisms like fungi, fatty acids are primarily synthesized through NADPH incorporation into acetyl-CoA<sup>132</sup>. During D<sub>2</sub>O treatment, rapid FAD/FADH<sub>2</sub>-catalyzed exchange between the hydrogen atom in NADPH and the deuterium atom in D<sub>2</sub>O results in the formation of NADPD. This NADPD can then be utilized in fatty acid synthesis in lieu of traditional NADPH, resulting in the incorporation of deuterium into fatty acids<sup>133</sup>. Thus, by quantifying the changes in C-D bonds formed under D<sub>2</sub>O treatment, it is possible to reveal changes in the fatty acid metabolism at a single-cell level. However, since C-D bonds are also capable of being incorporated within proteins under D<sub>2</sub>O metabolism, additional lipid profiling and quantification is needed to better determine the impact of catalase deactivation on lipid metabolism. GC-MS was chosen not only due to its ability to identify and quantify changes in fatty acids across millions of fungal cells but also because it would also be able to specify changes in specific fatty acids produced following light treatment. For light-treated *C. albicans*, C-D signal at 2165 cm<sup>-1</sup> was found to decrease by 58.8%, indicating a drastic loss in lipid production activity. In addition, GC-MS findings following blank subtraction and internal standard

normalization found that while 20 to 30% decreases in unsaturated fatty acids like oleic and linoleic fatty acids were observed, their decrease paled in comparison to the 75 to 80% decrease observed in the saturated fatty acids palmitic and stearic acids. These drastic decreases in saturated fatty acids point to a potential disruption in the overall synthesis of saturated fatty acids following light treatment. This disruption in saturated fatty acid production would potentially explain the inhibition in hyphae production following catalase deactivation, as the reduction in palmitic acid synthesis would in turn prevent the production of sphingolipids, as sphingolipid synthesis is dependent on palmitoyl-CoA and serine<sup>134</sup>. This sphingolipid biosynthesis inhibition would therefore in turn disrupt the overall growth and development of hyphae<sup>111</sup>. While the direct relationship between catalase and fatty acid production has not been fully determined, the susceptibility of fatty acid synthase to ROS damage during catalase deactivation within yeast cells points to a potential pathway in which light induced catalase deactivation can inhibit hyphae formation. These downstream effects of catalase inactivation are likely caused in part by the hyphae inducing conditions, as the increased ROS formed within the fungal cell during the yeast to hyphae transition would likely exert a significant amount of damage on the interior of the cell machinery without catalase present to neutralize the ROS, therefore maximizing potential damage<sup>114,115</sup>. The observed reduction in fatty acid production and synthesis, therefore, points to a cascading downstream effect induced by the deactivation of catalase and maximized by the byproducts formed within hyphae-inducing conditions. While both SRS imaging and GC-MS indicate disruptions in fatty acid production, additional research will need to be conducted to determine the full

impact of catalase deactivating light treatment on the lipid production pathway, such as evaluating the extent of damage exerted on specific lipid proteins like fatty acid synthase or desaturase.

While the effects of catalase deactivation on hyphae development can be observed *in vitro*, there is little practical application for this phenomenon unless it can be applied to interactions with the host immune system. Thus, translational explorations into interactions of light-treated *C. albicans* with immune cells both *in vitro* and *in vivo* were necessary to determine the effectiveness of light treatment at slowing hyphae growth and, by extension, reducing *C. albicans* virulence. As the most abundant white blood cells in circulation, neutrophils play a key role in the eradication of infections<sup>135</sup>. As such, neutrophils act as the major effector immune cells in fungal killing, using a combination of phagocytosis and extracellular traps to capture and kill *C. albicans* in both yeast and hyphae form<sup>136,137</sup>. Our studies on neutrophils treated with light treated *C. albicans* co-cultured with human harvested neutrophils found similar inhibition in overall hyphae growth and formation capabilities. Given that *C. albicans* germtube and hyphae formation is heavily stimulated upon neutrophil phagocytosis<sup>138</sup>, a near 50% reduction in hyphae length within neutrophil environments is even greater than the average hyphae reductions observed without neutrophils, indicating that the neutrophil activity on the light treated *C. albicans* further inhibited hyphal development. These results are also consistent with previous data collected on the interactions of light treated *C. albicans* with immune cells, as light treated fungi co-cultured with murine macrophages exhibit similar decreases in hyphae growth and survival<sup>86</sup>. The reduced hyphae forming

capabilities of light-treated *C. albicans* can provide immune cells with more opportunities to recognize and eradicate fungi with a reduction in the risk of fungal hyphae development and escape.

Based on the results, catalase deactivating blue light appears to easily exert its effects on *Candida* fungal cells *in vitro* and interacts well with immune cells. From here, the next step to determine the translatability of this technology would be to combine the hyphae-suppressing phenomenon with the ROS sensitizing capabilities of blue light and determining if aBL can demonstrate the same reduction in fungal virulence within animal models. Initial toxicity tests found that the conditions that render *Candida* cells susceptible to either ROS sensitization or hyphae suppression were well tolerated by mammalian CHO cells within *in vitro* assays. Based on these results, similar conditions were applied to *in vivo* murine models. Investigations into the impact of light-treated *C. albicans* on infected murine skin wounds not only found that light-treated *Candida* infected wounds exhibited greater sensitivity towards H<sub>2</sub>O<sub>2</sub>, but they also exhibited little to no significant hyphae formation, especially in comparison to untreated *C. albicans* wounds. From the histology images, strong neutrophil swarming can be observed in the untreated infections, indicating the hyphae development of the pathogens has triggered a strong immune response. Given that neutrophil swarming is intended to delay the growth and development of fungal clusters, the mass accumulation of neutrophils within the dermis layer indicates that the hyphae from *C. albicans* have significantly invaded through the epidermis and dermis<sup>139</sup>. As in untreated *C. albicans*, the strong initial hyphal penetration through tissue also runs the risk of further translocation which may result in

bloodstream access, resulting in the potential development of candidemia<sup>106,140</sup>. In contrast, the lack of hyphae development observed in the light-treated *C. albicans* infected wound is matched with low neutrophil presence, indicating a failure to successfully penetrate through the dermis. Blue light and H<sub>2</sub>O<sub>2</sub> treated infections also appear to show a drastically lower presence of *Candida* cells on the skin, in addition to the reduced hyphae development observed in the light only treated samples. This reduced *Candida* presence and hyphae development is also observed within the *ex vivo* model utilizing EpiDerm Skin Scaffolds, further validating the results. Taken together, these results indicate a potential therapeutic usage of light treatment as a method of reducing virulence of cutaneous fungal infections through both ROS sensitization and hyphae suppression.

With the following data, we have been able to demonstrate that catalase deactivation can reduce the virulence of *Candida* species within both *in vitro* and *in vivo* environments, providing a potential avenue of translation of this technology in the treatment of fungal skin infections. Antimicrobial blue light not only increases ROS sensitization of fungi, but its catalase deactivating capabilities also causes a downstream disruption in lipogenesis, inducing hyphae suppression. As one of the most significant *Candida* virulence factors, hyphae formation in particular has long been targeted not only due to its role in immune system invasion but also because of its capability to act as a precursor to fungal biofilm formation, potentially contributing to the development of antifungal resistance<sup>141</sup>. While several studies have established the hyphae inhibiting effects of antifungal drugs or small molecule inhibitors such as azoles, farnesol, and SR

compounds, the usage of external agents still carries the risk of eventual resistance development, as already observed with established antifungals like fluconazole<sup>142,143</sup>. Utilizing catalase deactivating aBL therefore offers a non-drug reliant method of achieving similar hyphae inhibiting effects to small molecule inhibitors while also providing the beneficial side effect of inducing ROS sensitization within the fungi as well. Preliminary investigation also indicates that this catalase deactivating phenomenon may also be applicable to a variety of non-*Candida* fungal strains, like the catalase positive fungi *Aspergillus fumigatus*, a filamentous mold responsible for both pulmonary and wound infections<sup>144-146</sup>. Future explorations of this technology can further investigate the effects of catalase deactivating blue light on additional non-*Candida* strains to determine potential applicability. Overall, this technology offers a noninvasive and non-antifungal reliant method of reducing *Candida* infection virulence within infected wounds and therefore can play a key role in the current fight against antifungal resistance development.

## **CHAPTER FOUR: Blue Light Induced Catalase Deactivation Improves Antimicrobial Efficiency of Silver Sulfadiazine**

The work and figures presented in this chapter was published in Photobiomodulation, Photomedicine, and Laser Surgery<sup>147</sup>. Reprinted with permission from Mary Ann Liebert, Inc., publishers. Copyright 2023, Mary Ann Liebert, Inc., publishers. DOI: 10.1089/photob.2022.0107

### **Introduction**

#### *Clinical Relevance of Hydrogen Peroxide and Systemic Antibiotics Against Skin Infections*

While the clear synergy offered between catalase deactivating blue light and H<sub>2</sub>O<sub>2</sub> offers an exciting method of treating pathogenic infections within both *in vitro* and *in vivo* conditions, significant problems remain regarding the usage of H<sub>2</sub>O<sub>2</sub>. Despite the high availability and accessibility of H<sub>2</sub>O<sub>2</sub>, hydrogen peroxide is not commonly used within wound care settings to treat most infected burns or wounds, as H<sub>2</sub>O<sub>2</sub> usage in wound care has been found to exhibit mixed results within clinical settings, failing to significantly alter infection rates or reduce the bacterial load within wounds<sup>148,149</sup>. In addition, the extremely short half-life of H<sub>2</sub>O<sub>2</sub> renders the compound generally unsuitable for long term treatment<sup>150</sup>. Usage of hydrogen peroxide for wound irrigation has also been found to hold an inherent risk of causing fatal oxygen embolism formation within patients<sup>151,152</sup>.

In contrast, while usage of systemic antibiotics through intravenous or oral administration is common in clinical environments, the usage of systemic antibiotics runs

the risk of requiring higher antibiotic dosages and altering the natural microbial flora of the human body<sup>153</sup>. In addition, the localized catalase deactivating effect of blue light is best taken advantage of immediately following light application, and usage of systemic antibiotics runs the risk of delivering the antibiotics to the site of action too slowly. As such, topical antibacterial antibiotics are better suited to properly synergize with the light treatment on skin infections within a clinical setting, as topical antibiotics have the advantage of allowing for the targeted delivery of a high drug concentration to the infection wound site while at the same time minimizing the risk of systemic side effects and toxicity<sup>153</sup>. Given these observations and concerns, if this phototherapy technology is expected to be implemented as a novel method of treating infected wounds within clinical settings, there exists a need to identify different topical ROS producing agents that are commonly used in clinical settings that can be used as an alternative to H<sub>2</sub>O<sub>2</sub>.

#### *Silver Sulfadiazine: Mechanisms and Clinical Usage*

Given the issues with utilizing H<sub>2</sub>O<sub>2</sub> for general wound care and treatment, an alternative synergistic agent to combine with catalase deactivating phototherapy is needed to allow for improved translation of this technology to clinical settings. Based on its topical nature, the antibiotic silver sulfadiazine (SSD) has emerged as an ideal alternative to H<sub>2</sub>O<sub>2</sub> for synergy with blue light. First introduced in 1968, silver sulfadiazine was first introduced as a therapeutic agent for the treatment of *P. aeruginosa* infected burns. Since then, this FDA-approved topical antibiotic has been widely adopted for the treatment of infected wounds and burns, and its 1% cream formulation is currently listed as one of the few dermatological medicines on the World Health

Organization's List of Essential Medicines<sup>154-158</sup>.

Literature indicates that SSD exerts its mechanism of action through the combined antimicrobial activity of the silver ions and sulfadiazine that make up the compound. The individual sulfadiazine component acts as a specific competitive inhibitor of dihydropteroate synthetase, preventing the synthesis of key folic acid derivatives like tetrahydrofolic acid in bacteria, disrupting amino and nucleic acid synthesis<sup>159</sup>. In contrast, silver ions released by SSD act in a much more broad-spectrum manner, binding to the amino, carboxyl, phosphate, imidazole, and thiol groups within bacterial proteins and triggering protein denaturation or enzyme inactivation<sup>160,161</sup>. However, while this protein denaturation induced by silver ion binding has been believed to be the driving cause of SSD antimicrobial activity, additional research has indicated that the intracellular ROS generation indirectly caused by silver ions binding and disrupting proteins within the bacterial respiratory chain plays a major role in the antimicrobial activity of silver ions, contributing up the half of the log reduction observed in model gram negative and positive bacterial models<sup>162</sup>. This significant ROS generating capability, alongside its clinical usage and topical nature, makes SSD an ideal compound to potentially synergize with catalase deactivation.

This theoretical synergy can also potentially improve the overall efficiency of SSD, helping minimize side effects like inhibited wound healing by improving bioburden clearance and reducing the SSD application duration<sup>163-165</sup>. Thus, we hypothesize that light induced catalase deactivation can improve the efficiency of SSD within both *in vitro* and *in vivo* environments.

## Methods and Materials

### *Bacterial Strains*

Wild type *E. coli* (BW25113) and its catalase deficient mutant *E. coli*  $\Delta katGE$  was obtained through Dr. Xilin Zhao of Rutgers University in New Brunswick, New Jersey, USA. MRSA (USA300), and *P. aeruginosa* PAO-1 (ATCC 47085) were obtained through Dr. Mohamed N. Seleem of Virginia Tech University in Blacksburg, Virginia, USA.

### *Silver Sulfadiazine Preparation*

For *in vitro* studies, silver sulfadiazine salt (481181, Sigma Aldrich) was dissolved in diluted (0.7% - 1.4%) ammonium hydroxide (NH<sub>4</sub>OH) (L13168, Alfa Aesar). For *in vivo* studies, topical 1% silver sulfadiazine cream (67877012450, Ascend) was used.

### *In Vitro Blue Light and Silver Sulfadiazine Treatment*

Bacterial strains were cultured overnight in tryptic soy broth (TSB) to stationary phase. The next day, bacteria was resuspended and diluted in 1x phosphate buffered saline (PBS) to an OD<sub>600</sub> of 1.0. For light treatment, bacterial aliquots were placed on a coverslip and exposed to 200 mW/cm<sup>2</sup> of CW-405. For a checkerboard assay, 2  $\mu$ L droplets were treated for 0, 2.5, 5, 10, 20, and 40 minutes, diluted in 2 mL of TSB, and plated in a 96-well plate. Following this, SSD was diluted 2-fold from a concentration of 64  $\mu$ g/mL to concentrations of 32, 16, 8, and 4  $\mu$ g/mL. The assay was incubated at 37 °C for 48 hours before the OD<sub>600</sub> was measured with a plate reader to identify the minimal inhibitory concentration (MIC) of CW-405 and SSD alone and in combination.

Synergistic interactions were determined by calculating the fractional inhibitory concentration index (FICI) defined by the following equation<sup>166</sup>:

$$\frac{\text{MIC}_A^{\text{Comb}}}{\text{MIC}_A^{\text{Alone}}} + \frac{\text{MIC}_B^{\text{Comb}}}{\text{MIC}_B^{\text{Alone}}} = \text{FIC}_A + \text{FIC}_B = \text{FICI}$$

$\text{MIC}^{\text{Alone}}$  refers to the MIC of isolated agents while  $\text{MIC}^{\text{Comb}}$  correspond to the MIC of agents in combination. For colony forming unit (CFU) studies, 10  $\mu\text{L}$  aliquots were treated for 5 minutes (60  $\text{J}/\text{cm}^2$ ). Once complete, the aliquot was removed and diluted within 990  $\mu\text{L}$  of either PBS or TSB. Varying concentrations of SSD dissolved in around 1% of  $\text{NH}_4\text{OH}$  were then added to each dilution. To account for the  $\text{NH}_4\text{OH}$  within the SSD solution, equal amounts of low concentration  $\text{NH}_4\text{OH}$  were added to non-SSD treated dilutions as well. Following the addition of SSD, samples were incubated for up to 2 hours within a 37 °C incubator at an RPM of 200. Once finished, samples were serially diluted and plated onto tryptic soy agar plates. The resulting CFU was then quantified.

#### *Catalase Rescue and Salvaging*

Overnight cultured PAO-1 and MRSA were subjected to light treatment as described previously. Following treatment, 100  $\mu\text{L}$  of 1 mg/mL bovine catalase (C9322, Sigma Aldrich) was added to 900  $\mu\text{L}$  of each suspension, adding 200-500 units of catalase to each solution. Next, 2  $\mu\text{g}/\text{mL}$  of SSD was added. The suspensions were incubated for 1 hour at 37 °C, plated, and quantified.

### *ROS Detection and Quantification*

ROS production was quantified through a hydroxyl radical and peroxyxynitrite sensor (HPF) dye (H36004, ThermoFisher Scientific). Overnight cultured PAO-1 and MRSA were treated to 60 J/cm<sup>2</sup> of CW-405 and 2 µg/mL of SSD in the process described above. Following SSD addition, 2 µM of HPF was added and suspensions were incubated for 30 minutes at 37 °C. Once complete, 100 µL of suspension was transferred to a 96-well plate and fluorescence (n = 3) was quantified at an excitation/emission setting of 490/515 nm. Background fluorescence was quantified by adding 2 µM of HPF to PBS and incubating the solution in 37 °C for 30 minutes. Measured fluorescence were normalized by subtracting the background fluorescence.

### *In Vivo Murine Model*

Murine abrasion wounds were generated following the procedure established by Dong et al<sup>34</sup>. 7–8-week-old BALB/c female mice (000651, Jackson Laboratory) were dorsally shaved and placed under isoflurane anesthesia. 1 cm<sup>2</sup> abrasion wounds were created by a #15 sterile scalpel. A 10 µL aliquot containing 10<sup>6</sup> CFU of log phase MRSA or 10<sup>8</sup> CFU of log phase PAO-1 was applied to the surface of each wound. Treatment began 2 hours after infection. For each bacteria tested, mice were separated into four groups: Untreated, Light Only, SSD Only, and Combination. Light treatment consisted of two 60 J/cm<sup>2</sup> CW-405 treatments applied onto wounds with 5-minute breaks between treatments. A single light session would consist of 120 J/cm<sup>2</sup> of exposure. For SSD treatment, 1% SSD cream was applied directly to the wound surface. In combination treated groups, mice would receive light treatment followed immediately by SSD cream application. For the MRSA

wounds, the untreated, SSD only, and combination groups consisted of  $n = 7$  wounds while the light only group consisted of  $n = 5$  wounds. MRSA groups were treated daily over 4 days for a total light dosage of  $480 \text{ J/cm}^2$ . 24 hours after the last treatment, MRSA infected mice were euthanized and the wounds were extracted, homogenized in 2 mL of PBS, and plated on *S. aureus* selective mannitol agar plates. For the PAO-1 model, each group consisted of  $n = 4$  wounds. PAO-1 groups were treated twice in the span of 24 hours, with 12-hour breaks between sessions, totaling to a final dosage of  $240 \text{ J/cm}^2$ . 4 hours after the last treatment, PAO-1 infected mice were euthanized and wounds were removed, homogenized, and plated on *P. aeruginosa* selective ceftrimide agar plates. The resulting CFU was then quantified.

#### *Statistical Analysis*

Student unpaired t-tests were used to conduct statistical analysis via GraphPad PRISM version 9.0.0. Significance (\*) was set at  $p$ -values less than 0.05.

#### *Study Approval*

Murine infected abrasion models were approved under protocol PROTO201800535 by the Institutional Animal Care and Use Committee (IACUC) at Boston University.

## Results

### *Blue Light and Silver Sulfadiazine Exhibit Synergistic Behavior*

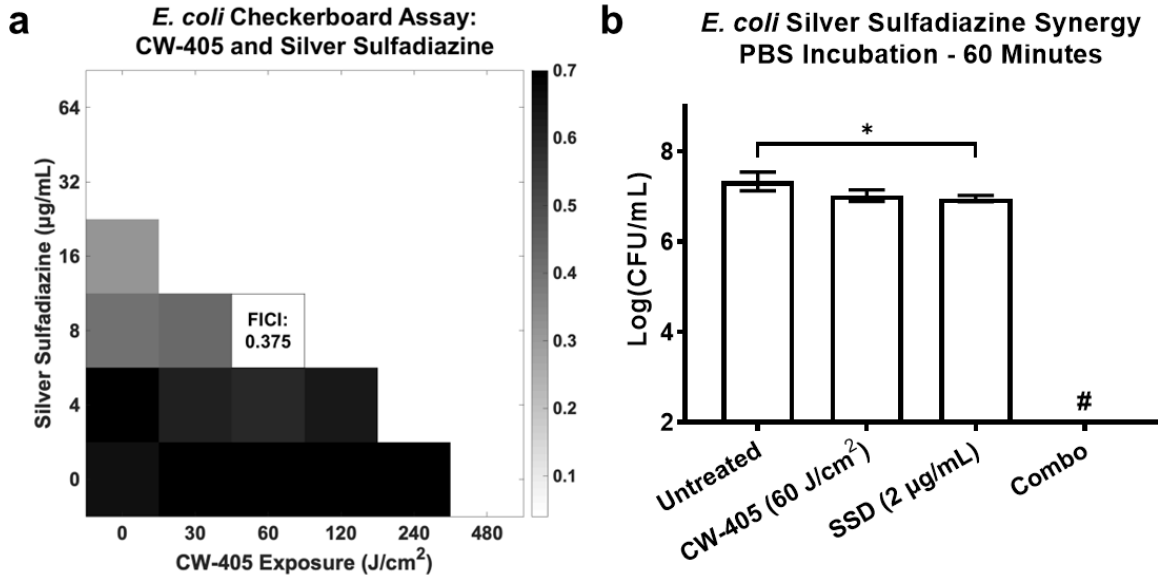


**Figure 23: Combination of catalase deactivating CW-405 and silver sulfadiazine results in synergistic interactions within model bacteria organism *E. coli* (BW25113). a) Checkerboard assay of *E. coli* exposed to varying dosages of CW-405 and silver sulfadiazine within tryptic soy broth. Treatment with 60 J/cm<sup>2</sup> of CW-405 and 8 µg/mL silver sulfadiazine results in a fractional inhibitory concentration index (FICI) of 0.375. FICI values below 0.5 indicate synergistic interactions. b) CFU measurements of bacterial population indicate combination of light and silver sulfadiazine resulted in complete eradication, further confirming the synergistic interactions. In contrast, light or silver sulfadiazine alone has little impact on the overall CFU. \*:  $p < 0.05$ , #: Below detection limit. Data published in Jusuf & Cheng, *Photobiomodulation, Photomedicine and Laser Surgery*, 2023<sup>147</sup>.**

To confirm synergy between blue light and SSD, a checkerboard assay was performed on the model bacteria *E. coli* (BW25113) to identify the fractional inhibitory concentration index (FICI) in TSB (**Figure 23a**). The FICI can be used to determine the type of interactions between two agents, with synergistic interactions identified through FICI values  $\leq 0.5$ <sup>167</sup>. *E. coli* was found to exhibit a MIC of 480 J/cm<sup>2</sup> for CW-405 and 32 µg/mL for SSD. In contrast, the MICs of the agents in combination was found to be 60

$\text{J}/\text{cm}^2$  for CW-405 and  $8 \mu\text{g}/\text{mL}$  for SSD. Based on the FICI equation listed, these values correspond to a FICI of 0.375, confirming the presence of synergy. To further explore the capability of light to improve SSD performance, the CFU of *E. coli* after light and SSD treatment was evaluated. Following 1 hour of incubation in PBS, both  $60 \text{ J}/\text{cm}^2$  light and  $2 \mu\text{g}/\text{mL}$  SSD reduced the CFU of *E. coli* by less than 0.5-log. In contrast, combination treatment completely eradicated the *E. coli* population beyond the detection limit (**Figure 23b**).

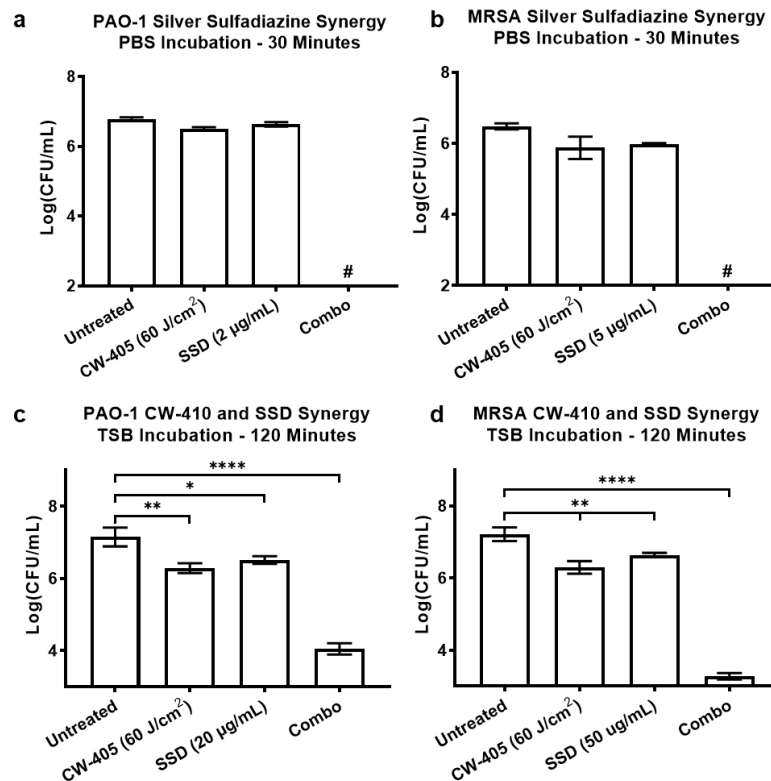


**Figure 24:** CFU measurements of CW-405 ( $60 \text{ J}/\text{cm}^2$ ) treated a) *P. aeruginosa* (PAO-1), and b) MRSA following incubation with silver sulfadiazine in PBS. Light or silver sulfadiazine alone has little impact on overall CFU, while the combination of the two agents results in complete eradication. In nutrient rich conditions, CFU measurements of CW-405 ( $60 \text{ J}/\text{cm}^2$ ) treated c) *P. aeruginosa* (PAO-1), and d) MRSA following incubation with silver sulfadiazine in tryptic soy broth indicate that while higher dosages of silver sulfadiazine are required, improved performance with CW-405 still occurs. \*\*\*\*:  $p < 0.0001$ , \*\*:  $p < 0.01$ , \*:  $p < 0.05$ , #: Below detection limit. Data published in Jusuf & Cheng, *Photobiomodulation, Photomedicine and Laser Surgery*, 2023<sup>147</sup>.

Next, the treatment was evaluated on gram-negative *P. aeruginosa* (PAO-1) and gram-positive MRSA. PAO-1 treated to either CW-405 or SSD (2 µg/mL) experienced a less than 0.5-log CFU reduction while combination treated samples experienced complete eradication (**Figure 24a**). MRSA treated to either CW-405 or SSD (5 µg/mL) resulted in a 0.5-log CFU reduction while the combination treatment also demonstrated full eradication (**Figure 24b**).

Within more nutrient rich environments, combination treatment conducted on bacteria incubated within TSB for 2 hours were found to require higher SSD concentrations to achieve an improved response. For PAO-1, CW-405 alone induced a 1-log CFU reduction while treatment with 20 µg/mL of SSD induced a 0.5 log reduction. Combination treatment of PAO-1 resulted in a 3-log CFU reduction (**Figure 24c**). For MRSA, treatment with CW-405 and 50 µg/mL of SSD resulted in a 1-log and 0.5-log CFU reduction respectively, identical to the PAO-1 results. However, combination treatment of MRSA was slightly more effective with a log CFU reduction of 4 (**Figure 24d**).

Mechanisms of Blue Light and Silver Sulfadiazine Interactions

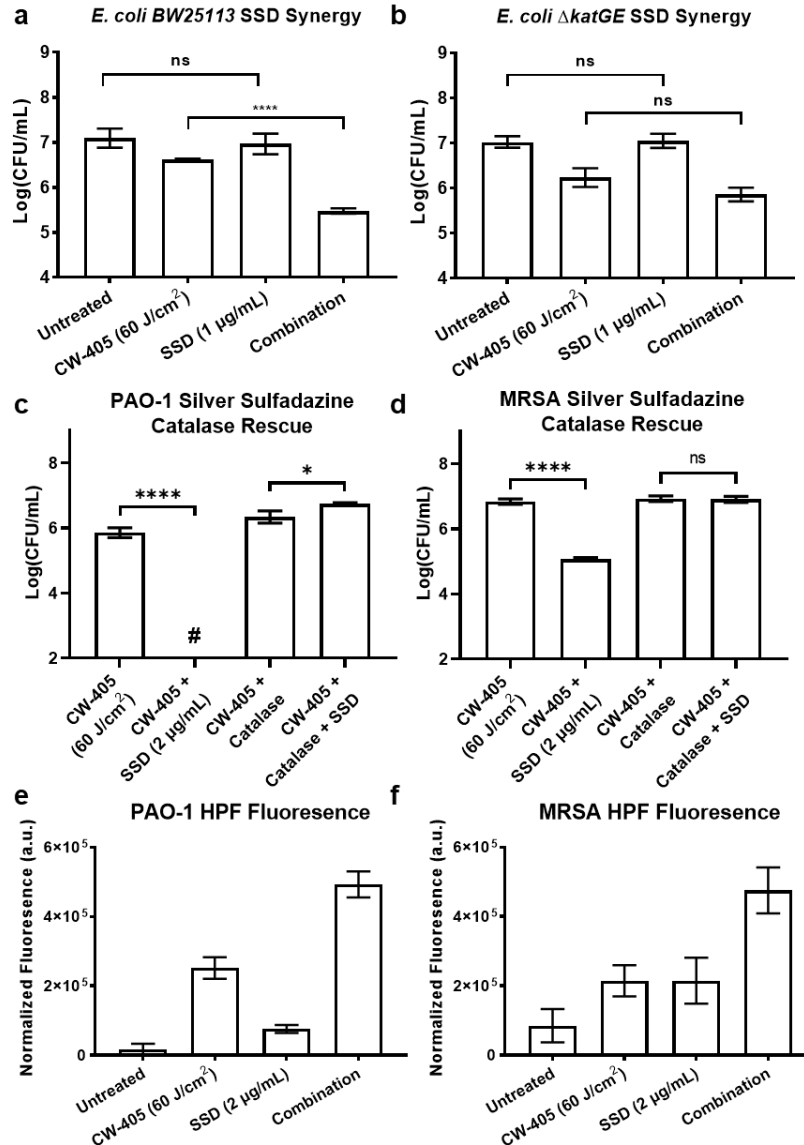


**Figure 25: Mechanisms of CW-405 and silver sulfadiazine synergy.** The combination of CW-405 ( $60 \text{ J/cm}^2$ ) and low concentration silver sulfadiazine results in a) a 1-log reduction in wild type *E. coli* but b) no significant reduction in catalase deficient *E. coli*  $\Delta katGE$  mutants. Further investigation in the possible role of catalase in the synergy reveal that the addition of exogenous bovine catalase completely neutralizes the synergistic effects of CW-405 and silver sulfadiazine in both c) PAO-1 and d) MRSA. The impact of catalase deactivation on the ROS production of silver sulfadiazine was further explored through an ROS detecting HPF dye. When applying the combination treatment to e) PAO-1 and f) MRSA, HPF dye reveals significant increases in ROS fluorescence for the combination treated samples. \*\*\*\*:  $p < 0.0001$ , \*:  $p < 0.05$ , ns = No Significance, #: Below detection limit.

**Data published in Jusuf & Cheng, *Photobiomodulation, Photomedicine and Laser Surgery*, 2023<sup>147</sup>.**

To investigate the mechanisms behind light and SSD synergy, the role of catalase against SSD activity was explored. In wild type *E. coli*, combination treatments of CW-405 and SSD (1 µg/mL) induced a 1-log CFU reduction compared to the light treated samples (**Figure 25a**). However, the same treatment applied to the catalase deficient mutant *E. coli*  $\Delta katGE$  resulted in no significant differences between the light treated mutant and the combination treated mutant (**Figure 25b**). Additional experiments revealed that the addition of exogenous catalase completely neutralized the effectiveness of the combination treatment in both PAO-1 and MRSA. For PAO-1, combination treatment alone resulted in the complete eradication of PAO-1, while the addition of catalase was found to slightly increase the CFU by less than 0.5-log (**Figure 25c**). For MRSA, while combination treatment alone resulted in a 2-log CFU reduction, the addition of catalases resulted in no differences between the light and combination treated samples (**Figure 25d**). These results indicate that increased ROS presence contributes to the increased antimicrobial activity of SSD, which exogenous catalase can neutralize. To confirm this, ROS levels were measured through a ROS detecting HPF dye. In PAO-1, individual treatments of CW-405 and SSD increased HPF fluorescence by a factor of 13.7 and 3.4 respectively. In comparison, the combination treatment increased fluorescence by a factor of 27.7 (**Figure 25e**). For MRSA, both CW-405 and SSD individually increased fluorescence by a factor of 1.5, while the combination treatment increased fluorescence by a factor of 4.6 (**Figure 25f**).

*Blue Light Improves Silver Sulfadiazine Performance In Vivo*

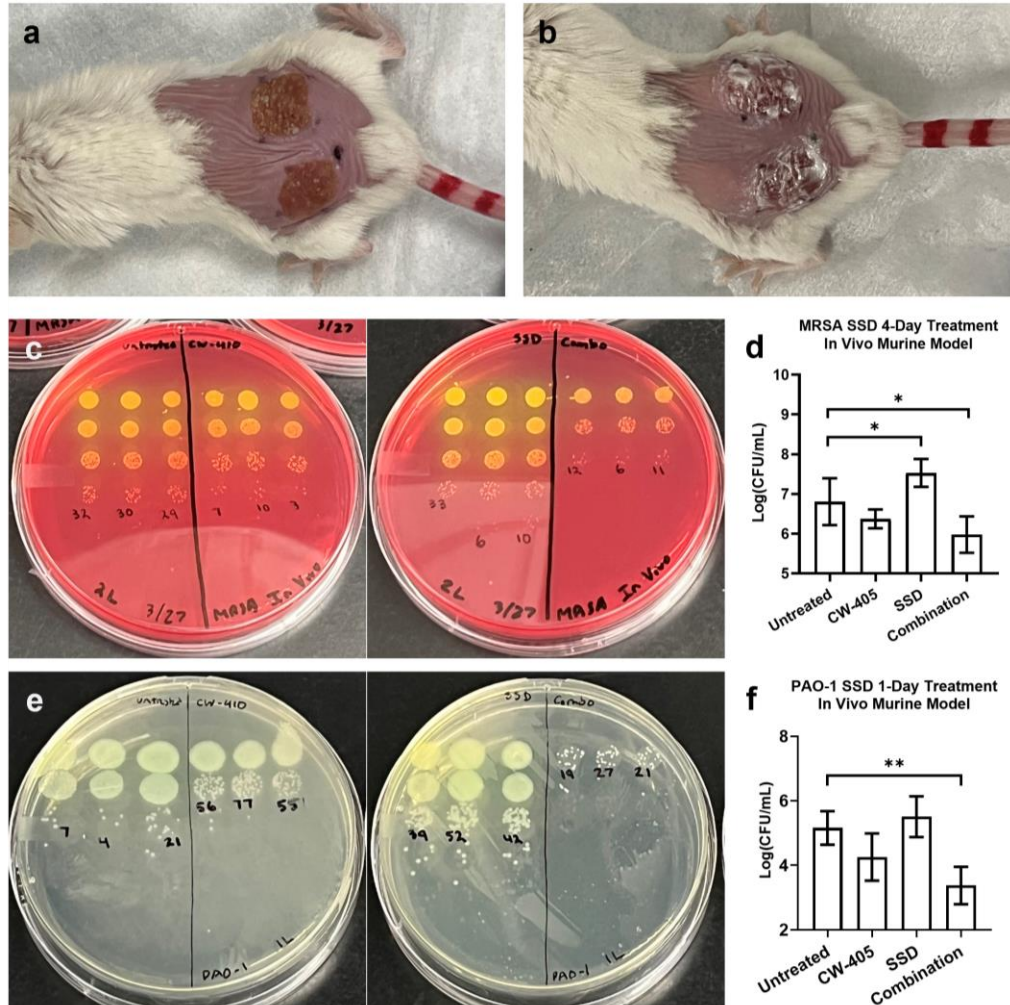


**Figure 26: MRSA and PAO-1 infected murine abrasion wound models were used to evaluate the effectiveness of blue light and silver sulfadiazine combination treatment. a) 1 cm<sup>2</sup> abrasion wounds were generated on the dorsal flanks of BALB/c mice and infected with bacterial loads. b) When applying 1% silver sulfadiazine cream to infected wounds, it was ensured that the wound would be covered by the silver sulfadiazine cream. MRSA infected wounds treated with daily application sessions of CW-405 (120 J/cm<sup>2</sup>) and 1% silver sulfadiazine cream for 4 days were c) quantified via CFU plating on mannitol salt agar and d) found to exhibit minor average improvement from the combination treatment in comparison to the untreated wounds. In PAO-1 infected wounds, wounds were treated with CW-405 (120 J/cm<sup>2</sup>) and silver sulfadiazine cream twice in 24 hours and e) plated on cetrimide agar were f) found to improve the efficacy of PAO-1 significantly, with a near 2-log reduction in CFU population observed from the untreated group. In both murine models, silver sulfadiazine alone was found to be either ineffective in the case of PAO-1 infected wounds or beneficial to bacterial growth in the case of MRSA infected wounds. \*\*:  $p < 0.01$ , \*:  $p < 0.05$ . Data published in Jusuf & Cheng, *Photobiomodulation, Photomedicine and Laser Surgery*, 2023<sup>147</sup>.**

A murine infected abrasion model was used to determine the effectiveness of blue light and SSD within *in vivo* conditions. Infected wounds (**Figure 26a**) were fully covered with SSD to maximize exposure (**Figure 26b**). CFU counts of MRSA wounds (**Figure 26c**) indicate that while the light treatment alone had no significant effect on the bioburden of the MRSA wounds, SSD treated MRSA wounds saw a near 4-fold increase in bioburden. Despite this, the combination treatment resulted in an 85% decrease in MRSA bioburden (**Figure 26d**). For PAO-1 infected wounds, CFU measurements (**Figure 26e**) indicated that individual CW-405 or SSD treatment had no significant effect on the bioburden. Combination treated wounds, however, were experienced a 98% reduction in CFU bioburden, constituting a significant improvement in effectiveness (**Figure 26f**).

### Discussion and Conclusion

Based on their FICI, the combination of catalase deactivating blue light and SSD exhibited strong synergistic interactions. The effectiveness of this treatment was further validated by the complete eradication of multiple bacterial strains within PBS upon treatment with both light and low dosage SSD. In comparison, the individual treatments of light or SSD exerted minimal impact on the bacteria, at most exerting a CFU log reduction of 0.5. These observed interactions between CW-405 and SSD behaved identically to the synergy observed between light and H<sub>2</sub>O<sub>2</sub>, indicating that SSD can act as a viable alternative to H<sub>2</sub>O<sub>2</sub><sup>34</sup>. Like H<sub>2</sub>O<sub>2</sub>, catalase deactivation allowed for bacterial eradication through SSD at sub-MIC concentrations, with *P. aeruginosa* reported to have a MIC range of 16-32 µg/mL while MRSA strains have a range of 64-128 µg/mL<sup>168</sup>.

Even within nutrient rich environments, the improved efficiency of SSD by CW-405 was found to remain, albeit requiring higher concentrations of SSD. The greater SSD dosage needed to achieve improved efficiency can be attributed to the active metabolism of bacteria within the media, as exposure to sub-lethal ROS sources would trigger the overexpression of oxidative stress defense genes in response<sup>169-171</sup>. Despite this, CW-405 incorporation significantly improves the performance of SSD by 3 to 4-log compared to the antibiotic alone.

The fact that light had no impact on the SSD activity in catalase deficient *E. coli* mutants indicates that it is the specific removal of catalase that contributes to the synergy between light and SSD. This is supported by the complete neutralization of the combination treatment observed by the addition of exogenous bovine catalase, which not only demonstrates the importance catalase plays as a defense mechanism against SSD, but also indicates that the intracellular ROS produced indirectly by SSD can diffuse out of the cell into the exterior environment<sup>162</sup>. Without catalase present, the intracellular ROS produced by light and SSD treated cells are likely increasing ROS levels within the bacterial environment, further propagating oxidative damage to surrounding cells. This increased ROS concentration caused by catalase removal is supported by the higher ROS levels detected within combination treated bacteria. For PAO-1 and MRSA, the combination treatment fluorescence increased 62% and 53% over the added individual fluorescence of CW-405 and SSD respectively. The increased ROS availability caused by the absence of catalase would provide more opportunities for the ROS to exert their antimicrobial activity on the cell, therefore increasing the efficiency of SSD following

exposure to light.

Interestingly, the MRSA HPF fluorescence was found to be significantly lower than the PAO-1 fluorescence. The lower fluorescence is likely caused by the presence of additional antioxidants like the membrane-bound staphyloxanthin pigment in MRSA neutralizing the ROS before they can react with HPF<sup>172,173</sup>. This pigment also likely contributes to the higher SSD resistance observed in MRSA.

While light and SSD exhibited clear synergy within an *in vitro* environment, *in vivo* studies showed promising results as well. Combination treatment in both MRSA and PAO-1 infected wounds significantly enhanced the antimicrobial activity of SSD and achieved significant bioburden reduction compared to their untreated counterparts. In contrast, individual light treatments did not significantly differentiate from untreated samples for both bacterial models. While SSD only treatment had no effect on PAO-1 infected wounds, MRSA wounds treated with SSD alone were observed to experience a 401.1% increase in bioburden. This increase in MRSA population can likely be attributed to a combination of factors, such as the tendency for mice to lick their own or other mice's back in response to cream application.<sup>174</sup> Such interference would significantly reduce the SSD concentration available on the wound and lead to subinhibitory dosages, resulting in potential growth driven by the hormetic effects of sub-inhibitory antibiotic concentrations<sup>175,176</sup>. Regardless, infected wounds exhibited greater vulnerability to combination treatment, with PAO-1 infections demonstrating greater sensitivity to the treatment, achieving a near 2-log CFU reduction compared to the less than 1-log CFU reduction CFU observed in MRSA. The sensitivity of PAO-1 to the combination

treatment suggests that catalase deactivation may provide a way of resensitizing SSD resistant *P. aeruginosa* to the drug, reviving the usage of the drug against previously resistant strains<sup>177,178</sup>. In addition, the increased effectiveness of SSD with light can allow for lower dosages and durations of SSD to be used against infected wounds, further minimizing potential side effects like wound healing inhibition<sup>163</sup>. The effectiveness of this treatment can also provide a strong foundation for additional studies examining the effectiveness of this treatment on other types of infected wounds, such as chronic wounds or diabetic ulcers<sup>179,180</sup>.

Overall, by combining catalase deactivating blue light with SSD, we have established a non-drug reliant method of sensitizing pathogens to an established clinical antibiotic. The improved effectiveness of SSD with CW-405 was found within a broad spectrum of pathogens in both PBS and nutrient rich conditions. Application of CW-405 and SSD was also found to be effective within *in vivo* environments, providing a foundation for the incorporation of light into traditional treatments. By establishing SSD as a viable alternative to H<sub>2</sub>O<sub>2</sub> in blue light synergy, we can provide a potential direction for the development of new antimicrobial agents that could be created to specifically synergize with light induced catalase deactivation within clinical and hospital settings.

## CHAPTER FIVE: Conclusion and Future Directions

### Conclusion

Overall, through the following work, we have successfully investigated various aspects regarding the mechanism and translation of blue light antimicrobial phototherapy. On the mechanistic sides, we have not only demonstrated the importance that antioxidant enzymes play in the antimicrobial activity of blue light, but we have also established the importance that catalase plays in the downstream effects of blue light on microbes, such as acting as the primary target responsible for the ROS sensitization observed in bacteria or contributing to the suppression of hyphae development within dimorphic *C. albicans*. On the translational side, we have found 410 nm aBL to be able to sensitize pathogenic bacteria to various treatments, ranging from conventional or topical antibiotics to the host immune system. We also were able to successfully take advantage of the downstream effects of catalase deactivating blue light technology within *in vivo* murine models, reducing the microbe virulence and bioburden of *PAO-1* or *C. albicans* infected abrasion wounds, increasing the efficiency and effectiveness of antimicrobial agents like silver sulfadiazine.

### Further Directions of Antimicrobial Phototherapy

#### *Applications of Pulsed Light*

Within this study, the bulk of aBL studies was performed with a blue light 405 nm LED device. However, while the dosages and powers used within the *in vivo* and other translational studies were generally in line with ANSI standards for medical skin laser

applications, it was observed that within the *in vivo* murine models, usage of continuous wave LED light resulted in a measurable increase in the surface temperature of the mice. While there are key differences in thermoregulation between humans and mice, such as the fact that mice lack the ability to sweat<sup>181</sup>, the increase in surface temperature by the LED light may prove to be an issue in translatability for clinical studies, as it may prove to be a source of mild discomfort for human patients. A solution to this would be to investigate the efficiency of pulsed light sources. Pulsed light would allow for the thermal cooling of the skin or wound to apply between light pulses, which would result in lower heat accumulation within the skin<sup>182</sup>. This would solve the problem of rising surface temperature in light treated skin tissue. While the Cheng Lab has been able to establish that nanosecond pulsed light sources are able to bleach catalase or antioxidant pigments more efficiently than continuous wave LEDs, there has been little investigation into the direction relationship between pulsed light frequency and bleaching within *in vivo* systems. Investigating the effects of different frequencies of pulsed light, as well as if pulsed light can retain the same bleaching efficiency across multiple conditions, can help better translate this technology towards clinical settings.

#### *Higher Wavelength Explorations*

While the mechanisms and translatability of antimicrobial blue light have been well explored within this work, one inherent limitation within the technology lies within the usage of blue light. While the 400 to 410 nm wavelengths utilized are theoretically safe for human application and medical use based on existing ANSI standards, the fact

remains that the blue light wavelength used is near the ultraviolet (UV-A) spectrum. While UV light is already used in environmental and medical settings for water and surface disinfection, it is not currently used in skin wound treatment<sup>183,184</sup>. UV light exposure is heavily associated with malignant skin melanoma, and specific studies have established that UV-A light induces persistent genomic instability in human keratinocytes<sup>185</sup>. The proximity of the wavelengths in this technology used to UV light may make adoption of this technology difficult. In addition, blue light is well known for its poor penetration through human skin, due in part to the high absorbance of blood and other heme containing molecules to the blue light wavelength<sup>186</sup>. This means that it would be difficult to apply this technology to deeper, more invasive skin infections. One solution to this problem is the usage of longer wavelengths like red or near-infrared (NIR) light, which is understood to exhibit strong penetration through human skin. While usage of red and NIR light in photodynamic therapy and acne treatment currently exist, there have been few investigations into the usage of this wavelength against skin infections<sup>187,188</sup>. Recent investigations by the Cheng Lab have revealed that the photosensitive staphyloxanthin (STX) pigment present within MRSA, which is normally photolyzed by 460 nm light, can also be photolyzed through 800 nm NIR light through a two photon photobleaching process. This STX photobleaching process through NIR light has been found to sensitize MRSA to ROS similar to blue light, and demonstrates an exciting future direction to explore further to expand the viability of antimicrobial phototherapy. These promising findings can not only allow for phototherapy to target deeper and more invasive MRSA infections, but the usage of red/NIR light on infective

wounds can allow these wounds to take advantage of the accelerated wound healing that red or NIR light has been capable of inducing within wounds<sup>189</sup>.

## APPENDIX

## Blue Light Application Devices



**Blue light application devices used in bacterial and fungal studies. Left) 405 nm LED system used to deliver continuous wave light to pathogens within in vitro and in vivo environments. Right) Tunable nanosecond pulsed laser device allowed for delivery of blue light between 410 and 480 nm.**

**BIBLIOGRAPHY**

1. Aminov RI. A brief history of the antibiotic era: lessons learned and challenges for the future. *Frontiers in Microbiology*. 2010;1:134. PubMed PMID: 21687759; PMCID: PMC3109405.
2. Gould K. Antibiotics: from prehistory to the present day. *Journal of Antimicrobial Chemotherapy*. 2016;71(3):572-575. PubMed PMID: 26851273.
3. Jackson N, Czaplowski L, Piddock LJV. Discovery and development of new antibacterial drugs: learning from experience? *Journal of Antimicrobial Chemotherapy*. 2018;73(6):1452-1459. PubMed PMID: 29438542.
4. Conly J, Johnston B. Where are all the new antibiotics? The new antibiotic paradox. *Canadian Journal of Infectious Diseases & Medical Microbiology*. 2005;16(3):159-160. PubMed PMID: 18159536; PMCID: PMC2095020.
5. Goldman E. Antibiotic abuse in animal agriculture: Exacerbating drug resistance in human pathogens. *Human and Ecological Risk Assessment*. 2004;10(1):121-134. PubMed PMID: WOS:000220374200012.
6. Shea KM. Antibiotic resistance: what is the impact of agricultural uses of antibiotics on children's health? *Pediatrics*. 2003;112(1 Pt 2):253-258. PubMed PMID: 12837918.
7. Ventola CL. The antibiotic resistance crisis: part 1: causes and threats. *P & T*. 2015;40(4):277-283. PubMed PMID: 25859123; PMCID: PMC4378521.
8. Ostrowsky B, Greenko J, Adams E, Quinn M, O'Brien B, Chaturvedi V, Berkow E, Vallabhaneni S, Forsberg K, Chaturvedi S, Lutterloh E, Blog D, Group CaIW. *Candida auris* Isolates Resistant to Three Classes of Antifungal Medications - New York, 2019. *MMWR: Morbidity and Mortality Weekly Report*. 2020;69(1):6-9. PubMed PMID: 31917780; PMCID: PMC6973342.
9. Graham CJ. The global threat of antibiotic resistance: what can be done? *Journal of Global Health Reports*. 2017;1.
10. Yoshikawa TT. Antimicrobial resistance and aging: beginning of the end of the antibiotic era? *Journal of the American Geriatrics Society*. 2002;50(7 Suppl):S226-229. PubMed PMID: 12121517.
11. Ahmad M, Khan AU. Global economic impact of antibiotic resistance: A review. *Journal of Global Antimicrobial Resistance*. 2019;19:313-316. PubMed PMID: 31176071.

12. Aslam B, Wang W, Arshad MI, Khurshid M, Muzammil S, Rasool MH, Nisar MA, Alvi RF, Aslam MA, Qamar MU, Salamat MKF, Baloch Z. Antibiotic resistance: a rundown of a global crisis. *Infection and Drug Resistance*. 2018;11:1645-1658. PubMed PMID: 30349322; PMCID: PMC6188119.
13. Zaman SB, Hussain MA, Nye R, Mehta V, Mamun KT, Hossain N. A Review on Antibiotic Resistance: Alarm Bells are Ringing. *Cureus*. 2017;9(6):e1403. PubMed PMID: 28852600; PMCID: PMC5573035.
14. Bertesteanu S, Triaridis S, Stankovic M, Lazar V, Chifiriuc MC, Vlad M, Grigore R. Polymicrobial wound infections: pathophysiology and current therapeutic approaches. *International Journal of Pharmaceutics*. 2014;463(2):119-126. PubMed PMID: 24361265.
15. Perera G, Hay R. A guide to antibiotic resistance in bacterial skin infections. *Journal of the European Academy of Dermatology and Venereology*. 2005;19(5):531-545. PubMed PMID: 16164705.
16. Boyanova L, Mitov I. Antibiotic resistance rates in causative agents of infections in diabetic patients: rising concerns. *Expert Review of Anti-Infective Therapy*. 2013;11(4):411-420. PubMed PMID: 23566150.
17. Gomes A, Teixeira C, Ferraz R, Prudencio C, Gomes P. Wound-Healing Peptides for Treatment of Chronic Diabetic Foot Ulcers and Other Infected Skin Injuries. *Molecules*. 2017;22(10):1743. PubMed PMID: 29057807; PMCID: PMC6151519.
18. Howell-Jones RS, Wilson MJ, Hill KE, Howard AJ, Price PE, Thomas DW. A review of the microbiology, antibiotic usage and resistance in chronic skin wounds. *Journal of Antimicrobial Chemotherapy*. 2005;55(2):143-149. PubMed PMID: 15649989.
19. Appelbaum PC. The emergence of vancomycin-intermediate and vancomycin-resistant *Staphylococcus aureus*. *Clinical Microbiology and Infection*. 2006;12 Suppl 1:16-23. PubMed PMID: 16445720.
20. Boneca IG, Chiosis G. Vancomycin resistance: occurrence, mechanisms and strategies to combat it. *Expert Opinion on Therapeutic Targets*. 2003;7(3):311-328. PubMed PMID: 12783569.
21. Sherry L, Ramage G, Kean R, Borman A, Johnson EM, Richardson MD, Rautemaa-Richardson R. Biofilm-Forming Capability of Highly Virulent, Multidrug-Resistant *Candida auris*. *Emerging Infectious Diseases*. 2017;23(2):328-331. PubMed PMID: 28098553; PMCID: PMC5324806.

22. Traugott KA, Echevarria K, Maxwell P, Green K, Lewis JS, 2nd. Monotherapy or combination therapy? The *Pseudomonas aeruginosa* conundrum. *Pharmacotherapy*. 2011;31(6):598-608. PubMed PMID: 21923444.
23. Mehta KC, Dargad RR, Borade DM, Swami OC. Burden of antibiotic resistance in common infectious diseases: role of antibiotic combination therapy. *Journal of Clinical and Diagnostic Research*. 2014;8(6):ME05-8. PubMed PMID: 25121020; PMCID: PMC4129256.
24. Worthington RJ, Melander C. Overcoming resistance to beta-lactam antibiotics. *Journal of Organic Chemistry*. 2013;78(9):4207-4213. PubMed PMID: 23530949; PMCID: PMC3644377.
25. Grzybowski A, Sak J, Pawlikowski J. A brief report on the history of phototherapy. *Clinics in Dermatology*. 2016;34(5):532-537. PubMed PMID: 27638430.
26. Kharkwal GB, Sharma SK, Huang YY, Dai T, Hamblin MR. Photodynamic therapy for infections: clinical applications. *Lasers in Surgery and Medicine*. 2011;43(7):755-767. PubMed PMID: 22057503; PMCID: PMC3449167.
27. Enwemeka CS. Antimicrobial blue light: an emerging alternative to antibiotics. *Photomedicine and Laser Surgery*. 2013;31(11):509-511. PubMed PMID: 24138170.
28. Wang Y, Wang Y, Wang Y, Murray CK, Hamblin MR, Hooper DC, Dai T. Antimicrobial blue light inactivation of pathogenic microbes: State of the art. *Drug Resistance Updates*. 2017;33-35:1-22. PubMed PMID: 29145971; PMCID: PMC5699711.
29. Amin RM, Bhayana B, Hamblin MR, Dai T. Antimicrobial blue light inactivation of *Pseudomonas aeruginosa* by photo-excitation of endogenous porphyrins: In vitro and in vivo studies. *Lasers in Surgery and Medicine*. 2016;48(5):562-568. PubMed PMID: 26891084; PMCID: PMC4914480.
30. Castano AP, Demidova TN, Hamblin MR. Mechanisms in photodynamic therapy: part one-photosensitizers, photochemistry and cellular localization. *Photodiagnosis and Photodynamic Therapy*. 2004;1(4):279-293. PubMed PMID: 25048432; PMCID: PMC4108220.
31. Hamblin MR, Hasan T. Photodynamic therapy: a new antimicrobial approach to infectious disease? *Photochemical & Photobiological Sciences*. 2004;3(5):436-450. PubMed PMID: 15122361; PMCID: PMC3071049.
32. Dong PT, Mohammad H, Hui J, Leanse LG, Li J, Liang L, Dai T, Seleem MN, Cheng JX. Photolysis of Staphyloxanthin in Methicillin-Resistant *Staphylococcus*

- aureus Potentiates Killing by Reactive Oxygen Species. *Advanced Science*. 2019;6(11):1900030. PubMed PMID: 31179216; PMCID: PMC6548961.
33. Jusuf S, Dong PT, Hui J, Ulloa ER, Liu GY, Cheng JX. Granadaene Photobleaching Reduces the Virulence and Increases Antimicrobial Susceptibility of *Streptococcus agalactiae*. *Photochemistry and Photobiology*. 2021;97(4):816-25. PubMed PMID: 33502005; PMCID: PMC8277675.
  34. Dong PT, Jusuf S, Hui J, Zhan Y, Zhu Y, Liu GY, Cheng JX. Photoinactivation of catalase sensitizes a wide range of bacteria to ROS-producing agents and immune cells. *JCI Insight*. 2022;7(10). PubMed PMID: 35446788; PMCID: PMC9220836.
  35. Lück H. *Catalase. Methods of enzymatic analysis*: Elsevier; 1965. p. 885-894.
  36. Aebi H. [13] *Catalase in vitro. Methods in enzymology*: Elsevier; 1984. p. 121-126.
  37. Becker K, Skov RL, von Eiff C. *Staphylococcus, Micrococcus, and other catalase - positive cocci. Manual of clinical microbiology*. 2015:354-382.
  38. Imlay JA. Diagnosing oxidative stress in bacteria: not as easy as you might think. *Current Opinion in Microbiology*. 2015;24:124-131. PubMed PMID: 25666086; PMCID: PMC4380616.
  39. Flannagan RS, Heit B, Heinrichs DE. Antimicrobial Mechanisms of Macrophages and the Immune Evasion Strategies of *Staphylococcus aureus*. *Pathogens*. 2015; 4(4):826-868. PubMed PMID: 26633519; PMCID: PMC4693167.
  40. Kobayashi SD, Voyich JM, Burlak C, DeLeo FR. Neutrophils in the innate immune response. *Archivum Immunologiae et Therapiae Experimentalis*. 2005;53(6):505-517. PubMed PMID: 16407783.
  41. Day WA, Jr., Sajecki JL, Pitts TM, Joens LA. Role of catalase in *Campylobacter jejuni* intracellular survival. *Infection and Immunity*. 2000;68(11):6337-6345. PubMed PMID: 11035743; PMCID: PMC97717.
  42. Crane D, Masters C. On the role of catalase in the oxidation of tissue fatty acids. *Archives of Biochemistry and Biophysics*. 1984;229(1):104-111. PubMed PMID: 6703689.
  43. Gabriel F, Accoceberry I, Bessoule J-J, Salin B, Lucas-Guérin M, Manon S, Dementhon K, Noël T. A Fox2-dependent fatty acid  $\beta$ -oxidation pathway coexists both in peroxisomes and mitochondria of the ascomycete yeast *Candida lusitanae*. *PLoS One*. 2014;9(12):e114531.

44. Díaz A, Loewen PC, Fita I, Carpena X. Thirty years of heme catalases structural biology. *Archives of Biochemistry and Biophysics*. 2012;525(2):102-110.
45. Sies H, Bucher T, Oshino N, Chance B. Heme occupancy of catalase in hemoglobin-free perfused rat liver and of isolated rat liver catalase. *Archives of Biochemistry and Biophysics*. 1973;154(1):106-116. PubMed PMID: 4689773.
46. Miller LG, Eisenberg DF, Liu H, Chang CL, Wang Y, Luthra R, Wallace A, Fang C, Singer J, Suaya JA. Incidence of skin and soft tissue infections in ambulatory and inpatient settings, 2005-2010. *BMC Infectious Diseases*. 2015;15:362. PubMed PMID: 26293161; PMCID: PMC4546168.
47. Lee G, Boyd N, Lawson K, Frei C. Incidence and cost of skin and soft tissue infections in the United States. *Value in Health*. 2015;18(3):A245.
48. Kaye KS, Petty LA, Shorr AF, Zilberberg MD. Current Epidemiology, Etiology, and Burden of Acute Skin Infections in the United States. *Clinical Infectious Diseases*. 2019;68(Suppl 3):S193-S199. PubMed PMID: 30957165; PMCID: PMC6452002.
49. Kaye KS, Patel DA, Stephens JM, Khachatryan A, Patel A, Johnson K. Rising United States Hospital Admissions for Acute Bacterial Skin and Skin Structure Infections: Recent Trends and Economic Impact. *PLoS One*. 2015;10(11):e0143276. PubMed PMID: 26599005; PMCID: PMC4657980.
50. Ray GT, Suaya JA, Baxter R. Trends and characteristics of culture-confirmed *Staphylococcus aureus* infections in a large U.S. integrated health care organization. *Journal of Clinical Microbiology*. 2012;50(6):1950-1957. PubMed PMID: 22422853; PMCID: PMC3372166.
51. Moet GJ, Jones RN, Biedenbach DJ, Stilwell MG, Fritsche TR. Contemporary causes of skin and soft tissue infections in North America, Latin America, and Europe: report from the SENTRY Antimicrobial Surveillance Program (1998-2004). *Diagnostic Microbiology and Infectious Disease*. 2007;57(1):7-13. PubMed PMID: 17059876.
52. Petkovsek Z, Elersic K, Gubina M, Zgur-Bertok D, Starcic Erjavec M. Virulence potential of *Escherichia coli* isolates from skin and soft tissue infections. *Journal of Clinical Microbiology*. 2009;47(6):1811-1817. PubMed PMID: 19357208; PMCID: PMC2691073.
53. Wroblewska M. Novel therapies of multidrug-resistant *Pseudomonas aeruginosa* and *Acinetobacter* spp. infections: the state of the art. *Archivum Immunologiae et Therapiae Experimentalis*. 2006;54(2):113-120. PubMed PMID: 16648971.

54. Smith R, Russo J, Fiegel J, Brogden N. Antibiotic delivery strategies to treat skin infections when innate antimicrobial defense fails. *Antibiotics*. 2020;9(2):56.
55. Eisenstein BI. Treatment challenges in the management of complicated skin and soft-tissue infections. *Clinical Microbiology and Infection*. 2008;14 Suppl 2:17-25. PubMed PMID: 18226086.
56. Ogbodo S, Okeke A, Ugwuoru C, Chukwurah E. Possible alternatives to reduce antibiotic resistance. *Life Sciences and Medicine Research*. 2011;2011:1-9.
57. Dai TH, Gupta A, Huang YY, Yin R, Murray CK, Vrahas MS, Sherwood ME, Tegos GP, Hamblin MR. Blue Light Rescues Mice from Potentially Fatal *Pseudomonas aeruginosa* Burn Infection: Efficacy, Safety, and Mechanism of Action. *Antimicrobial Agents and Chemotherapy*. 2013;57(3):1238-1245. PubMed PMID: WOS:000314968100018.
58. Zhang Y, Zhu Y, Gupta A, Huang Y, Murray CK, Vrahas MS, Sherwood ME, Baer DG, Hamblin MR, Dai T. Antimicrobial blue light therapy for multidrug-resistant *Acinetobacter baumannii* infection in a mouse burn model: implications for prophylaxis and treatment of combat-related wound infections. *Journal of Infectious Diseases*. 2014;209(12):1963-1971. PubMed PMID: 24381206; PMCID: PMC4038138.
59. Hoenes K, Bauer R, Spellerberg B, Hessling M. Microbial photoinactivation by visible light results in limited loss of membrane integrity. *Antibiotics*. 2021;10(3):341.
60. Ramakrishnan P, Maclean M, MacGregor SJ, Anderson JG, Grant MH. Cytotoxic responses to 405nm light exposure in mammalian and bacterial cells: Involvement of reactive oxygen species. *Toxicology In Vitro*. 2016;33:54-62. PubMed PMID: 26916085.
61. Nitzan Y, Salmon-Divon M, Shporen E, Malik Z. ALA induced photodynamic effects on gram positive and negative bacteria. *Photochemical & Photobiological Sciences*. 2004;3(5):430-435. PubMed PMID: 15122360.
62. Kim M-J, Yuk H-G. Antibacterial mechanism of 405-nanometer light-emitting diode against *Salmonella* at refrigeration temperature. *Applied and Environmental Microbiology*. 2017;83(5):e02582-16.
63. Seaver LC, Imlay JA. Alkyl hydroperoxide reductase is the primary scavenger of endogenous hydrogen peroxide in *Escherichia coli*. *Journal of Bacteriology*. 2001;183(24):7173-7181.

64. Ferrandiz MJ, Martin-Galiano AJ, Arnanz C, Zimmerman T, de la Campa AG. Reactive Oxygen Species Contribute to the Bactericidal Effects of the Fluoroquinolone Moxifloxacin in *Streptococcus pneumoniae*. *Antimicrobial Agents and Chemotherapy*. 2016;60(1):409-417. PubMed PMID: 26525786; PMCID: PMC4704168.
65. Wang X, Zhao X, Malik M, Drlica K. Contribution of reactive oxygen species to pathways of quinolone-mediated bacterial cell death. *Journal of Antimicrobial Chemotherapy*. 2010;65(3):520-524. PubMed PMID: 20067982; PMCID: PMC2818107.
66. von Ossowski I, Mulvey MR, Leco PA, Borys A, Loewen PC. Nucleotide sequence of *Escherichia coli* katE, which encodes catalase HPII. *Journal of Bacteriology*. 1991;173(2):514-520.
67. Van Acker H, Coenye T. The Role of Reactive Oxygen Species in Antibiotic-Mediated Killing of Bacteria. *Trends in Microbiology*. 2017;25(6):456-466. PubMed PMID: 28089288.
68. Brown A, Lo D, Sharpe C, Tong C. Increased intracellular hydrogen peroxide observed in *Escherichia coli* in the presence of two classes of antibiotics. *Journal of Experimental Microbiology and Immunology*. 2012;16:17-23. [https://www.microbiology.ubc.ca/sites/default/files/roles/drupal\\_ungrad/JEMI/16/JEMI16\\_17-23.pdf](https://www.microbiology.ubc.ca/sites/default/files/roles/drupal_ungrad/JEMI/16/JEMI16_17-23.pdf)
69. Goswami M, Mangoli SH, Jawali N. Involvement of reactive oxygen species in the action of ciprofloxacin against *Escherichia coli*. *Antimicrobial Agents and Chemotherapy*. 2006;50(3):949-954. PubMed PMID: 16495256; PMCID: PMC1426460.
70. Reis J, Massari M, Marchese S, Ceccon M, Aalbers FS, Corana F, Valente S, Mai A, Magnani F, Mattevi A. A closer look into NADPH oxidase inhibitors: Validation and insight into their mechanism of action. *Redox Biology*. 2020;32:101466.
71. Linley E, Denyer SP, McDonnell G, Simons C, Maillard J-Y. Use of hydrogen peroxide as a biocide: new consideration of its mechanisms of biocidal action. *Journal of Antimicrobial Chemotherapy*. 2012;67(7):1589-1596.
72. Dai T, Kharkwal GB, Tanaka M, Huang YY, Bil de Arce VJ, Hamblin MR. Animal models of external traumatic wound infections. *Virulence*. 2011;2(4):296-315. PubMed PMID: 21701256; PMCID: PMC3173676.
73. Loewen P. Probing the structure of catalase HPII of *Escherichia coli*--a review. *Gene*. 1996;179(1):39-44. PubMed PMID: 8955627.

74. Panek HR, O'Brian MR. KatG is the primary detoxifier of hydrogen peroxide produced by aerobic metabolism in *Bradyrhizobium japonicum*. *Journal of Bacteriology*. 2004;186(23):7874-7880. PubMed PMID: 15547258; PMCID: PMC529082.
75. Kremer M. Mechanism of the Fenton reaction. Evidence for a new intermediate. *Physical Chemistry Chemical Physics*. 1999;1(15):3595-3605.
76. Belcher JD, Beckman JD, Balla G, Balla J, Vercellotti G. Heme degradation and vascular injury. *Antioxidants & Redox Signaling*. 2010;12(2):233-248.
77. Winterbourn CC. Toxicity of iron and hydrogen peroxide: the Fenton reaction. *Toxicology Letters*. 1995;82-83:969-974. PubMed PMID: 8597169.
78. Brandi G, Cattabeni F, Albano A, Cantoni O. Role of hydroxyl radicals in *Escherichia coli* killing induced by hydrogen peroxide. *Free Radical Research Communications*. 1989;6(1):47-55.
79. Nagababu E, Rifkind JM. Reaction of hydrogen peroxide with ferrylhemoglobin: superoxide production and heme degradation. *Biochemistry*. 2000;39(40):12503-12511. PubMed PMID: 11015232.
80. Das D, Saha SS, Bishayi B. Intracellular survival of *Staphylococcus aureus*: correlating production of catalase and superoxide dismutase with levels of inflammatory cytokines. *Inflammation Research*. 2008;57(7):340-349. PubMed PMID: 18607538.
81. Guerra FE, Borgogna TR, Patel DM, Sward EW, Voyich JM. Epic Immune Battles of History: Neutrophils vs. *Staphylococcus aureus*. *Frontiers in Cellular and Infection Microbiology*. 2017;7:286. PubMed PMID: 28713774; PMCID: PMC5491559.
82. Sender R, Fuchs S, Milo R. Are we really vastly outnumbered? Revisiting the ratio of bacterial to host cells in humans. *Cell*. 2016;164(3):337-340.
83. Laser Institute of America. American National Standard for Safe Use of Lasers ANSI Z136. 1-2014. American National Standards Institute, Inc.; 2014.
84. Molano-Arevalo JC, Jeanne Dit Fouque K, Pham K, Miksovska J, Ridgeway ME, Park MA, Fernandez-Lima F. Characterization of Intramolecular Interactions of Cytochrome c Using Hydrogen-Deuterium Exchange-Trapped Ion Mobility Spectrometry-Mass Spectrometry and Molecular Dynamics. *Analytical Chemistry*. 2017;89(17):8757-8765. PubMed PMID: 28742962; PMCID: PMC5653375.

85. Jusuf S, Zhan Y, Zhang M, Alexander NJ, Viens A, Mansour MK, Cheng JX. Blue Light Deactivation of Catalase Suppresses Candida Hyphae Development Through Lipogenesis Inhibition. *Photochemistry and Photobiology*. 2022. <https://doi.org/10.1111/php.13719>
86. Dong PT, Zhan Y, Jusuf S, Hui J, Dagher Z, Mansour MK, Cheng JX. Photoinactivation of Catalase Sensitizes Candida albicans and Candida auris to ROS-Producing Agents and Immune Cells. *Advanced Science*. 2022:e2104384. PubMed PMID: 35119220.
87. Bongomin F, Gago S, Oladele RO, Denning DW. Global and Multi-National Prevalence of Fungal Diseases-Estimate Precision. *Journal of Fungi*. 2017;3(4). PubMed PMID: 29371573; PMCID: PMC5753159.
88. Kainz K, Bauer MA, Madeo F, Carmona-Gutierrez D. Fungal infections in humans: the silent crisis. *Microbial Cell*. 2020;7(6):143-145. PubMed PMID: 32548176; PMCID: PMC7278517.
89. Papon N, Courdavault V, Clastre M, Bennett RJ. Emerging and emerged pathogenic Candida species: beyond the Candida albicans paradigm. *PLoS Pathogens*. 2013; 9(9):e1003550. PubMed PMID: 24086128; PMCID: PMC3784480.
90. Nucci M, Queiroz-Telles F, Tobon AM, Restrepo A, Colombo AL. Epidemiology of opportunistic fungal infections in Latin America. *Clinical Infectious Diseases*. 2010; 51(5):561-570. PubMed PMID: 20658942.
91. Walmsley S, Devi S, King S, Schneider R, Richardson S, Ford-Jones L. Invasive Aspergillus infections in a pediatric hospital: a ten-year review. *Pediatric Infectious Disease Journal*. 1993;12(8):673-682. PubMed PMID: 8414781.
92. van Burik JA, Colven R, Spach DH. Cutaneous aspergillosis. *Journal of Clinical Microbiology*. 1998;36(11):3115-3121. PubMed PMID: 9774549; PMCID: PMC105285.
93. Blutfield MS, Lohre JM, Pawich DA, Vlahovic TC. The Immunologic Response to Trichophyton Rubrum in Lower Extremity Fungal Infections. *Journal of Fungi*. 2015;1(2):130-137. PubMed PMID: 29376904; PMCID: PMC5753105.
94. Sosa L, Clares B, Alvarado HL, Bozal N, Domenech O, Calpena AC. Amphotericin B releasing topical nanoemulsion for the treatment of candidiasis and aspergillosis. *Nanomedicine*. 2017;13(7):2303-2312. PubMed PMID: 28712917.
95. Nusbaum AG, Kirsner RS, Charles CA. Biofilms in dermatology. *Skin Therapy Letter*. 2012;17(7):1-5. PubMed PMID: 22825648.

96. Chen SC, Sorrell TC. Antifungal agents. *Medical Journal of Australia*. 2007;187(7):404-409. PubMed PMID: 17908006.
97. Ghannoum MA, Rice LB. Antifungal agents: mode of action, mechanisms of resistance, and correlation of these mechanisms with bacterial resistance. *Clinical Microbiology Reviews*. 1999;12(4):501-517. PubMed PMID: 10515900; PMCID: PMC88922.
98. Whaley SG, Berkow EL, Rybak JM, Nishimoto AT, Barker KS, Rogers PD. Azole Antifungal Resistance in *Candida albicans* and Emerging Non-*albicans* *Candida* Species. *Frontiers in Microbiology*. 2016;7:2173. PubMed PMID: 28127295; PMCID: PMC5226953.
99. Du H, Bing J, Hu T, Ennis CL, Nobile CJ, Huang G. *Candida auris*: Epidemiology, biology, antifungal resistance, and virulence. *PLoS Pathogens*. 2020;16(10):e1008921. PubMed PMID: 33091071; PMCID: PMC7581363 inhibitors and diagnostics of biofilms.
100. Wysong DR, Christin L, Sugar AM, Robbins PW, Diamond RD. Cloning and sequencing of a *Candida albicans* catalase gene and effects of disruption of this gene. *Infection and Immunity*. 1998;66(5):1953-1961. PubMed PMID: 9573075; PMCID: PMC108149.
101. Calderone RA, Fonzi WA. Virulence factors of *Candida albicans*. *Trends in Microbiology*. 2001;9(7):327-335. PubMed PMID: 11435107.
102. Alfonso-Prieto M, Biarnes X, Vidossich P, Rovira C. The molecular mechanism of the catalase reaction. *Journal of the American Chemical Society*. 2009;131(33):11751-11761. PubMed PMID: 19653683.
103. El-Benna J, Hurtado-Nedelec M, Marzaioli V, Marie JC, Gougerot-Pocidallo MA, Dang PM. Priming of the neutrophil respiratory burst: role in host defense and inflammation. *Immunological Reviews*. 2016;273(1):180-193. PubMed PMID: 27558335.
104. Nakagawa Y, Kanbe T, Mizuguchi I. Disruption of the human pathogenic yeast *Candida albicans* catalase gene decreases survival in mouse-model infection and elevates susceptibility to higher temperature and to detergents. *Microbiology and Immunology*. 2003;47(6):395-403. PubMed PMID: 12906099.
105. Sudbery P, Gow N, Berman J. The distinct morphogenic states of *Candida albicans*. *Trends in Microbiology*. 2004;12(7):317-324. PubMed PMID: 15223059.

106. Brand A. Hyphal growth in human fungal pathogens and its role in virulence. *International Journal of Microbiology*. 2012;2012:517529. PubMed PMID: 22121367; PMCID: PMC3216317.
107. Sudbery PE. Growth of *Candida albicans* hyphae. *Nature Reviews. Microbiology*. 2011;9(10):737-748. PubMed PMID: 21844880.
108. Kumamoto CA, Vences MD. Contributions of hyphae and hypha-co-regulated genes to *Candida albicans* virulence. *Cellular Microbiology*. 2005;7(11):1546-1554. PubMed PMID: 16207242.
109. Mukaremera L, Lee KK, Mora-Montes HM, Gow NAR. *Candida albicans* Yeast, Pseudohyphal, and Hyphal Morphogenesis Differentially Affects Immune Recognition. *Frontiers in Immunology*. 2017;8:629. PubMed PMID: 28638380; PMCID: PMC5461353.
110. Mukherjee PK, Zhou G, Munyon R, Ghannoum MA. *Candida* biofilm: a well-designed protected environment. *Medical Mycology*. 2005;43(3):191-208. PubMed PMID: 16010846.
111. Martin SW, Konopka JB. Lipid raft polarization contributes to hyphal growth in *Candida albicans*. *Eukaryotic Cell*. 2004;3(3):675-684. PubMed PMID: 15189988; PMCID: PMC420133.
112. Yano K, Yamada T, Banno Y, Sekiya T, Nozawa Y. Modification of Lipid Composition in a Dimorphic Fungus, *Candida albicans* during the Yeast Cell to Hypha Transformation. *Japanese Journal of Medical Mycology*. 1982;23(2):159-165.
113. Nakagawa Y. Catalase gene disruptant of the human pathogenic yeast *Candida albicans* is defective in hyphal growth, and a catalase-specific inhibitor can suppress hyphal growth of wild-type cells. *Microbiology and Immunology*. 2008;52(1):16-24. PubMed PMID: 18352908.
114. Schroter C, Hipler UC, Wilmer A, Kunkel W, Wollina U. Generation of reactive oxygen species by *Candida albicans* in relation to morphogenesis. *Archives of Dermatological Research*. 2000;292(5):260-264. PubMed PMID: 10867815.
115. Rossi DCP, Gleason JE, Sanchez H, Schatzman SS, Culbertson EM, Johnson CJ, McNees CA, Coelho C, Nett JE, Andes DR, Cormack BP, Culotta VC. *Candida albicans* FRE8 encodes a member of the NADPH oxidase family that produces a burst of ROS during fungal morphogenesis. *PLoS Pathogens*. 2017;13(12): e1006763. PubMed PMID: 29194441; PMCID: PMC5728582.

116. Nasution O, Srinivasa K, Kim M, Kim YJ, Kim W, Jeong W, Choi W. Hydrogen peroxide induces hyphal differentiation in *Candida albicans*. *Eukaryotic Cell*. 2008;7(11):2008-2011. PubMed PMID: 18791036; PMCID: PMC2583538.
117. Cabiscol E, Piulats E, Echave P, Herrero E, Ros J. Oxidative stress promotes specific protein damage in *Saccharomyces cerevisiae*. *Journal of Biological Chemistry*. 2000;275(35):27393-27398. PubMed PMID: 10852912.
118. Sousa AB, Manzano H, Soto-Blanco B, Gorniak SL. Toxicokinetics of cyanide in rats, pigs and goats after oral dosing with potassium cyanide. *Archives of Toxicology*. 2003;77(6):330-334. PubMed PMID: 12799772.
119. Banerjee O, Singh S, Prasad SK, Bhattacharjee A, Banerjee A, Banerjee A, Saha A, Maji BK, Mukherjee S. Inhibition of catalase activity with 3-amino-1,2,4-triazole intensifies bisphenol A (BPA)-induced toxicity in granulosa cells of female albino rats. *Toxicology and Industrial Health*. 2018;34(11):787-797. PubMed PMID: 30269681.
120. Hopke A, Nicke N, Hidu EE, Degani G, Popolo L, Wheeler RT. Neutrophil Attack Triggers Extracellular Trap-Dependent *Candida* Cell Wall Remodeling and Altered Immune Recognition. *PLoS Pathogens*. 2016;12(5):e1005644. PubMed PMID: 27223610; PMCID: PMC4880299.
121. Barros N, Alexander N, Viens A, Timmer K, Atallah N, Knooihuizen SAI, Hopke A, Scherer A, Dagher Z, Irimia D, Mansour MK. Cytokine Augmentation Reverses Transplant Recipient Neutrophil Dysfunction against the human fungal pathogen, *Candida albicans*. *Journal of Infectious Diseases*. 2021;224(5):894–902. PubMed PMID: 33417688.
122. Zhang M, Hong W, Abutaleb NS, Li J, Dong PT, Zong C, Wang P, Seleem MN, Cheng JX. Rapid Determination of Antimicrobial Susceptibility by Stimulated Raman Scattering Imaging of D2O Metabolic Incorporation in a Single Bacterium. *Advanced Science*. 2020;7(19):2001452. PubMed PMID: 33042757; PMCID: PMC7539191.
123. Breil C, Abert Vian M, Zemb T, Kunz W, Chemat F. "Bligh and Dyer" and Folch Methods for Solid-Liquid-Liquid Extraction of Lipids from Microorganisms. Comprehension of Solvation Mechanisms and towards Substitution with Alternative Solvents. *International Journal of Molecular Sciences*. 2017;18(4). PubMed PMID: 28346372; PMCID: PMC5412294.
124. Kruger NJ, von Schaewen A. The oxidative pentose phosphate pathway: structure and organisation. *Current Opinion in Plant Biology*. 2003;6(3):236-246. PubMed PMID: 12753973.

125. Xue J, Balamurugan S, Li DW, Liu YH, Zeng H, Wang L, Yang WD, Liu JS, Li HY. Glucose-6-phosphate dehydrogenase as a target for highly efficient fatty acid biosynthesis in microalgae by enhancing NADPH supply. *Metabolic Engineering*. 2017;41:212-221. PubMed PMID: 28465173.
126. Walther TC, Farese RV, Jr. Lipid droplets and cellular lipid metabolism. *Annual Review of Biochemistry*. 2012;81:687-714. PubMed PMID: 22524315; PMCID: PMC3767414.
127. Dai T, Bil de Arce VJ, Tegos GP, Hamblin MR. Blue dye and red light, a dynamic combination for prophylaxis and treatment of cutaneous *Candida albicans* infections in mice. *Antimicrobial Agents and Chemotherapy*. 2011;55(12):5710-5717. PubMed PMID: 21930868; PMCID: PMC3232820.
128. Faway E, Lambert de Rouvroit C, Poumay Y. In vitro models of dermatophyte infection to investigate epidermal barrier alterations. *Experimental Dermatology*. 2018;27(8):915-922. PubMed PMID: 29957851.
129. VanderVen BC, Yates RM, Russell DG. Intrapagosomal measurement of the magnitude and duration of the oxidative burst. *Traffic*. 2009;10(4):372-378. PubMed PMID: 19183302; PMCID: PMC2736473.
130. Steinberg G. Hyphal growth: a tale of motors, lipids, and the Spitzenkorper. *Eukaryotic Cell*. 2007;6(3):351-360. PubMed PMID: 17259546; PMCID: PMC1828937.
131. Patton JL, Lester RL. The phosphoinositol sphingolipids of *Saccharomyces cerevisiae* are highly localized in the plasma membrane. *Journal of Bacteriology*. 1991;173(10):3101-3108. PubMed PMID: 1827112; PMCID: PMC207903.
132. Wakil SJ. Fatty acid synthase, a proficient multifunctional enzyme. *Biochemistry*. 1989;28(11):4523-4530. PubMed PMID: 2669958.
133. Zhang Z, Chen L, Liu L, Su X, Rabinowitz JD. Chemical Basis for Deuterium Labeling of Fat and NADPH. *Journal of the American Chemical Society*. 2017;139(41):14368-14371. PubMed PMID: 28911221; PMCID: PMC5748894.
134. Futerman AH, Riezman H. The ins and outs of sphingolipid synthesis. *Trends in Cell Biology*. 2005;15(6):312-318. PubMed PMID: 15953549.
135. Amulic B, Cazalet C, Hayes GL, Metzler KD, Zychlinsky A. Neutrophil function: from mechanisms to disease. *Annual Review of Immunology*. 2012;30:459-489. PubMed PMID: 22224774.

136. Gazendam RP, van Hamme JL, Tool AT, van Houdt M, Verkuijlen PJ, Herbst M, Liese JG, van de Veerdonk FL, Roos D, van den Berg TK, Kuijpers TW. Two independent killing mechanisms of *Candida albicans* by human neutrophils: evidence from innate immunity defects. *Blood*. 2014;124(4):590-597. PubMed PMID: 24948657.
137. Urban CF, Reichard U, Brinkmann V, Zychlinsky A. Neutrophil extracellular traps capture and kill *Candida albicans* yeast and hyphal forms. *Cellular Microbiology*. 2006;8(4):668-676. PubMed PMID: 16548892.
138. Ermert D, Niemiec MJ, Rohm M, Glenthøj A, Borregaard N, Urban CF. *Candida albicans* escapes from mouse neutrophils. *Journal of Leukocyte Biology*. 2013; 94(2):223-236. PubMed PMID: 23650619.
139. Hopke A, Scherer A, Kreuzburg S, Abers MS, Zerbe CS, Dinauer MC, Mansour MK, Irimia D. Neutrophil swarming delays the growth of clusters of pathogenic fungi. *Nature Communications*. 2020;11(1):2031. PubMed PMID: 32341348; PMCID: PMC7184738.
140. Kuhbacher A, Burger-Kentischer A, Rupp S. Interaction of *Candida* Species with the Skin. *Microorganisms*. 2017;5(2). PubMed PMID: 28590443; PMCID: PMC5488103.
141. Tsui C, Kong EF, Jabra-Rizk MA. Pathogenesis of *Candida albicans* biofilm. *Pathogens and Disease*. 2016;74(4):ftw018. PubMed PMID: 26960943; PMCID: PMC5975230.
142. Jacobsen ID, Wilson D, Wachtler B, Brunke S, Naglik JR, Hube B. *Candida albicans* dimorphism as a therapeutic target. *Expert Review of Anti-Infective Therapy*. 2012;10(1):85-93. PubMed PMID: 22149617.
143. Berkow EL, Lockhart SR. Fluconazole resistance in *Candida* species: a current perspective. *Infection and Drug Resistance*. 2017;10:237-245. PubMed PMID: 28814889; PMCID: PMC5546770.
144. Köhler JR, Casadevall A, Perfect J. The spectrum of fungi that infects humans. *Cold Spring Harbor Perspectives in Medicine*. 2015;5(1):a019273.
145. Jerome TJ, Kandasamy L, Terrence TK, Bhalaji S, Shanmugasundaram B. *Aspergillus flavus* Infection of Lower Limb in an Immune-Competent Patient. *Cureus*. 2020;12(7):e9342. PubMed PMID: 32850216; PMCID: PMC7444893.
146. Que AT, Nguyen NT, Do NA, Nguyen NL, Tran ND, Le TA. Infection of burn wound by *Aspergillus fumigatus* with gross appearance of fungal colonies. *Medical*

- Mycology Case Reports. 2019;24:30-32. PubMed PMID: 30949425; PMCID: PMC6429549.
147. Jusuf S, Cheng JX. Blue Light Improves Antimicrobial Efficiency of Silver Sulfadiazine Via Catalase Inactivation. *Photobiomodulation, Photomedicine, and Laser Surgery*. 2023;41(2):80-87. PubMed PMID: 36780574; PMCID: PMC9963486.
  148. Kapoor P, Kumar S. Hydrogen peroxide in dermatology. *Indian Journal of Dermatology, Venereology and Leprology*. 2021:1-3. PubMed PMID: 34623047.
  149. Lau WY, Wong SH. Randomized, prospective trial of topical hydrogen peroxide in appendectomy wound infection. High risk factors. *American Journal of Surgery*. 1981;142(3):393-397. PubMed PMID: 7283035.
  150. Cambiaso-Daniel J, Boukavalas S, Bitz GH, Branski LK, Herndon DN, Culnan DM. Topical Antimicrobials in Burn Care: Part 1-Topical Antiseptics. *Annals of Plastic Surgery*. 2018. PubMed PMID: 29319571; PMCID: PMC6037606.
  151. Mut M, Yemisci M, Gursoy-Ozdemir Y, Ture U. Hydrogen peroxide-induced stroke: elucidation of the mechanism in vivo. *Journal of Neurosurgery*. 2009;110(1): 94-100. PubMed PMID: 18928358.
  152. Beattie C, Harry LE, Hamilton SA, Burke D. Cardiac arrest following hydrogen peroxide irrigation of a breast wound. *Journal of Plastic, Reconstructive & Aesthetic Surgery*. 2010;63(3):e253-254. PubMed PMID: 19632911.
  153. Bandyopadhyay D. Topical Antibacterials in Dermatology. *Indian Journal of Dermatology*. 2021;66(2):117-125. PubMed PMID: 34188265; PMCID: PMC8208253.
  154. Oaks RJ, Cindass R. *Silver Sulfadiazine*: StatPearls Publishing, Treasure Island (FL); 2021.
  155. Hoffmann S. Silver Sulfadiazine: an Antibacterial Agent for Topical use in Burns. *Scandinavian Journal of Plastic and Reconstructive Surgery*. 1984;18(1):119-126.
  156. Carr HS, Wlodkowski TJ, Rosenkranz HS. Silver sulfadiazine: in vitro antibacterial activity. *Antimicrobial Agents and Chemotherapy*. 1973;4(5):585-587. PubMed PMID: 4791493; PMCID: PMC444599.
  157. Fox CL, Jr. Silver sulfadiazine--a new topical therapy for Pseudomonas in burns. Therapy of Pseudomonas infection in burns. *Archives of Surgery*. 1968;96(2):184-188. PubMed PMID: 5638080.

158. World Health Organization. The selection and use of essential medicines: report of the WHO Expert Committee on Selection and Use of Essential Medicines, 2019 (including the 21st WHO Model List of Essential Medicines and the 7th WHO Model List of Essential Medicines for Children) 2019. <https://apps.who.int/iris/rest/bitstreams/50531/retrieve>
159. Achari A, Somers DO, Champness JN, Bryant PK, Rosemond J, Stammers DK. Crystal structure of the anti-bacterial sulfonamide drug target dihydropteroate synthase. *Nature Structural Biology*. 1997;4(6):490-497. PubMed PMID: 9187658.
160. Gordon O, Vig Slenters T, Brunetto PS, Villaruz AE, Sturdevant DE, Otto M, Landmann R, Fromm KM. Silver coordination polymers for prevention of implant infection: thiol interaction, impact on respiratory chain enzymes, and hydroxyl radical induction. *Antimicrobial Agents and Chemotherapy*. 2010;54(10):4208-4218. PubMed PMID: 20660682; PMCID: PMC2944614.
161. Fox CL, Jr., Modak SM. Mechanism of silver sulfadiazine action on burn wound infections. *Antimicrobial Agents and Chemotherapy*. 1974;5(6):582-8. PubMed PMID: 15825409; PMCID: PMC429018.
162. Park HJ, Kim JY, Kim J, Lee JH, Hahn JS, Gu MB, Yoon J. Silver-ion-mediated reactive oxygen species generation affecting bactericidal activity. *Water Research*. 2009;43(4):1027-1032. PubMed PMID: 19073336.
163. Cho Lee AR, Leem H, Lee J, Park KC. Reversal of silver sulfadiazine-impaired wound healing by epidermal growth factor. *Biomaterials*. 2005;26(22):4670-4676. PubMed PMID: 15722137.
164. Fuller FW. The side effects of silver sulfadiazine. *Journal of Burn Care & Research*. 2009;30(3):464-470. PubMed PMID: 19349889.
165. Akhoondinasab MR, Akhoondinasab M, Saberi M. Comparison of healing effect of aloe vera extract and silver sulfadiazine in burn injuries in experimental rat model. *World Journal of Plastic Surgery*. 2014;3(1):29-34. PubMed PMID: 25489521; PMCID: PMC4236981.
166. Botelho MG. Fractional inhibitory concentration index of combinations of antibacterial agents against cariogenic organisms. *Journal of Dentistry*. 2000;28(8):565-570. PubMed PMID: 11082524.
167. Odds FC. Synergy, antagonism, and what the checkerboard puts between them. *Journal of Antimicrobial Chemotherapy*. 2003;52(1):1. PubMed PMID: 12805255.
168. Hamilton-Miller JM, Shah S, Smith C. Silver sulphadiazine: a comprehensive in vitro reassessment. *Chemotherapy*. 1993;39(6):405-409. PubMed PMID: 8222868.

169. Elkins JG, Hassett DJ, Stewart PS, Schweizer HP, McDermott TR. Protective role of catalase in *Pseudomonas aeruginosa* biofilm resistance to hydrogen peroxide. *Applied and Environmental Microbiology*. 1999;65(10):4594-4600. PubMed PMID: 10508094; PMCID: PMC91612.
170. Storz G, Tartaglia LA, Farr SB, Ames BN. Bacterial defenses against oxidative stress. *Trends in Genetics*. 1990;6(11):363-368. PubMed PMID: 1965068.
171. Martins D, English AM. Catalase activity is stimulated by H<sub>2</sub>O<sub>2</sub> in rich culture medium and is required for H<sub>2</sub>O<sub>2</sub> resistance and adaptation in yeast. *Redox Biology*. 2014;2:308-313.
172. Liu GY, Essex A, Buchanan JT, Datta V, Hoffman HM, Bastian JF, Fierer J, Nizet V. *Staphylococcus aureus* golden pigment impairs neutrophil killing and promotes virulence through its antioxidant activity. *Journal of Experimental Medicine*. 2005;202(2):209-215. PubMed PMID: 16009720; PMCID: PMC2213009.
173. Hall JW, Yang J, Guo H, Ji Y. The *Staphylococcus aureus* AirSR Two-Component System Mediates Reactive Oxygen Species Resistance via Transcriptional Regulation of Staphyloxanthin Production. *Infection & Immunity*. 2017;85(2). PubMed PMID: 27872240; PMCID: PMC5278164.
174. Berbudi A, Fadlillah AA, Afni M, Atik N. Effect of *Curcuma longa* Crude Extract, Curcumin and Nano Curcumin-based Gel Topical Administration on Excised Skin Wound Healing in Swiss-Webster Mice. *Biomedical and Pharmacology Journal*. 2021;14(2):635-641.
175. Davies J, Spiegelman GB, Yim G. The world of subinhibitory antibiotic concentrations. *Current Opinion in Microbiology*. 2006;9(5):445-453. PubMed PMID: 16942902.
176. Iavicoli I, Fontana L, Agathokleous E, Santocono C, Russo F, Vetrani I, Fedele M, Calabrese EJ. Hormetic dose responses induced by antibiotics in bacteria: A phantom menace to be thoroughly evaluated to address the environmental risk and tackle the antibiotic resistance phenomenon. *Science of the Total Environment*. 2021;798:149255. PubMed PMID: 34340082.
177. Heggers JP, Robson MC. The emergence of silver sulphadiazine-resistant *pseudomonas aeruginosa*. *Burns*. 1978;5(2):184-187.
178. Pirnay JP, De Vos D, Cochez C, Bilocq F, Pirson J, Struelens M, Duinslaeger L, Cornelis P, Zizi M, Vanderkelen A. Molecular epidemiology of *Pseudomonas aeruginosa* colonization in a burn unit: persistence of a multidrug-resistant clone and a silver sulfadiazine-resistant clone. *Journal of Clinical Microbiology*. 2003;41(3):1192-1202. PubMed PMID: 12624051; PMCID: PMC150314.

179. Landis SJ. Chronic Wound Infection and Antimicrobial Use. *Advances in Skin & Wound Care*. 2008;21(11):531-540. PubMed PMID: 00129334-200811000-00010.
180. Chang M, Nguyen TT. Strategy for Treatment of Infected Diabetic Foot Ulcers. *Accounts of Chemical Research*. 2021;54(5):1080-1093. PubMed PMID: 33596041.
181. Gordon CJ. The mouse thermoregulatory system: Its impact on translating biomedical data to humans. *Physiology & Behavior*. 2017;179:55-66.
182. Goldberg DJ. Current trends in intense pulsed light. *The Journal of Clinical and Aesthetic Dermatology*. 2012;5(6):45.
183. Chen J, Loeb S, Kim J-H. LED revolution: fundamentals and prospects for UV disinfection applications. *Environmental Science: Water Research & Technology*. 2017;3(2):188-202.
184. Raeiszadeh M, Adeli B. A critical review on ultraviolet disinfection systems against COVID-19 outbreak: applicability, validation, and safety considerations. *ACS Photonics*. 2020;7(11):2941-2951.
185. Phillipson RP, Tobi SE, Morris JA, McMillan TJ. UV-A induces persistent genomic instability in human keratinocytes through an oxidative stress mechanism. *Free Radical Biology and Medicine*. 2002;32(5):474-480.
186. Finlayson L, Barnard IR, McMillan L, Ibbotson SH, Brown CTA, Eadie E, Wood K. Depth penetration of light into skin as a function of wavelength from 200 to 1000 nm. *Photochemistry and Photobiology*. 2022;98(4):974-981.
187. Xu J, Gulzar A, Liu Y, Bi H, Gai S, Liu B, Yang D, He F, Yang P. Integration of IR - 808 sensitized upconversion nanostructure and MoS<sub>2</sub> nanosheet for 808 nm NIR light triggered phototherapy and bioimaging. *Small*. 2017;13(36):1701841.
188. Na JI, Suh DH. Red light phototherapy alone is effective for acne vulgaris: randomized, single - blinded clinical trial. *Dermatologic Surgery*. 2007;33(10):1228-1233.
189. Trelles MA, Allones I. Red light - emitting diode (LED) therapy accelerates wound healing post - blepharoplasty and periocular laser ablative resurfacing. *Journal of Cosmetic and Laser Therapy*. 2006;8(1):39-42.

**CURRICULUM VITAE**

